UNIVERSITY OF MANITOBA

NEXT TO LEADING ORDER AND HARD-PHOTON BREMSSTRAHLUNG EFFECTS IN ELECTROWEAK ELECTRON-NUCLEON SCATTERING

By

Aleksandrs Aleksejevs

A THESIS

Submitted to the Faculty of Graduate Studies
of the University of Manitoba
in partial fulfillment of the requirements for
the degree of Doctor of Philosophy

Winnipeg, Manitoba
June 20, 2005

THE UNIVERSITY OF MANITOBA

FACULTY OF GRADUATE STUDIES
*****
COPYRIGHT PERMISSION

Next to Leading Order and Hard-Photon Bremsstrahlung Effects in Electroweak Electron-Nucleon Scattering

BY

Aleksandrs Aleksejevs

A Thesis/Practicum submitted to the Faculty of Graduate Studies of The University of

Manitoba in partial fulfillment of the requirement of the degree

Of

Doctor of Philosophy

Aleksandrs Aleksejevs © 2005

Aleksandrs Aleksejevs

NEXT TO LEADING ORDER AND HARD-PHOTON BREMSSTRAHLUNG EFFECTS IN ELECTROWEAK ELECTRON-NUCLEON SCATTERING   June 20, 2005

Parity-violating electron-proton scattering experiments are a rapidly developing area dedicated not only to measuring the weak nucleon form factors, but also, more generally, to search for effects beyond the Standard Model of Particle Physics.

The main purpose of the present work is to take into consideration the next to leading order effects in parity-violating (PV) electron-nucleon scattering with realistic form factors for the hadronic currents, and to compute corrections to the weak charges of the proton and neutron. We do so without using the usual zero momentum transfer approximation. A complete analytical example for the $\gamma - Z$ box type of correction for electron-proton scattering is considered.

The method for evaluation of the electron-nucleon radiative corrections most commonly found in the literature is to follow the Feynman rules for the elementary particles of the Standard Model, and calculate electron-

quark corrections first. Then the single quark terms are combined to form hadronic vector and axial vector corrections. However, this approach leaves us with infrared divergences generated by the integration in the loops involving massless particles. One way to treat such infrared divergences of the electroweak radiative corrections is by adding PV soft-photon emission graphs. Although reasonable, the results are left with a logarithmic dependence on the photon detector acceptance, which can only be eliminated by considering PV hard-photon bremsstrahlung (HPB) graphs. We present what we believe to be the first complete treatment of HPB for electroweak scattering. Parity-violating HPB differential cross sections for electron-proton scattering have been computed using the experimental values of form factors in the diagram vertices. It allows us to avoid uncertainties associated with unknown quark dynamics.

The final results are conveniently expressed through kinematical parameters, making it possible to apply the computed HPB asymmetries to virtually any PV electron-nucleon scattering process. We also provide a complete set of numerical results for one-loop electron-nucleon radiative corrections for SAMPLE, HAPPEX, G0, A4, and Q-Weak experiments. The methods developed for electron-nucleon scattering are applied to calculations of the weak charges of nuclei. Several numerical results are

listed, and found to be in good agreement with the current experimental

data.

Contents

List of Figures

List of Tables

ACKNOWLEGEMENTS

1 Introduction

The Standard Model introduces an asymmetry between left- and right-handed particles, and predicts a parity-violating interference between the weak and electromagnetic forces. These interference effects are small, but have been clearly detected in recent experiments [1]. Extracting the physics of interest from the measured asymmetry requires evaluating radiative corrections to electroweak scattering at very high precision. Naturally, one-loop[1] radiative corrections will give the dominant contribution. Electroweak radiative corrections to intermediate energy, parity non-conserving semi-leptonic neutral current interactions have been addressed previously in Refs. [2, 3, 4, 5, 6]. Later work in Ref. [7] improved the techniques for one-quark radiative corrections computation by retaining analytical momentum-dependent expressions and providing the precise numerical evaluations of 446 one-loop diagrams. However, in Ref. [7], even after regulating infrared divergences through soft-photon emission, the calculated one-quark radiative corrections showed a logarithmic dependence on the detector's photon acceptance parameter.

The thesis presented here proves that elimination of this dependence can be

---

[1] Here one-loop refers to the leading order correction in perturbation theory, generally involving one integration over virtual internal four-momenta in a topological closed-loop Feynman diagram.

achieved by adding the Hard-Photon Bremsstrahlung (HPB) term. For one-quark radiative corrections, the HPB term is hard to account for due to the poorly known quark dynamics. Thus, we have to define the next to leading order hadronic radiative corrections for the electron-nucleon parity-violating scattering directly. This approach has its own challenges and advantages. In the case of the HPB computation for electron-proton scattering, we can avoid this theoretical uncertainty by representing cumulative quark dynamics directly through an experimentally determined set of form factors. Using a monopole approximation for the form factors, we modify general electroweak couplings by inserting appropriate form factors into vertices and construct a HPB factor as a function of Mandelstam invariants.

In the current work, we provide a detailed description of both hard- and soft-photon emission treatment. For each set of experimental constraints, integration over the emitted photon phase space can be performed numerically.

One-loop corrections are generally sub-divided into three topological classes: boxes, self energies, and vertex (triangle) graphs. To preserve gauge invariance, we include all the possible bosons of the Standard Model in these topological classes, and develop partially-computerized techniques applicable for each class.

Our theoretical predictions are in excellent agreement with the currently available results from the atomic parity-violating experiments for the weak charges. We plan to provide the radiative corrections for the ongoing Q-Weak experiment, which is directly

focused on the measurements of the weak charge of the proton. One-quark radiative corrections have a theoretical error associated with uncertainty of quark dynamics. In this work, we take into consideration the next to leading order effects in parity-violating electron scattering with realistic form factors for the hadronic currents, and compute corrections along with the weak charges of the proton and neutron. Thus, we are be able to avoid uncertainties associated with one-quark radiative effects by absorbing terms which are responsible for the quark dynamics into experimentally measured electromagnetic form factors. Previously, the estimates were done for the case of $\gamma - Z$ box (Ref. [8]) in the zero momentum transfer approximation. The rest of the corrections used for calculations of the weak charges of the nuclei in Ref. [8] are on the one-quark level only. We hope that modification of the couplings with model-dependent form factors and replacement of one-quark corrections with the hadronic ones developed in this thesis will contribute more clarity to tests of the Standard Model. Also, in the treatment of the infrared divergences with the hard-photon bremsstrahlung, it is more natural to consider photon emission from the proton instead of the quark. By this, we expect to reduce theoretical error up to the level of uncertainty of current electromagnetic form factor measurements. Finally, preserving the momentum transfer dependence in all types of our radiative corrections makes it easier to adopt our results to the current parity-violating experiments.

The thesis is constructed as follows. The next chapter, "Standard Model", out-

lines the general features of the Glashow-Salam-Weinberg model, focusing on electroweak interactions. The chapter briefly explains the concept of spontaneous symmetry breaking and corresponding gauge theories. It also lists the Feynman rules used as a starting point for our calculations. Special attention is paid to the regularization, tensor decomposition, and tensor reduction methods. Three selected types of regularization schemes are explained (Pauli-Villars, lattice, and dimensional regularization (DR)), and our choice for DR scheme is justified.

The equivalence at the one-loop level of our chosen method, Constrained Differential Renormalization (CDR), to regularization by dimensional reduction is explained in Chapter 3. This chapter also lists four rules for the Constrained Differential Renormalization, allowing us to renormalize any one-loop Feynman graph. A set of Ward-Takahashi identities which simplifies our work by reducing the number of independent renormalization constants is given. Chapter 3 also shows the relation of the renormalized parameters to the bare parameters, and the counterterms chosen in the on-shell renormalization scheme in the 't Hooft-Feynman gauge.

Chapter 4, "Radiative Effects", is the most important part of this work. It starts with expressions for realistic Pauli and Dirac couplings in terms of fermion weak and electric charges, and the definition and classification of one-loop radiative corrections. After that, a complete analytical example for the $\{\gamma - Z\}$ box type of correction for electron-proton scattering is considered. The key idea here is to avoid uncertainties

associated with one-quark radiative effects by absorbing terms which are responsible for the quark dynamics into experimentally measured electromagnetic form factors. The numerical results are compared with Ref. [9]. Parts 4.5 and 4.6 give computational details for the self-energy graphs and vertex correction graphs, respectively.

Chapter 5 is dedicated to the soft- and hard-photon bremsstrahlung effects. The proper account for these effects allows us to achieve final results that are free both of infrared divergences and a logarithmic dependence on the detector's photon acceptance parameter. Again, when computing hard-photon bremsstrahlung terms for electron-proton scattering, we replace the unknown quark dynamics by the measured set of form factors. Using the monopole approximation, we modify general electroweak couplings by inserting appropriate form factors directly into the vertices and construct a HPB factor as a function of Mandelstam invariants. For the several selected experiments, SAMPLE [10, 11], HAPPEX [12], G0 [13], A4 [14], and Q-Weak [15], we provide a complete set of numerical results for one-loop electron-nucleon radiative corrections. Although a very valuable result on its own, the radiative corrections for electron-proton scattering are considered only as a numerical example here. Our work on bremsstrahlung effects is methodological, and the same technique can be expanded to many other processes.

Chapter 6, "Discussion and Analysis", shows how the methods described above for electron-nucleon scattering can be applied to calculations of the weak charges

of nuclei. Several numerical results are listed, and found to be in good agreement with the current experimental data. Some directions for the improvement of our computational model which can be pursued in the near future are discussed.

2 Standard Model

The Glashow-Salam-Weinberg model [16], originally developed for leptons, has become the "Standard Model" of electroweak interactions after being successfully extended to the hadronic sector by incorporating the concept of Cabbibo-Kobayashi-Maskawa mixing. The Standard Model is the most comprehensive formulation of a theory of the unified electroweak interaction at present [17]. It is theoretically consistent and in agreement with all known phenomena of electroweak origin.

The Standard Model asserts that the material in the universe is made up of elementary fermions interacting through fields, of which they are the sources. The elementary fermions of the Standard Model are of two types: leptons and quarks. The particles associated with the interaction fields are bosons. Out of four types of interaction fields, the Standard Model excludes the gravitational field from consideration . The quanta of the electromagnetic interaction field between electrically charged fermions are the massless photons. The quanta of the weak interaction fields between fermions are the charged W+ and W- bosons and the neutral Z boson, discovered at CERN in 1983. Since these carry mass, the weak interaction is short ranged. The quanta of the strong interaction field, the gluons, have zero mass, and, like photons might be expected to have infinite range. However, unlike the electromagnetic field, the gluon fields are confining.

The Standard Model, like the QED it contains, is a theory of interacting fields,

whose construction has been guided by principles of symmetry. Some of the symmetries are not exact because of the different quark masses and different quark charges. The symmetry breaking due to quark mass differences precedes over the electromagnetic.

The electroweak Standard Model is a non-Abelian gauge theory based on the gauge group $SU(2) \times U(1)$, where the ideas of Yang-Mills theories, isospin invariance, spontaneous symmetry breaking, and Higgs mechanism merge in one common concept. The renormalizability of this class of theories was proven by 't Hooft in 1971 [18]. It gives the possibility to perform perturbative calculations for measurable quantities order by order, using a few input parameters. The input parameters themselves cannot be predicted but have to be taken from appropriate experiments.

The renormalizability makes it possible to calculate higher order quantum effects (i.e. radiative corrections) to the processes accessible by experimental facilities. Such processes include the weak decays of particles, neutrino-lepton and neutrino-nucleon scattering, electron-nucleon scattering, and electron-positron annihilation. If hadrons[2] are involved, the basic electroweak processes are considered to be the corresponding subreactions at the level of quarks as their constituents. Thus, these kind of fundamental reactions are all a type of 4-fermion process.

Electroweak processes between fermions can essentially be described with the help

---

[2] A hadron is a strongly interacting composite particle which either a fermion (baryon) or boson (meson).

of three input parameters, besides the masses of the fermions themselves and CKM mixing angles: the non-Abelian $SU(2)$ gauge coupling constant g_2, Abelian $U(1)$ coupling g_1, and the Higgs field vacuum expectation value v. This set can be replaced by any other set of three independent parameters, having theoretical relations to the previous set. Since the input parameters eventually have to be taken from experiment, it is practical to choose a set of more or less well measured quantities.

One of the examples would be [19]:

- the fine structure constant $\alpha = 1/137.03599976(50)$

- the Fermi coupling constant $G_\mu = 1.16639(1) \times 10^{-5} \ GeV^{-2}$

- the Weinberg mixing angle $\sin^2 \theta_W = 0.23113(15)$ (Z-pole, $\overline{MS}$ renormalization).

Another possible choice of parameters could include the masses of $W^\pm$ and Z bosons:

$$M_W^2 = \frac{\pi \alpha}{\sqrt{2} G_\mu \sin^2 \theta_W} \tag{1}$$

$$\frac{M_W^2}{M_Z^2} = 1 - \sin^2 \theta_W \tag{2}$$

2.1 Electroweak Lagrangian: Weinberg-Salam model

The lowest order description of a 4-fermion process starts with the classical Lagrangian. According to the general principles of constructing a gauge invariant field theory with a spontaneous symmetry breaking mechanism, the electroweak classical

Lagrangian consists of the following gauge, Higgs, and fermion parts [17]:

$$L_{classical} = L_{gauge} + L_{Higgs} + L_{fermion}. \tag{3}$$

The gauge Lagrangian L_{gauge} formed from the isotriplet of vector fields $\overrightarrow{W_\mu} = (W_\mu^1, W_\mu^2, W_\mu^3)$ (we will use notation W_μ^a, $a = 1, 2, 3$) and the isosinglet vector field B_μ transforming under a gauge transformation according to the adjoint representation of the gauge group $SU(2) \times U(1)$, and leading to the field strength tensors

$$W_{\mu\nu}^a = \partial_\mu W_\nu^a - \partial_\nu W_\mu^a - g_2 \epsilon^{abc} W_\mu^b W_\nu^c, \tag{4}$$

$$B_{\mu\nu} = \partial_\mu B_\nu - \partial_\nu B_\mu. \tag{5}$$

Using the field tensors Eq. (4) and (5), we can form the pure gauge field Lagrangian:

$$L_{gauge} = -\frac{1}{4} W_{\mu\nu}^a W^{\mu\nu,a} - \frac{1}{4} B_{\mu\nu} B^{\mu\nu}. \tag{6}$$

Now let us consider the Higgs field components.

The electric charge operator Q is built from the generators $\overrightarrow{T}$ of the weak isospin and the weak hypercharge Y:

$$Q = T_{w3} + \frac{Y}{2}. \tag{7}$$

T_{w3} is assigned a quantum number of $+\frac{1}{2}(-\frac{1}{2})$ for the upper (lower) component of left-handed fermion doublets of Table 1 and zero for all right-handed fermions.

Quarks	$q_L \equiv$	$\begin{pmatrix} u \\ d \end{pmatrix}_L$ up down	$\begin{pmatrix} c \\ s \end{pmatrix}_L$ charm strange	$\begin{pmatrix} t \\ b \end{pmatrix}_L$ top bottom
	$q_R \equiv$	$u_R, \; d_R$	$c_R, \; s_R$	$t_R, \; b_R$
Leptons	$l_L \equiv$	$\begin{pmatrix} \nu_e \\ e \end{pmatrix}_L$ $e-$neutrino electron	$\begin{pmatrix} \nu_\mu \\ \mu \end{pmatrix}_L$ $\mu-$neutrino muon	$\begin{pmatrix} \nu_\tau \\ \tau \end{pmatrix}_L$ $\tau-$neutrino tau
	$l_R \equiv$	e_R	μ_R	τ_R

Table 1: Fermions of the Standard Model.

2.2 Spontaneous Symmetry Breaking

Mass generation for fermions and gauge bosons proceeds by means of spontaneous breaking of the $SU(2) \times U(1)$ symmetry [20]. Due to the presence of $SU(2)$, a non-Abelian group, self-interactions occur between the gauge bosons. The corresponding field tensors yield the gauge-kinetic Lagrangian.

We shall only know for sure what breaks the electroweak symmetry when we can see the scattering of W's and Z's at very high energies, of the order of 1 TeV. This should be possible at the LHC – the Large Hadron Collider, expected to operate at CERN in the first decade of the this millennium.

For spontaneous breaking of the $SU(2) \times U(1)$ symmetry leaving the electromagnetic gauge subgroup $U(1)$ unbroken, a single complex scalar doublet field with hyper

charge $Y = 1$

$$\Phi(x) = \begin{pmatrix} \phi^+(x) \\ \phi^0(x) \end{pmatrix} \tag{8}$$

is coupled to the gauge fields

$$L_{Higgs} = (D_\mu \Phi)^* (D^\mu \Phi) - V(\Phi) \tag{9}$$

with the covariant derivative

$$D_\mu = \partial_\mu - i g_2 T_a W_\mu^a + i \frac{g_1}{2} B_\mu. \tag{10}$$

The Higgs field self-interaction is constructed in a way that it gives rise to spontaneous symmetry breaking:

$$V(\Phi) = -\mu^2 \Phi^+ \Phi + \lambda (\Phi^+ \Phi)^2. \tag{11}$$

Here, coefficients μ and λ are related to the non-vanishing vacuum expectation value v as

$$v = \frac{\mu}{\sqrt{\lambda}}. \tag{12}$$

Using Eq. (12), let us re-write Eq. (8) in the following way:

$$\Phi(x) = \begin{pmatrix} \phi^+(x) \\ (v + H(x) + i\chi(x))/\sqrt{2} \end{pmatrix},$$

where the components ϕ^+, H and χ now have zero vacuum expectation values.

The real component $H(x)$ describes a physical neutral scalar particle with mass

$$M_H = \mu, \tag{13}$$

12

i.e. Higgs boson, which has so far escaped experimental detection at present colliders. This non-observation allows one to set a lower bound of $M_H > 114.3$ GeV [19].

At the European Laboratory for Particle Physics (CERN) in Geneva [21], a new particle accelerator, the Large Hadron Collider (LHC) is presently being constructed. In the year 2007 beams of protons are expected to collide at a center of mass energy of 14 TeV. In parallel to the accelerator two general purpose detectors, ATLAS and CMS, are being constructed to investigate proton-proton collisions in the new energy domain and to study fundamental questions of particle physics. The ATLAS experiment will be capable of detecting the Higgs boson with a high significance ($> 5\sigma$) in the mass range from 100 GeV to 1 TeV.

The Higgs field components have cubic and quartic self couplings following from V, and couplings to the gauge fields via the kinetic term of Eq. (9). Yukawa couplings give masses to the charged fermions, although the values of these masses are not specified by the Standard Model.

The left-handed fermion fields of each quark and lepton family are grouped into $SU(2)$ doublets

$$\psi_j^L = \begin{pmatrix} \psi_{j+}^L \\ \psi_{j-}^L \end{pmatrix}, \tag{14}$$

where j is the doublet index and $+/-$ refers to the component index ($\sigma = \pm$). The right-handed fields form singlets:

$$\psi_j^R = \psi_{j\sigma}^R \tag{15}$$

13

The left-handed fermion doublets and right-handed fermion singlets, included into our calculations, are listed in the Table 1. Each left and right-handed multiplet is an eigenstate of the weak hypercharge Y according to Eq. (7). The covariant derivative (see Eq. (10))

$$D_\mu = \partial_\mu - ig_2 T_a W_\mu^a + ig_1 \frac{Y}{2} B_\mu \tag{16}$$

induces the fermion-gauge field interaction.

The interaction with the Higgs field is expressed in terms of Yukawa couplings:

$$L_{fermion} = \sum_{j,\sigma} \left\{ \psi_j^L i\gamma^\mu D_\mu \psi_j^L + \psi_{j,\sigma}^R i\gamma^\mu D_\mu \psi_{j,\sigma}^R \right\} + L_{Yukawa} \, , \tag{17}$$

with

$$L_{Yukawa} = -g_l(\overline{\nu}_L \phi^+ l_R + \overline{l}_R \phi^- \nu_L + \overline{l}_L \phi^0 l_R + \overline{l}_R \phi^{0*} l_L). \tag{18}$$

Here, ϕ^- denotes the adjoint of ϕ^+. The Yukawa coupling g_l constants are directly related to the masses of the charged fermions as will be specified later. For one family of leptons and quarks only (let's say u and d) and neglecting quark mixing, Eq. (18) will look as follows:

$$
\begin{aligned}
L_{Yukawa} \;\; = \;\; & -g_d(\overline{u}_L \phi^+ d_R + \overline{d}_R \phi^- u_L + \overline{d}_L \phi^0 d_R + \overline{d}_R \phi^{0*} d_L) \\
& -g_u(\overline{u}_R \phi^+ d_L + \overline{d}_L \phi^- u_R + \overline{u}_R \phi^0 u_L + \overline{u}_L \phi^{0*} u_R)
\end{aligned}
\tag{19}
$$

According to the expressions above, the Standard Model has included parameters

$$\mu^2, \; \lambda, \; g_1, \; g_2, \; g_{j\sigma} \tag{20}$$

14

i.e. two parameters coming from the Higgs self-interaction Eq. (11) μ^2 and λ (which are positive but otherwise arbitrary), gauge couplings g_1 and g_2, and Yukawa coupling constants $g_{j\sigma}$. None of them is physical and can be measured directly, so we have to find a way to replace the original set Eq. (20) by the set of some physical, measurable quantities.

The symmetry is manifested in terms of fields W_μ^a, B_μ. The gauge invariant Higgs gauge field interaction in the kinetic part of Eq. (9) leads to mass terms for the vector bosons in the non-diagonal form

$$2 \left(\frac{g_2}{4}v\right)^2 (W_1^2 + W_2^2) + \frac{v^2}{8}(W_\mu^3, B_\mu) \begin{pmatrix} g_2^2 & -g_1 g_2 \\ -g_1 g_2 & g_2^2 \end{pmatrix} \begin{pmatrix} W_\mu^3 \\ B_\mu \end{pmatrix}. \tag{21}$$

Let us now transform W_μ^a, B_μ to the physical fields $W_\mu^\pm$ and Z_μ, A_μ :

$$W_\mu^\pm = \frac{1}{\sqrt{2}}(W_\mu^1 \mp i W_\mu^2) \tag{22}$$

$$Z_\mu = \cos\theta_W W_\mu^3 - \sin\theta_W B_\mu \tag{23}$$

$$A_\mu = \sin\theta_W W_\mu^3 + \cos\theta_W B_\mu$$

where θ_W is called the Weinberg or weak mixing angle (although Glashow was the first to introduce the idea). The $SU(2)_L \times U(1)_Y$ proposal made by Glashow in 1961 was extended to accommodate massive vector bosons by Weinberg (1967) and Salam (1968). It is important to remember that $\sin\theta_W$ is a scheme dependent parameter, i.e. its value depends on the renormalization scheme used.

In Eq. (23), A_μ is the regular electric (photon) field which is massless and couples to the electron via the electric charge $e = \sqrt{4\pi\alpha}$. $W_\mu^\pm$ and Z_μ describe two charged $W^\pm$ and one neutral Z heavy vector bosons.

In these fields the mass term Eq. (21) is diagonal and has the form

$$M_W^2 W_\mu^+ W^{\mu-} + \frac{1}{2}(A_\mu, Z_\mu)\begin{pmatrix} 0 & 0 \\ 0 & M_Z^2 \end{pmatrix}\begin{pmatrix} A^\mu \\ Z^\mu \end{pmatrix} \tag{24}$$

with

$$\begin{aligned} M_W &= \frac{1}{2}g_2 v \\ M_Z &= \frac{1}{2}v\sqrt{g_1^2 + g_2^2} \end{aligned} \tag{25}$$

if the mixing angle in Eq. (23) is chosen as

$$\cos\theta_W = \frac{M_W}{M_Z} = \frac{g_2}{\sqrt{g_1^2 + g_2^2}} \tag{26}$$

The electric charge e can be expressed in terms of the gauge couplings in the following way

$$e = \frac{g_1 g_2}{\sqrt{g_1^2 + g_2^2}} \tag{27}$$

or

$$g_1 = \frac{e}{\cos\theta_W}, \quad g_2 = \frac{e}{\sin\theta_W}. \tag{28}$$

The fermion masses can be obtained from the Yukawa coupling terms Eq. (19) as

$$m_{j\sigma} = g_{j\sigma}\frac{v}{\sqrt{2}}.$$

16

Quantity	Value	Quantity	Value
m_u	47 MeV	m_e	0.51100 MeV
m_d	47 MeV	m_μ	105.66 MeV
m_s	150 MeV	m_τ	1777.0 MeV
m_c	1.25 GeV	M_Z	91.1882 GeV
m_b	4.2 GeV	M_W	80.419 GeV
m_t	174.3 GeV	M_H	100 GeV

Table 2: Standard Model parameters used in this calculation. Here, light quark masses are calculated from the fit presented in the subsection "Self-Energy Graphs". Other parameters are taken from Ref. [19].

Thus, instead of the original set of non-physical parameters Eq. (20), we have the equivalent set where every parameter can be measured directly:

$$m_{j\sigma}, \ M_W, \ M_Z, \ M_H, \ e \tag{29}$$

The values used in this work are summarized in the adjacent table (Table 2).

The quark mass eigenstates are not the same as the weak eigenstates, and the matrix relating these bases is called the Cabibbo-Kobayashi-Maskawa (CKM) matrix, or the quark mixing matrix $\mathbb{V}$. Its matrix elements are not predicted by the Standard Model and must be extracted from experiment.

For three quark generations, the matrix is expressed by convention in terms of a 3×3 unitary matrix $\mathbb{V}$ operating on the lower ($\sigma-$) quarks mass eigenstates (d, s,

and b):

$$\begin{pmatrix} d' \\ s' \\ b' \end{pmatrix} = \begin{pmatrix} V_{ud} & V_{us} & V_{ub} \\ V_{cd} & V_{cs} & V_{cb} \\ V_{td} & V_{ts} & V_{tb} \end{pmatrix} \begin{pmatrix} d \\ s \\ b \end{pmatrix}, \tag{30}$$

with current experimental magnitudes [19]

$$\mathbb{V} = \begin{pmatrix} 0.9741 \text{ to } 0.9756 & 0.219 \text{ to } 0.226 & 0.0025 \text{ to } 0.0048 \\ 0.219 \text{ to } 0.226 & 0.9732 \text{ to } 0.9748 & 0.038 \text{ to } 0.044 \\ 0.004 & 0.037 \text{ to } 0.044 & 0.9990 \text{ to } 0.9993 \end{pmatrix} \tag{31}$$

For some elements the values can be obtained from the weak decays of the relevant quarks or from deep inelastic neutrino scattering. The rest are restricted using unitarity constraints. See [19] for more experimental details. We actually do not use these values directly in the evaluation of the weak charges of the nucleon. We substitute $\mathbb{V}$ by the unitary matrix there. However, in the case of the one-quark radiative corrections supplementing the Hard-Photon Bremsstrahlung effects, the parametrization, involving the four angles θ_1, θ_2, θ_3, and δ, was used:

$$\begin{pmatrix} d' \\ s' \\ b' \end{pmatrix} = \begin{pmatrix} c_1 & -s_1 c_3 & -s_1 s_3 \\ s_1 c_2 & c_1 c_2 c_3 - s_2 s_3 e^{i\delta} & c_1 c_2 s_3 + s_2 c_3 e^{i\delta} \\ s_1 s_2 & c_1 s_2 c_3 + c_2 s_3 e^{i\delta} & c_1 s_2 s_3 - c_2 c_3 e^{i\delta} \end{pmatrix} \begin{pmatrix} d \\ s \\ b \end{pmatrix}, \tag{32}$$

where $c_i = \cos\theta_i$ and $s_i = \sin\theta_i$ for $i = 1, 2, 3$.

18

2.3 Gauge Theories

Gauge theories have an invariance of Lagrangian under group transformations $g(x)$ which depend on a point in the space-time manifold. Fields in such theories are divided into two classes: matter fields $\psi^i(x)$ and gauge fields $A_\mu^\alpha(x)$. The number of gauge fields is equal to the number of group generators. The gauge fields are vector fields; the matter fields can have an arbitrary Lorentz structure. Their internal components are transformed according to some representation of the group. Let $\widehat{D}(\omega)$ be an operator which performs an infinitesimal transformation of fields under the local gauge transformation. For matter fields we have

$$\hat{D}(\omega)\psi(x) = i\omega^\alpha(x)\hat{\tau}\psi(x). \tag{33}$$

For gauge fields the local gauge transformations are defined by

$$(\hat{D}(\omega)A_\mu)^\alpha(x) = f_{\beta\gamma}^\alpha A_\mu^\beta(x)\omega^\gamma(x) + \partial_\mu\omega^\alpha(x). \tag{34}$$

To construct a local invariant Lagrangian, we need to define a covariant derivative and a gauge field tensor:

$$\nabla_\mu\psi(x) = \partial_\mu\psi(x) - \hat{D}(A_\mu)\psi(x) = \partial_\mu\psi(x) - iA_\mu^\alpha(x)\hat{\tau}_\alpha\psi(x), \tag{35}$$

$$F_{\mu\nu}^\alpha(x) = \partial_\mu A_\nu^\alpha(x) - \partial_\nu A_\mu^\alpha(x) + f_{\beta\gamma}^\alpha A_\mu^\beta(x)A_\nu^\gamma(x).$$

19

In these terms, the Lagrangian of gauge theory is defined by [22] or [23] as the following:

$$L = -\frac{1}{4g^2}F^\alpha_{\mu\nu}F^{\mu\nu}_\alpha + L_m(\nabla_\mu\psi, \psi), \tag{36}$$

where g is the coupling constant and $L_m(\nabla_\mu\psi, \psi)$ is some Lagrangian of the matter fields which is invariant under the global gauge transformations. In order to quantize the gauge theory we must add to Eq.(36) a gauge fixing term and the corresponding Faddeev-Popov term [24]. The first term breaks the gauge symmetry and in this way removes the divergence of the functional integral. The general form of the gauge fixing term is

$$L_{GF}(x) = -\frac{1}{2}\sum_\alpha(\Phi^\alpha(x))^2, \tag{37}$$

where $\Phi^\alpha(x)$ corresponds to the vector boson fields of the theory.

For example, in the case of t'Hooft-Feynman gauge we use in this work, the gauge fixing terms are

$$L_{GF}(x) = -\frac{1}{2}(\partial^\mu A_\mu)^2 - \frac{1}{2}(\partial^\mu Z_\mu + M_Z Z_f)^2 - \left|\partial^\mu W^+_\mu + M_W W^+_f\right|^2, \tag{38}$$

where the squared Goldstone field terms $(M_Z Z_f)^2$ give a mass to the Goldstone particle equal to the mass of the corresponding vector boson field.

The second term we have to add to Eq.(36) improves the integration measure to provide correct predictions for gauge invariant observables. The corresponding

20

Faddeev-Popov term is

$$L_{FP}(x) = -\bar{c}_\alpha(x)(\widehat{D}(c)[\Phi^\alpha])c_\alpha(x), \tag{39}$$

where $\bar{c}_\alpha(x)$ and $c_\alpha(x)$ are the auxiliary anti-commutative fields, called the Faddeev-Popov ghosts and $\widehat{D}(c)$ defined by the Eq.(34).
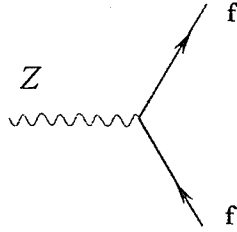
Based on the specific form of the Lagrangian, we can develop a set of Feynman rules applicable for the given physical situation. Some of Feynman rules we use most often for semi-leptonic electroweak processes are listed in the following section.

2.4 Feynman Rules

The full set of electroweak Feynman rules can found in [25]. Below are shown selected rules most commonly applied in the present work, expressed in terms of bare parameters.

$$-i\frac{g_2}{2\sqrt{2}}V_{ij}\gamma_\mu(1-\gamma^5)$$
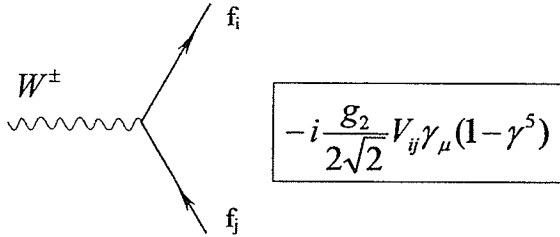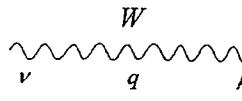
Fermion W-boson vertex.
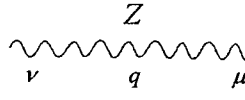
$$-i\frac{g_2}{2\cos\theta_W}\gamma_\mu(g_V^f - g_A^f\gamma^5)$$

Fermion Z-boson vertex.
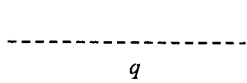
$$\frac{i}{q^2 - M_W^2}\left[-g_{\mu\nu} + \frac{q_\mu q_\nu(1-\xi_+)}{q^2 - \xi_+ M_W^2}\right]$$

W-boson propagator

$$\frac{i}{q^2 - M_Z^2}\left[-g_{\mu\nu} + \frac{q_\mu q_\nu(1-\xi_Z)}{q^2 - \xi_Z M_Z^2}\right]$$

Z-boson propagator.

$$\frac{i}{q^2 - \xi_+ M_w^2}$$

Unphysical charged Higgs propagator.

We use notation ξ for the gauge-fixing parameter. The limit of $\xi \to 0$ corresponds to the Landau gauge, whereas the limit $\xi \to \infty$ defines the unitary gauge. In the unitary gauge only physical polarization states of the incoming and outgoing $W^\pm$ and Z bosons are considered. Consequently, in the unitary gauge all ghost and Goldstone fields may be omitted.

For our case, the most convenient choice is the 't Hooft-Feynman gauge, defined

by setting all the gauge-fixing parameters to unity, $\xi = 1$. In this gauge, the lowest order propagators for the physical gauge bosons and unphysical Higgs and ghost fields have poles at either M_W^2 or M_Z^2. This condition can be maintained in higher order by a suitable renormalization of the gauge-fixing parameters [20].

As one can see from the expressions above, all boson propagators are gauge dependent. The more detailed consideration of different gauge choices is given in the next section, "Renormalization".

The reader should note that all the couplings chosen in an example above are defined for the point-like particles of the Standard Model. Much more complicated couplings applicable for the electron-nucleon vertex will be derived later.

The vector and axial-vector "charges" of the fermion, g_V^f and g_A^f, are defined as

$$g_V^f \;=\; T_{w3}^f - 2Q_f \sin^2 \theta_W, \tag{40}$$

$$g_A^f \;=\; T_{w3}^f, \tag{41}$$

The same quantities are also called "coupling constants".

More specifically, for the electron and the (u, d, s) quarks we have:

$$
\begin{aligned}
g_V^e &= -\frac{1}{2} + 2\sin^2 \theta_W, & g_A^e &= -\frac{1}{2}, \\
g_V^u &= +\frac{1}{2} - \frac{4}{3}\sin^2 \theta_W, & g_A^u &= +\frac{1}{2}, \\
g_V^{d,s} &= -\frac{1}{2} + \frac{2}{3}\sin^2 \theta_W, & g_A^{d,s} &= -\frac{1}{2}.
\end{aligned}
\tag{42}
$$

23

Let us form combinations

$$\psi_L = \frac{1 - \gamma_5}{2}\psi,$$ (43)

$$\psi_R = \frac{1 + \gamma_5}{2}\psi,$$

where "1" represents the unit 4×4 matrix. The quantities ψ_L and ψ_R are Dirac equation solutions of definite chirality, i.e. handedness. For zero mass particles, chirality coincides with helicity. The matrices

$$\varpi_{R,L} = \frac{1 \pm \gamma_5}{2}$$ (44)

are chirality projection operators. We re-define ω_L as ϖ_- , and ω_R as ϖ_+ . In this thesis, it was found more convenient to define amplitudes using chirality projection operators $\varpi_+ = \frac{1+\gamma_5}{2}$ and $\varpi_- = \frac{1-\gamma_5}{2}$ instead of explicit Dirac matrices γ_5. Thus,

$$g_V = \frac{g_L + g_R}{2},$$

and

$$g_A = \frac{g_R - g_L}{2}.$$ (45)

2.5   Coupling Constants

At a generic level, for vertex $\{F - F - V_\mu\}$ we can write

$$\{F - F - V_\mu\} \rightarrow \overline{u}_F \Gamma(F, F, V_\mu) u_F,$$ (46)

24

where $C(F, F, V_\mu)$ is a generic coupling defined from the SM Lagrangian as

$$\Gamma(F, F, V_\mu) = \left(\gamma_\mu \varpi_-, \quad \gamma_\mu \varpi_+ \right) \vec{G}_{FFV} \tag{47}$$

where $\vec{G}_{FFV}$ is a coupling matrix containing couplings of the classes up to the desired counterterm order. In the case of one-loop calculations, we restrict coupling matrices up to the first counterterm order only (zero order – tree level, first order – one-loop, etc.). We define five types of fermion-fermion-vector boson coupling matrix $\vec{G}_{FFV}$: $\vec{G}_{f,f,\gamma}$ (any fermions, photon), $\vec{G}_{f,f,Z}$ (any fermions, Z-boson), $\vec{G}_{l,l',W}$ (leptons only, charged W-boson), $\vec{G}_{q_i^{(up)}, q_j^{(down)}, W}$ (up and down type quarks only, W^--boson), and $\vec{G}_{q_i^{(down)}, q_j^{(up)}, W}$ (down and up type quarks only, W^+-boson).

Let us start with the coupling matrix $\vec{G}_{f,f,\gamma}$ (fermion-fermion-photon vertex):

$$\vec{G}_{f,f,\gamma} = ie \begin{pmatrix} -Q_f & -Q_f(\delta e + \frac{\delta Z_{\gamma\gamma}}{2} + \mathrm{Re}[\delta f_L^f]) + g_L^{l-Z} \frac{\delta Z_{Z\gamma}}{2} \\ -Q_f & -Q_f(\delta e + \frac{\delta Z_{\gamma\gamma}}{2} + \mathrm{Re}[\delta f_R^f]) + g_R^{l-Z} \frac{\delta Z_{Z\gamma}}{2} \end{pmatrix}, \tag{48}$$

where the first column represents tree level coupling and the second one one loop counterterm. Furthermore, we give a list of the generic couplings for various interactions, as well as coupling matrices up to the first order counterterm, where necessary.

The rest of the coupling matrices entering Eq. (47) have the following structure:

$$\vec{G}_{f,f,Z} = ie \begin{pmatrix} g_L^{f-Z} & g_L^{f-Z} \frac{\delta Z_{ZZ}}{2} + \delta g_L^{f-Z} - Q_f \frac{\delta Z_{\gamma Z}}{2} + g_L^{f-Z} \mathrm{Re}[\delta f_L^f] \\ g_R^{f-Z} & g_R^{f-Z} \frac{\delta Z_{ZZ}}{2} + \delta g_R^{f-Z} - Q_f \frac{\delta Z_{\gamma Z}}{2} + g_R^{f-Z} \mathrm{Re}[\delta f_R^f] \end{pmatrix}, \tag{49}$$

$$\vec{G}_{l,l',W} = ie \begin{pmatrix} \frac{1}{\sqrt{2} s_W} \\ 0 \end{pmatrix}, \tag{50}$$

25

$$\overrightarrow{G}_{q_i^{(up)}, q_j^{(down)}, W} = ie \begin{pmatrix} \frac{1}{\sqrt{2}s_W} U_{ij} \\ \\ 0 \end{pmatrix}, \tag{51}$$

$$\overrightarrow{G}_{q_i^{(down)}, q_j^{(up)}, W} = ie \begin{pmatrix} \frac{1}{\sqrt{2}s_W} U_{ij}^* \\ \\ 0 \end{pmatrix}. \tag{52}$$

Combining Eq. (47) with Eq. (48) and Eqs. (49-52), we obtain the couplings needed to construct vertex, boxes and self-energy graphs.

To construct counterterm amplitudes for self-energy graphs, generic coupling for $\Gamma\left(V_\mu\left(k_1\right), V_\nu\left(k_2\right)\right)$ has been used:

$$\Gamma\left(V_\mu\left(k_1\right), V_\nu\left(k_2\right)\right) = \begin{pmatrix} -g_{\mu\nu}\left(k_1 k_2\right) & g_{\mu\nu} & -k_{1\mu}k_{2\nu} \end{pmatrix} \overrightarrow{G}_{VV}, \tag{53}$$

where

$$\overrightarrow{G}_{ZZ} = i \begin{pmatrix} 0 & \delta Z_{ZZ} \\ 0 & m_Z^2\, \delta Z_{ZZ} + \delta m_Z^2 \\ 0 & -\delta Z_{ZZ} \end{pmatrix}, \tag{54}$$

and

$$\overrightarrow{G}_{\gamma Z} = \frac{i}{2} \begin{pmatrix} 0 & \delta Z_{\gamma Z} + \delta Z_{Z\gamma} \\ 0 & m_Z^2\, \delta Z_{\gamma Z} \\ 0 & -\delta Z_{\gamma Z} - \delta Z_{Z\gamma} \end{pmatrix}. \tag{55}$$

As an example, let us consider an electron interacting with an up-quark via $Z-$boson exchange on tree level:
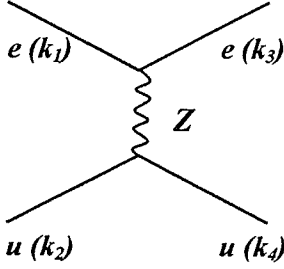
According to the Feynman rules stated above and for the momenta specified on

the diagram, we obtain the following parity-violating amplitude:

$$
\mathcal{M}^{Z-tree} = \bar{u}(k_3, m_e)\left[\frac{ie(-\frac{1}{2} + \sin^2\theta_W)\gamma_\mu\, \varpi_-}{\cos\theta_W \sin\theta_W} + \frac{ie\sin\theta_W\, \gamma_\mu\, \varpi_+}{\cos\theta_W}\right] u(k_1, m_e) \quad (56)
$$

$$
\times \bar{u}(k_4, m_u)\left[\frac{ie(\frac{1}{2} - \frac{2}{3}\sin^2\theta_W)\gamma_\nu\, \varpi_-}{\cos\theta_W \sin\theta_W} - \frac{2ie\sin\theta_W\, \gamma_\nu\, \varpi_+}{3\cos\theta_W}\right] u(k_2, m_u)
$$

$$
\times \frac{g_{\mu\nu}}{(k_4 - k_2)^2 - M_Z^2}
$$

Let us now consider the ZZ-box diagram as a simple example of a one-loop process:
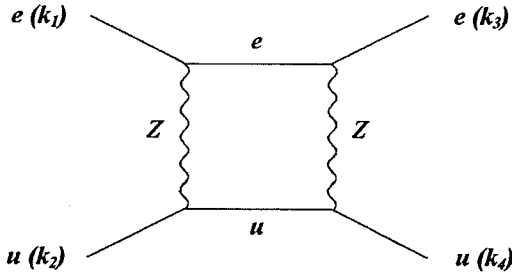
This amplitude will include four propagators (last line) and require integration

over 4-dimensional momenta in the loop:

$$
\mathcal{M}^{\{Z-Z\}box} = \frac{i}{16\pi^4}\int d^4q\; \bar{u}(k_3, m_e)\left[\frac{ie(-\frac{1}{2} + \sin^2\theta_W)\gamma_\mu\, \varpi_-}{\cos\theta_W \sin\theta_W} + \frac{ie\sin\theta_W\, \gamma_\mu\, \varpi_+}{\cos\theta_W}\right]
$$

$$
\times (m_e + (\slashed{k}_3 + \slashed{k}_4 - \slashed{k}_2 - \slashed{q}))
$$

27

$$\times \left[\frac{ie(-\frac{1}{2} + \sin^2\theta_W)\gamma_\nu\,\varpi_-}{\cos\theta_W \sin\theta_W} + \frac{ie\sin\theta_W\,\gamma_\nu\,\varpi_+}{\cos\theta_W} \right] u(k_1, m_e)$$

$$\times\overline{u}(k_4, m_u) \left[\frac{ie(\frac{1}{2} - \frac{2}{3}\sin^2\theta_W)\gamma_\sigma\,\varpi_-}{\cos\theta_W \sin\theta_W} - \frac{2ie\sin\theta_W\,\gamma_\sigma\,\varpi_+}{3\cos\theta_W} \right] (m_u + (\not{k}_2 + \not{q})) \quad (57)$$

$$\times \left[\frac{ie(\frac{1}{2} - \frac{2}{3}\sin^2\theta_W)\gamma_\rho\,\varpi_-}{\cos\theta_W \sin\theta_W} - \frac{2ie\sin\theta_W\,\gamma_\rho\,\varpi_+}{3\cos\theta_W} \right] u(k_2, m_u)$$

$$\times \frac{1}{q^2 - M_Z^2} \cdot \frac{1}{(k_2 + q)^2 - m_u^2} \cdot \frac{1}{(k_2 + q - k_4)^2 - M_Z^2} \cdot \frac{g_{\nu\rho}g_{\mu\sigma}}{(k_2 + q - k_4 - k_3)^2 - m_e^2}$$

The task of constructing an amplitude according to the Feynman rules is relatively straightforward. The amplitude shown above is not divergent. The integration will require more of an effort if the amplitude is divergent. The vacuum polarization tensor, entering all self-energies and triangles, is divergent due to singular high momentum behavior. Generally speaking, we can tell whether the integral diverges by simply counting the powers of q in a given Feynman graph. Each fermion propagator contributes q^{-1}, each boson propagator contributes q^{-2}, each loop contributes a loop integration with q^4, and each vertex with n derivatives contributes at most n powers to q. If, as a result, you have q^m and $m \geq 0$, the graph diverges. The methods of regularization and renormalization applicable here are discussed in the next section.

2.6 Regularization

To interpret the behavior of the divergent integrals, a wide variety of regularization schemes have been developed over the decades, each with its own advantages and disadvantages. Let us consider three selected types: Pauli-Villars, Lattice, and

Dimensional regularizations.

In the Pauli-Villars regularization scheme, we cut off the integrals by assuming the existence of a fictitious particle of mass M. The propagator becomes modified by

$$\frac{1}{q^2 - m^2} - \frac{1}{q^2 - M^2} = \frac{m^2 - M^2}{(q^2 - m^2)(q^2 - M^2)},$$

where relative minus sign means that the new particle is a ghost, i.e. it has negative norm. The propagator now behaves as $1/q^4$, rendering all graphs finite. Then, we make M^2 go to infinity so that the unphysical fermion decouples from theory. The Pauli-Villar scheme preserves local gauge invariance and Ward identities in QED, but they get broken for higher groups [26].

Lattice regularization is the most widely used regularization scheme in QCD for non-perturbative calculations. Combined with Monte-Carlo techniques, it makes it possible to extract qualitative and even some quantitative information from QCD. Here, we assume that space-time is actually a set of discrete points arranged in some kind of hyper cubical array. The lattice spacing then serves as the cutoff for the space-time integral. Because this method is defined in Euclidean space, it allows to calculate only the "static" properties of QCD.

In this work, we choose to employ the method of dimensional regularization. According to this method, we consider the vacuum polarization tensor as the four-dimensional limit of a function defined in d dimensions. To follow the standard convention, let us introduce the variable $\varepsilon = 4 - d$ for continuation away from the

physical space-time dimension. Now, mathematical operations like summing over Lorentz indices or evaluating loop integrals, can be carried out in d dimensions, with the results expressed as an expansion of ε. The divergences from loop integrals will take the form of poles in ε. The last step is to continue the results back to $d = 4$.

Although in the dimensional regularization procedure we define our functions in d dimensions, all physical parameters entering the theory must retain the original dimensionality. To maintain the units corresponding to $d = 4$ while dimensionally regularizing Feynman integrals, we introduce an arbitrary quantity μ having dimension of mass. The parameter μ allows us to modify the integration measure over momentum as

$$\int \frac{d^4p}{(2\pi)^4} \rightarrow \mu^{\varepsilon} \int \frac{d^dp}{(2\pi)^d}. \tag{58}$$

Of course, the arbitrary mass parameter μ shall not change the relationships between physical observables. Indeed, it does not, as it serves only in the intermediate parts of calculations.

2.7   Tensor Decomposition

In the CDR scheme, Feynman diagrams are considered completely in four dimensions. Thereafter, the reduction of singular basic functions (products of propagators and their derivatives) has been renormalized into the sum of "regular" ones by implementing a set of rules in such a way that Ward identities are satisfied. It was

30
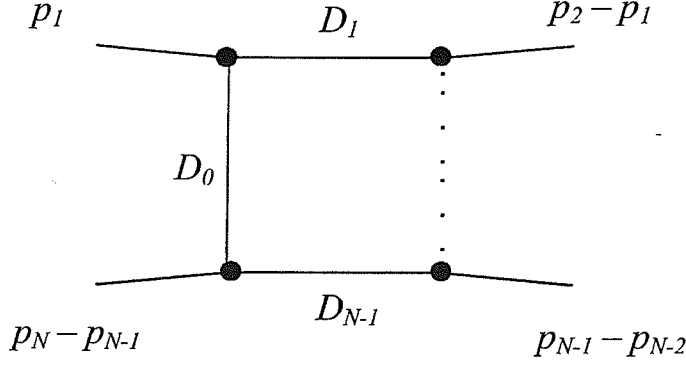
Figure 1: General form of one-loop diagram with N propagators.

proven in Ref. [27] that CDR is equivalent at the one-loop level to regularization by dimensional reduction [28], after taking the Fourier transform of the basic renormalized functions into momentum space. This last approach corresponds to a modified dimensional regularization, where one-loop integrals are considered in d dimensions, but all the tensors and spinors are kept 4-dimensional [28]. To preserve gauge invariance in dimensional reduction, one should use $\widehat{g}_{\mu\nu}$ $\left(\widehat{g}_{\mu}^{\mu} = d\right)$ with $g_{\mu\nu}\widehat{g}^{\nu\rho} = \widehat{g}_{\mu}^{\rho}$ for the tensor decomposition.

In dimensional regularization, the general structure of one-loop tensor integral can be written in the form:

$$J_{\mu_1\ldots\mu_P}^N = \frac{(2\pi\mu)^{4-d}}{i\pi^2} \int d^d q \, \frac{q_{\mu_1}\cdots q_{\mu_P}}{D_0 D_1 \cdot\cdot D_{N-1}}. \tag{59}$$

which corresponds to the one-loop diagram shown in Fig. (1).

Unlike at Born level, where all momenta running along the internal lines of a

Feynman diagram are fixed by the overall momentum conservation, at one loop level there remains one momentum q which must be integrated over. The (q_μ)'s in the numerator arise from fermion propagators or from vertices that correspond to terms with derivatives in the Lagrangian.

The denominators of Eq. (59) arise from the propagators running in the loop:

$$
\begin{aligned}
D_0 &= q^2 - m_0^2, & &(60) \\
D_i &= (q + p_i^2) - m_i^2, \quad i = 1, ..., N-1.
\end{aligned}
$$

P, the number of (q_μ)'s in the numerator, determines the Lorentz tensor structure of the whole integral, e.g. $P = 0$ denotes a scalar integral, $P = 1$ a vector integral, etc.

To have the proper units for the integral in d space–time dimensions, we have to introduce an arbitrary reference mass μ. Basically, μ means the regularization scale parameter of dimensional reduction, which is related to the CDR renormalization scale by $\log\left(\bar{M}^2\right) = \log\left(\mu^2\right) + 2$. The final renormalized amplitude will be independent of μ, of course.

The integrals with a tensor structure can be reduced to linear combinations of scalar integrals. Because the integrals Eq.(59) are symmetric, Lorentz covariant tensors (i.e. they transform in a definite way under Lorentz transformations), they can be decomposed into a tensor basis formed from the linearly independent external momenta p_i and the metric tensor $g_{\mu\nu}$. The choice of this basis is not unique; the basis

32

can be chosen such that the coefficients are totally symmetric in their indices [29].
Using the Passarino-Veltman [30] method for tensor decomposition, we can represent
the above integral as the linear combination of tensor coefficient functions, which
reads explicitly

$$B'_\mu = k_{1\mu}B_1,$$

$$B'_{\mu\nu} = \widehat{g}_{\mu\nu}B_{00} + k_{1\mu}k_{1\nu}B_{11},$$

$$C'_\mu = \sum_{i=1}^{2} k_{i\mu}C_i,$$

$$C'_{\mu\nu} = \widehat{g}_{\mu\nu}C_{00} + \sum_{i,j=1}^{2} k_{i\mu}k_{j\nu}C_{ij},$$

$$C'_{\mu\nu\rho} = \sum_{i=1}^{2} \left(\widehat{g}_{\mu\nu}k_{i\rho} + \widehat{g}_{\nu\rho}k_{i\mu} + \widehat{g}_{\mu\rho}k_{i\nu}\right)C_{00i} + \sum_{i,j,\xi=1}^{2} k_{i\mu}k_{j\nu}k_{\xi\rho}C_{ij\xi},$$

$$D'_\mu = \sum_{i=1}^{3} k_{i\mu}D_i, \tag{61}$$

$$D'_{\mu\nu} = \widehat{g}_{\mu\nu}D_{00} + \sum_{i,j=1}^{3} k_{i\mu}k_{j\nu}D_{ij},$$

$$D'_{\mu\nu\rho} = \sum_{i=1}^{3} \left(\widehat{g}_{\mu\nu} k_{i\rho} + \widehat{g}_{\nu\rho} k_{i\mu} + \widehat{g}_{\mu\rho} k_{i\nu} \right) D_{00i} + \sum_{i,j,\xi=1}^{2} k_{i\mu} k_{j\nu} k_{\xi\rho} D_{ij\xi},$$

$$D'_{\mu\nu\rho\sigma} = \left(\widehat{g}_{\mu\nu} \widehat{g}_{\rho\sigma} + \widehat{g}_{\mu\rho} \widehat{g}_{\nu\sigma} + \widehat{g}_{\mu\sigma} \widehat{g}_{\nu\rho} \right) D_{0000}$$

$$+ \sum_{i,j=1}^{3} \left(\begin{array}{c} \widehat{g}_{\mu\nu} k_{i\rho} k_{j\sigma} + \widehat{g}_{\nu\rho} k_{i\mu} k_{j\sigma} + \widehat{g}_{\mu\rho} k_{i\nu} k_{j\sigma} \\ \\ + \widehat{g}_{\mu\sigma} k_{i\nu} k_{j\rho} + \widehat{g}_{\nu\sigma} k_{i\mu} k_{j\rho} + \widehat{g}_{\rho\sigma} k_{i\mu} k_{j\nu} \end{array} \right) D_{00ij}$$

$$+ \sum_{i,j,\xi,m=1}^{3} k_{i\mu} k_{j\nu} k_{\xi\rho} k_{m\sigma} D_{ij\xi m},$$

Here (B', C', D') mean two, three, and four point tensor integrals, with two, three, and four propagators, respectively. The rank of the above tensors is equal to the number of integrable momenta $(q_{\mu_1} q_{\mu_2} \ldots q_{\mu_P})$ in the numerator of Eq. (59). The standard notation is A for $N = 1$, B for $N = 2$, C for $N = 3$, etc. The scalar integrals are denoted by a subscripted zero: A_0, B_0, etc. In four dimensions, only A_0 and B_0 are divergent; they depend, in dimensional regularization, on the scale parameter μ. As we are dealing with one-loop diagrams only, the maximum N we can have is 4. Thus, the Passarino-Veltman approach deals with two, three, and four point tensor integrals with two, three, and four propagators, respectively.

34

2.8 Tensor Reduction

To reduce the number of Lorentz indices, we contract with p_k^μ:

$$
\begin{aligned}
2q_\mu p_k^\mu &= (q+p_k)^2 - q^2 - p_k^2 \tag{62} \\[1em]
&= [(q+p_k)^2 - m_k^2] - [q^2 - m_0^2] - p_k{}^2 + m_k^2 - m_0^2 \\[1em]
&= D_k - D_0 - p_k^2 + m_k^2 - m_0^2 \\[1em]
&= D_k - D_0 - f_k \,,
\end{aligned}
$$

where

$$
f_k = p_k^2 - m_k^2 + m_0^2.
$$

Thus,

$$
\begin{aligned}
p_k^{\mu_P} J^N_{\mu_1...\mu_P} &= \frac{(2\pi\mu)^{4-d}}{2i\pi^2} \int d^d q \, \frac{q_{\mu_1} \cdots q_{\mu_{P-1}}(D_k - D_0 - f_k)}{D_0 D_1 \cdot \cdot D_{N-1}} \tag{63} \\[1em]
&= \frac{1}{2}(J^{N-1,\not{k}}_{\mu_1...\mu_{P-1}} - J^{N-1,\not{0}}_{\mu_1...\mu_{P-1}} - f_k J^N_{\mu_1...\mu_{P-1}}),
\end{aligned}
$$

where $\not{k}$ indicated that D_k has been cancelled.

If we contract with $g^{\mu\nu}$,

$$
g^{\mu\nu} q_\mu q_\nu = (q^2 - m_0^2) + m_0^2 = D_0 + m_0^2. \tag{64}
$$

and

$$
\begin{aligned}
g^{\mu_{P-1}\mu_P} J^N_{\mu_1...\mu_P} &= \frac{(2\pi\mu)^{4-d}}{i\pi^2} \int d^d q \, \frac{q_{\mu_1} \cdots q_{\mu_{P-1}}(D_0 + m_0^2)}{D_0 D_1 \cdot \cdot D_{N-1}} \tag{65} \\[1em]
&= J^{N-1,\not{0}}_{\mu_1...\mu_{P-1}\mu_{P-2}} - m_0^2 J^N_{\mu_1...\mu_{P-1}\mu_{P-2}}.
\end{aligned}
$$

Let us introduce notations

$$R^{N,k}_{\mu_1\ldots\mu_{P-1}} \equiv \frac{1}{2}(J^{N-1,\not{k}}_{\mu_1\ldots\mu_{P-1}} - J^{N-1,0'}_{\mu_1\ldots\mu_{P-1}} - f_k J^{N}_{\mu_1\ldots\mu_{P-1}}), \tag{66}$$

$$R^{N,00}_{\mu_1\ldots\mu_{P-2}} \equiv J^{N-1,0'}_{\mu_1\ldots\mu_{P-1}\mu_{P-2}} - m_0^2 J^{N}_{\mu_1\ldots\mu_{P-1}\mu_{P-2}}.$$

We have now N linear equations relating the rank P tensors with rank $P-1$ and $P-2$ tensors:

$$R^{N,k}_{\mu_1\ldots\mu_{P-1}} = p_k^{\mu_P} J^{N}_{\mu_1\ldots\mu_P}, \tag{67}$$

$$R^{N,00}_{\mu_1\ldots\mu_2} = g^{\mu_{P-1}\mu_P} J^{N}_{\mu_1\ldots\mu_P},$$

with k running from 1 to $N-1$. Substituting Eq. (61) in the above yields linear equations relating the coefficient functions $J^{N}_{i_1\ldots i_P}$, $R^{N,k}_{i_1\ldots i_{P-1}}$ and $R^{N,00}_{i_1\ldots i_{P-2}}$, which have to be solved for $J^{N}_{i_1\ldots i_P}$. In d dimensions, the solutions are given by

$$J^{N}_{00i_1\ldots i_{P-2}} = \frac{1}{d+P-N-1}\left[R^{N,00}_{i_1\ldots i_{P-2}} - \sum_{k=1}^{N-1} R^{N,00}_{i_1\ldots i_{P-2}}\right], \tag{68}$$

and

$$J^{N}_{ki_1\ldots i_{P-2}} = (X_{N-1}^{-1})_{kk'}\left[R^{N,k'}_{i_1\ldots i_{P-2}} - \sum_{r=1}^{P-1} \delta_{i_r k'} J^{N}_{00i_1\ldots i_{r-1}i_{r+1}\ldots i_{P-1}}\right], \tag{69}$$

where X_{N-1} is non-singular Gram matrix:

$$X_{N-1} = \begin{pmatrix} p_1^2 & p_1 p_2 & \cdots & p_1 p_{N-1} \\ p_2 p_1 & p_2^2 & \cdots & p_1 p_{N-1} \\ \vdots & & \ddots & \vdots \\ p_{N-1}p_1 & p_{N-1}p_1 & \cdots & p_{N-1}^2 \end{pmatrix}. \tag{70}$$

This procedure of Eq. (68) - Eq. (70) can be iterated until all tensor coefficients are reduced to scalar functions.

It is worth noting here, that it is not directly possible to calculate radiative corrections for exact forward or backward scattering, because the external momenta become linearly dependent in this case, and the Gram matrix in Eq. (69) becomes singular.

3 Renormalization

Divergences found in Quantum Field Theory came from the transition to an infinite number of degrees of freedom from a finite number found in Quantum Mechanics. We have to sum continually over an infinite number of internal modes in loop integration, which leads to divergences. Not all theories are renormalizable. Renormalizability of Yang-Mills theory, proven by 't Hooft, made it possible to successfully apply Quantum Field Theory to the weak interactions in order to calculate effects beyond the tree level.

There are numerous renormalization proposals with the details varying from scheme to scheme, but they all share the same basic physical features. The divergences are absorbed into a set of "bare" physical parameters such as the coupling constants and particles masses. Those parameters are, consequently, divergent and unmeasurable. The divergences of these parameters are chosen in a way so that they cancel against the ultraviolet infinities coming from infinite classes of Feynman diagrams. After the divergences are absorbed by the bare parameters, parameters become renormalized and "dressed", i.e. physical and measurable. Here, the schematic point of view is presented. For more comprehensive descriptions, the reader is directed to Refs. [26], [29], [31], [32], and [33].

3.1 CDR Scheme

At the one-loop level, Constrained Differential Renormalization (CDR) was introduced in Ref.[34]. Standard dimensional renormalization manipulates singular objects as if they were well-defined, expresses them in terms of simple singular functions, and substitutes these by their renormalized value. In the CDR scheme, Feynman diagrams are considered completely in four dimensions. Thereafter, the reduction of singular basic functions (products of propagators and their derivatives) has been renormalized into the sum of "regular" ones by implementing a set of rules in such a way that Ward identities are satisfied. It was proven in Ref. [27] that CDR is equivalent at the one-loop level to regularization by dimensional reduction [28], after taking the Fourier transform of the basic renormalized functions into momentum space. This last approach corresponds to a modified dimensional regularization, where one-loop integrals are considered in D dimensions, but all the tensors and spinors are kept 4-dimensional [28]. To preserve gauge invariance in dimensional reduction, one should use $\widehat{g}_{\mu\nu}$ $\left(\widehat{g}_\mu^\mu = D\right)$ with $g_{\mu\nu}\widehat{g}^{\nu\rho} = \widehat{g}_\mu^\rho$ for the tensor decomposition.

If the renormalized expressions are compatible with a minimal set of consistent formal manipulations, i.e. rules, the ambiguities and arbitrary renormalization scales of DR are fixed and the resulting renormalized Green functions automatically preserve Ward identities. Ref.[34] proposes the following set of rules, allowing us to renormalize any one-loop Feynman graph:

39

3.2   Rules for CDR:

I. Differential reduction. In two steps, singular expressions are substituted by derivatives of regular ones:

a) Functions with singular behavior worse than logarithmic ($\sim x^{-4}$) are reduced to derivatives of logarithmically singular functions without introducing extra constants.

b) Logarithmically singular functions are written as derivatives of regular functions, which are solutions of the Lorentz invariant differential equation $\Box f(x) = \log(xM)^n/x^4$,

$$\left[\frac{1}{x^4}\right]^R = -\frac{1}{4}\Box\frac{\log(x^2 M^2)}{x^2},$$

$$(\Box = \partial\!\!\!/\,\,\partial\!\!\!/)$$

where M is a constant to make argument of the logarithmic function dimensionless. It has dimensions of mass, plays the role of the renormalization group scale, and is the only a constant needed for the whole process.

II. Formal integration by parts. Derivatives act formally by parts on test functions, i.e.

$$[\partial F]^R = \partial F^R,$$

where F is an arbitrary function and superscript R labels for renormalized function.

III. Delta function renormalization rule:

$$[F(x, x_1, x_2, ..., x_n)\delta(x - y)]^R = [F(x, x_1, x_2, ..., x_n)]^R \delta(x - y)$$

40

IV. Propagator equation:

$$[F(x, x_1, x_2, ..., x_n)(\Box^2 - m^2)\Delta_m(x)]^R = [F(x, x_1, x_2, ..., x_n)(-\delta(x))]^R,$$

with

$$\Delta_m(x) = \frac{1}{4\pi^2} \frac{mK_1(mx)}{x},$$

where $K_1(mx)$ is the modified Bessel function of the second kind.

Rule I and Rule II reduce the degree of singularity, connecting singular and regular expressions. The actual procedure of renormalization involves two steps:

1) express a Feynman diagram in terms of basic functions, and

2) replace the basic functions by their renormalized value.

As an example, let us consider a Feynman-like gauge, so propagators of the gauge fields are proportional to the scalar Feynman propagator. The formalism can be directly extended to general covariant gauges. Table (3) summarizes the singular basic functions for renormalizable theories in four dimensions. N stands for the number of propagators in the given Feynman graph. Rows are ordered according to the number of propagators and columns according to the degree of singularity.

It is important to distinguish basic functions with contracted and uncontracted differential operators, because contraction of Lorentz indices does not in general commute with CDR, i.e,

$$T^R[\Box] = [\delta_{\mu\nu}T[\partial_\mu\partial_\nu]]^R \neq \delta_{\mu\nu}T^R[\partial_\mu\partial_\nu].$$

41

N	logarithmic	linear	quadratic	cubic
1			$A_m[1]$	$A_m[\partial_\mu]$
2	$B_{m_1 m_2}[1]$	$B_{m_1 m_2}[\partial_\mu]$	$B_{m_1 m_2}[\square]$ $B_{m_1 m_2}[\partial_\mu \partial_\nu]$	
3	$T_{m_1 m_2 m_3}[\square]$ $T_{m_1 m_2 m_3}[\partial_\mu \partial_\nu]$	$T_{m_1 m_2 m_3}[\square \partial_\mu]$ $T_{m_1 m_2 m_3}[\partial_\mu \partial_\nu \partial_\rho]$		
4	$Q_{m_1 m_2 m_3 m_4}[\square \square]$ $Q_{m_1 m_2 m_3 m_4}[\square \partial_\mu \partial_\nu]$ $Q_{m_1 m_2 m_3 m_4}[\partial_\mu \partial_\nu \partial_\rho \partial_\sigma]$			

Table 3: Singular basic functions for renormalizable theories in four dimensions.

As the simplest example of point contraction, let us consider the renormalization of $A_m[1]$ and $B_{m_1 m_2}[1]$. For the massless case, renormalized expressions of massless one- and two-point functions are given by:

$$A^R[1] = 0$$

$$A^R[\partial_\mu] = 0$$

$$B^R[1] = -\frac{1}{64\pi^2} \square \frac{\log x^2 M^2}{x^2}$$

$$B^R[\partial_\mu] = \frac{1}{2} \partial_\mu B^R[1]$$

$$B^R[\square] = 0$$

$$B^R[\partial_\mu \partial_\nu] = \frac{1}{3}(\partial_\mu \partial_\nu - \frac{1}{4}\delta_{\mu\nu}\square)B^R[1] + \frac{1}{288\pi^2}(\partial_\mu \partial_\nu - \delta_{\mu\nu}\square)\delta(x)$$

For massive basic functions, we have to use the recurrence relations among modified Bessel functions to obtain the expressions for non-singular points. In this case,

$$
\begin{aligned}
B^R_{m_1 m_2}[1] &= \frac{1}{16\pi^4}\left[\frac{m_1 K_1(m_1 x) m_2 K_1(m_2 x)}{x^2}\right]^R \\
&= \frac{1}{32\pi^4}\frac{m_1 m_2}{m_1 + m_2}[\Box - (m_1 + m_2)^2]\frac{K_0(m_1 x)K_1(m_2 x) + K_0(m_2 x)K_1(m_1 x)}{x} \\
&\quad + \frac{1}{16\pi^2}\left(\log\frac{(2M/\gamma_E)^2}{m_1 m_2} + \frac{m_1 - m_2}{m_1 + m_2}\log\frac{m_1}{m_2}\right)\delta(x),
\end{aligned}
$$

where $\gamma_E = 1.781$ is Euler's constant. The massive one-point function $A^R_m[1]$ can be determined from $A^R[1]$ and $B^R_{m_1 m_2}$ as

$$
A^R_m[1] = \frac{1}{16\pi^2}m^2\left(1 - \log\frac{(2M/\gamma_E)^2}{m^2}\right)\delta(x).
$$

The renormalization of the remaining basic functions is obtained from $B^R_{m_1 m_2}[1]$ and $A^R_m[1]$ by recurrence relations based on Rules II-IV.

The functions listed above, including the amplitude, are defined in coordinate space. If we take the Fourier transform of the amplitude, thus expressing it in momentum space, the resulting expression will include the Passarino-Veltman many-point tensor coefficients. These are exactly the amplitudes obtained in momentum space by the dimensional reduction in on-shell renormalization. The next section will contrast and compare the CDR and dimensional regularization in on-shell renormalization.

3.3 CDR to On-Shell Connection

As was established earlier, CDR and dimensional reduction are equivalent at the one-loop level (Ref. [27]). One-loop integrals in D dimensions satisfy the relations im-

posed by the CDR rules. Once CDR has been translated into momentum space, the minimally subtracted D-dimensional tensor integrals are identical in the limit $D \to 4$ to the Fourier transforms of the corresponding renormalized basic functions of CDR. As we are free to choose the renormalization scale, a discrepancy which can arise in the initial conditions is not a problem. All the algebra outside tensor integrals has 4 dimensions in both CDR and dimensional reduction. Thus, in dimensional reduction, where it is possible to contract the 4-dimensional metric with D-dimensional integration momenta before performing the integrals, we have

$$
\begin{aligned}
g^{\mu\nu}C_{\mu\nu} &= g^{\mu\nu}(\hat{g}_{\mu\nu}C_{00} + \sum_{i,j=1}^{2} p_{i\mu}p_{j\nu}C_{ij}) = \hat{g}_{\mu}^{\mu}C_{00} + \sum_{i,j=1}^{2}(p_i p_j)C_{ij} \\
&= DC_{00} + \sum_{i,j=1}^{2}(p_i p_j)C_{ij} = 4C_{00} - \frac{1}{2} + \sum_{i,j=1}^{2}(p_i p_j)C_{ij}.
\end{aligned}
$$

The resulting contracted tensor integrals also satisfy the CDR relations. As C_{00} and C_{ij} are the same in both methods, we only need to add the extra local term, $-\frac{1}{2}$, to obtain the tensor integral C_{μ}^{μ} from $g^{\mu\nu}$ times the renormalized tensor integral $C_{\mu\nu}$ in CDR.

The results in D and 4 dimensions will differ for the electron self-energy in QED. Electron self-energy by dimensional regularization is

$$
\mathcal{M}_{d.reg.} = -\frac{e^2}{16\pi^2}[4m_e B_0(k^2, m_e^2, 0) + 2 \not{k}B_1(k^2, m_e^2, 0) + \not{k} - 2m_e],
$$

but CDR gives

$$
\mathcal{M}_{CDR} = -\frac{e^2}{16\pi^2}[4m_e B_0(k^2, m_e^2, 0) + 2 \not{k}B_1(k^2, m_e^2, 0)].
$$

44

where B_0 and B_1 are two-point functions. As a result, we chose to use the CDR idea and just add local terms, which allows us to work completely in 4 dimensions.

The most natural choice for the renormalization scheme in electroweak theory is the on-shell renormalization scheme [33]. The difference between renormalization schemes is reflected mostly by various definitions of the weak mixing angle. The on-shell scheme is the simplest conceptually, carrying the tree level relation, $\cos\theta_W = \frac{M_W}{M_Z}$, to all orders.

3.4   Ward-Takahashi Identities

Dimensional regularization preserves all properties of the theory that are independent of the dimension of space-time, such as the Ward-Takahashi identities. Actually, the Ward-Takahashi identities are required to prove the renormalizability of gauge theories. A set of Ward-Takahashi identities ([35]) also simplifies our work by reducing the number of independent renormalization constants. Because we have introduced more renormalization constants than physical parameters, we are free to fix the extra constants by requiring the residue to be equal to one for a corresponding number of propagators. Traditionally, these residue conditions are applied for the photon and the charged lepton propagators.

The renormalization conditions include the on-shell subtraction of the self energies which makes the particle content of the theory evident ([17]). Figure (2) gives an example of graphical representation of the on-shell subtraction conditions.

$$Re \quad \underset{W,\,Z \qquad\qquad W,\,Z}{\text{\Large(blob)}} \quad \Big|_{k^2 \,=\, M^2_{W,\,Z}} \quad = 0$$

$$Re \quad \underset{H \qquad\qquad H}{\text{\Large(blob)}} \quad \Big|_{k^2 \,=\, M^2_{H}} \quad = 0$$

$$Re \quad \underset{f \qquad\qquad f}{\text{\Large(blob)}} \quad \Big|_{k^2 \,=\, m^2_{f}} \quad = 0$$

Figure 2: Graphical representation of renormalization conditions. Class 1.

Here, the shaded blobs denote the renormalized one-particle irreducible amputated two-point functions, i.e. self-energies. It is equivalent to demanding that

$$Re\widehat{\Sigma}^{W}(M_W^2) = Re\widehat{\Sigma}^{Z}(M_Z^2) = Re\widehat{\Sigma}^{f}(m_f^2) = 0. \tag{71}$$

Another class of conditions is depicted in Fig. (3), with the corresponding equations:

$$\begin{aligned}
\widehat{\Gamma}_{\mu}^{\gamma ee}(k^2 &= 0, \ \not{p} = \not{q} = m_e) = ie\gamma, \\
\widehat{\Sigma}^{\gamma Z}(0) &= 0, \tag{72} \\
\frac{\partial \widehat{\Sigma}^{\gamma}}{\partial k^2}(0) &= 0, \\
\lim_{\not{k} \to m_-} \frac{1}{\not{k} - m_-}\widehat{\Sigma}^{f}(k)u_-(k) &= 0.
\end{aligned}$$

In the last condition, u_- is the spinor for charged leptons and quarks with $I_3 = -1/2$. It implies the condition for the renormalization constants Z_L and Z_R^- for the left-

$$\gamma \quad \begin{array}{c} e \\ \\ e \end{array} \bigg|_{k^2 = 0, \ \not{p} = \not{q} = m_e} = ie\gamma_\mu$$

$$\gamma \quad\quad\quad\quad Z \bigg|_{k^2 = 0} = 0$$

$$\frac{\partial}{\partial k^2}\left(\quad\quad\quad \right)\bigg|_{k^2 = 0} = 0$$

$$\frac{1}{\not{k} - m_-}\left(\begin{array}{ccc} & & \\ f_- & & f_- \end{array} \right)\bigg|_{\not{k} - m_-} = 0$$

Figure 3: Graphical representation of renormalization conditions. Class 2.

and right-handed fermion fields. The constant Z_R^+ corresponding to the right-handed quark fields can be fixed so that the renormalized left- and right-handed parts of the up-type propagators have equal residues at $k^2 = m_+^2$.

Let us consider an example of extracting two constraints on renormalization constants using the Ward-Takahashi identities and the expression for the renormalized self-energy,

$$\widehat{\Sigma}^Z(k^2) = \Sigma^Z(k^2) - \delta M_Z^2 + \delta Z_2^Z(k^2 - M_Z^2). \tag{73}$$

First, in Eq. (73) we set $k^2 = M_Z^2$ and leave only the real part. After obtaining immediately

$$Re\widehat{\Sigma}^Z(M_Z^2) = Re\Sigma^Z(M_Z^2) - \delta M_Z^2, \tag{74}$$

47

we use the Ward-Takahashi identities from Eq. (71):

$$Re\widehat{\Sigma}^Z(M_Z^2) = 0. \tag{75}$$

It is obvious now that δM_Z^2 is

$$\delta M_Z^2 = Re\widehat{\Sigma}^Z(M_Z^2). \tag{76}$$

Thus, we have derived the mass renormalization condition entering the set of Eq. (94) given in the next section.

Now, let us go back to Eq. (73), differentiate it with respect to k^2, take the real part, and set $k^2 = M_Z^2$, just as done previously:

$$Re\left(\frac{\partial\widehat{\Sigma}^Z(k^2)}{\partial k^2}\right)_{k^2=M_Z^2} = Re\left(\frac{\partial\Sigma^Z(k^2)}{\partial k^2}\right)_{k^2=M_Z^2} + \delta Z_2^Z. \tag{77}$$

Using the condition similar to the third line in Eq. (72), but for Z :

$$\frac{\partial\widehat{\Sigma}^Z}{\partial k^2}(M_Z^2) = 0, \tag{78}$$

we arrive at

$$\delta Z_2^Z = -Re\left(\frac{\partial\Sigma^Z(k^2)}{\partial k^2}\right)_{k^2=M_Z^2}, \tag{79}$$

which we will encounter again in Eq. (89), describing the wave function renormalization.

Another example will refer to the more abstract case of the arbitrary symmetry

$$\varphi_a(x) \rightarrow \varphi_a(x) + \varepsilon\Delta\varphi_a(x), \tag{80}$$

48

where we can use the Schwinger-Dyson equation as the Ward Takahashi identity:

$$\langle \partial_\mu j^\mu(x)\varphi_a(x_1)\varphi_b(x_2)\rangle \tag{81}$$

$$= -i\langle (\Delta\varphi_a(x_1)\delta(x-x_1))\varphi_b(x_2) + \varphi_a(x_1)(\Delta\varphi_b(x_2)\delta(x-x_2))\rangle .$$

Now, how does an expression like Eq. (81) help us to reduce the number of independent renormalization constants? Let us consider the simplest example of the electron-photon vertex, where on the left hand side of Eq. (81) we would have the three-point function with one entering (p) and one exiting $(p+k)$ electron and one external photon (k). Then the Ward Takahashi identity reads ([31]):

$$S(p+k)[-iek_\mu\Gamma^\mu(p+k,p)]S(p) = e(S(p) - S(p+k)), \tag{82}$$

where quantities S are the electron propagators and Γ^μ is the vertex. Multiplying both sides by $S^{-1}(p)$ and $S^{-1}(p+k)$ gives:

$$-ik_\mu\Gamma^\mu(p+k,p) = S^{-1}(p+k) - S^{-1}(p). \tag{83}$$

Let us now define the renormalization factors Z_1 and Z_2 as

$$\Gamma^\mu(p+k,p) \to Z_1^{-1}\gamma^\mu \tag{84}$$

for $k \to 0$, and

$$S(p) \sim \frac{iZ_2}{\not{p}-m}. \tag{85}$$

49

Setting p near the mass shell and expanding Eq. (82) about $k = 0$, for the first-order terms we obtain:

$$-iZ_1^{-1}\,\not{k} = -iZ_2^{-1}\,\not{k}, \tag{86}$$

i.e.

$$Z_1 = Z_2. \tag{87}$$

In this section, we introduced the general idea defining the the Ward Takahashi identities helpful in reducing the number of independent renormalization constants. Eqs. (76), Eq. (79) and (87) were derived to serve as examples. The full sets of constraints imposed on the renormalization constants necessary in our calculations are given in the following section.

3.5 Renormalization Constants

Generally, tensor coefficient functions are ultraviolet divergent (inversely proportional to the parameter $\varepsilon = 4-D$). In order to cancel divergences and transform bare parameters into physical observables one has to introduce a renormalization scheme. The renormalized parameters are related to the bare parameters (denoted by a subscript 0) as follows:

$$M_{Z,0}^2 = M_Z^2 + \delta M_Z^2,$$

$$M_{W,0}^2 = M_W^2 + \delta M_W^2,$$

$$M_{H,0}^2 = M_H^2 + \delta M_H^2,$$

50

$$m_{f_i,0} = m_{f_i} + \delta m_{f_i},$$

$$e_0 = (1 + \delta e)\, e,$$

$$\begin{pmatrix} Z_0 \\ A_0 \end{pmatrix} = \begin{pmatrix} 1 + \frac{1}{2}\delta Z^{ZZ} & \frac{1}{2}\delta Z^{ZA} \\ \frac{1}{2}\delta Z^{AZ} & 1 + \frac{1}{2}\delta Z^{AA} \end{pmatrix} \begin{pmatrix} Z \\ A \end{pmatrix},$$

$$W_0^{\pm} = \left(1 + \frac{1}{2}\delta Z^{WW}\right) W^{\pm},$$

$$H_0 = \left(1 + \frac{1}{2}\delta Z^{H}\right) H,$$

$$f_{i,0}^{L} = \left(\delta_{ij} + \frac{1}{2}(\delta f_L^f)_{ij}\right) f_j^{L},$$

$$f_{i,0}^{R} = \left(\delta_{ij} + \frac{1}{2}(\delta f_R^f)_{ij}\right) f_j^{R}.$$

(88)

Counterterms were chosen in the On-Shell Renormalization (OSR) scheme in the 't Hooft-Feynman gauge, where the gauge parameter $\xi = 1$ with the following renormalization constants (Ref.[29]):

Wave function renormalization:

$$\delta Z^{ZZ} = -\mathrm{Re}\left(\frac{\partial}{\partial k^2}\Sigma_{\perp}^{ZZ}\left(k^2\right)\right)_{k^2=M_Z^2},$$

$$\delta Z^{ZA} = 2\mathrm{Re}\left(\frac{\Sigma_{\perp}^{AZ}\left(0\right)}{M_Z^2}\right),$$

(89)

$$\delta Z^{AA} = -\mathrm{Re}\left(\frac{\partial}{\partial k^2}\Sigma_{\perp}^{AA}\left(k^2\right)\right)_{k^2=0},$$

$$\delta Z^{AZ} = -2\mathrm{Re}\left(\frac{\Sigma_{\perp}^{AZ}\left(M_Z^2\right)}{M_Z^2}\right),$$

(90)

51

$$\delta Z^{WW} = -\text{Re}\left(\frac{\partial}{\partial k^2}\Sigma_\perp^{WW}\left(k^2\right)\right)_{k^2=M_W^2},$$

$$\delta Z^H = -\text{Re}\left(\frac{\partial}{\partial k^2}\Sigma^H\left(k^2\right)\right)_{k^2=M_H^2}, \tag{91}$$

$$\delta Z^\chi = -\text{Re}\left(\frac{\partial}{\partial k^2}\Sigma^\chi\left(k^2\right)\right)_{k^2=M_Z^2},$$

$$\delta Z^\phi = -\text{Re}\left(\frac{\partial}{\partial k^2}\Sigma^\phi\left(k^2\right)\right)_{k^2=M_W^2},$$

$$(\delta f_L^f)_{ii} = -\text{Re}\left(\Sigma_{ii}^{f,L}\left(m_{f_i}^2\right)\right) \tag{92}$$

$$-m_{f_i}^2\text{Re}\left(\frac{\partial}{\partial p^2}\left[\Sigma_{ii}^{f,L}\left(p^2\right)+\Sigma_{ii}^{f,R}\left(p^2\right)+2\Sigma_{ii}^{f,S}\left(p^2\right)\right]\right)_{p^2=m_{f_i}^2},$$

$$(\delta f_R^f)_{ii} = -\text{Re}\left(\Sigma_{ii}^{f,R}\left(m_{f_i}^2\right)\right)$$

$$-m_{f_i}^2\text{Re}\left(\frac{\partial}{\partial p^2}\left[\Sigma_{ii}^{f,L}\left(p^2\right)+\Sigma_{ii}^{f,R}\left(p^2\right)+2\Sigma_{ii}^{f,S}\left(p^2\right)\right]\right)_{p^2=m_{f_i}^2}. \tag{93}$$

Mass renormalization:

$$\delta M_Z^2 = \text{Re}\left(\Sigma_\perp^{ZZ}\left(M_Z^2\right)\right),$$

$$\delta M_W^2 = \text{Re}\left(\Sigma_\perp^{WW}\left(M_W^2\right)\right), \tag{94}$$

$$\delta M_H^2 = \text{Re}\left(\Sigma^H\left(M_H^2\right)\right),$$

$$\delta m_{f_i} = \frac{1}{2}m_{f_i}\text{Re}\left(\Sigma_{ii}^{f,L}\left(m_{f_i}^2\right)+\Sigma_{ii}^{f,R}\left(m_{f_i}^2\right)+2\Sigma_{ii}^{f,S}\left(m_{f_i}^2\right)\right).$$

Here L and R correspond to left- and right-handed fermions, Σ means the one-loop

integral of the truncated self-energy graph, and $\perp$ denotes the transverse part only.

Charge and mixing angle renormalization:

$$\delta(\sin^2\theta_W) = \cos^2\theta_W \left(\frac{\delta M_Z^2}{M_Z^2} - \frac{\delta M_W^2}{M_W^2} \right), \tag{95}$$

$$\delta(\cos^2\theta_W) = -\delta(\sin^2\theta_W), \tag{96}$$

$$\delta e = -\frac{1}{2}\left(\delta Z^{AA} + \frac{\sin^2\theta_W}{\cos^2\theta_W}\delta Z^{ZA} \right),$$

with $\sin^2\theta_W = 1 - M_W^2/M_Z^2$.

4 Radiative Effects

4.1 Introduction

The ongoing Q-Weak experiment is directly focused on measurements of the weak charge of the proton. One-quark radiative corrections have theoretical error associated with the uncertainty of quark dynamics, and must be accounted for the valid test of the Standard Model. If we take into consideration the next to leading order effects in parity-violating scattering with realistic Pauli and Dirac parts of the coupling, and compute corrections along with the weak charges of the proton and neutron, we will be able to avoid uncertainties associated with one-quark radiative effects by absorbing terms which are responsible for the quark dynamics into experimentally measured electromagnetic form factors. Estimates have been already done for the case of $\gamma - Z$ box (Ref. [8]) in the zero momentum transfer approximation. The rest of the corrections used for calculations of the weak charges of the nuclei in Ref. [8] are on the one-quark level. Modification of the couplings with model-dependent form factors and replacement of one-quark corrections with hadronic ones will contribute more clarity in situation where the Standard Model is tested. Also, in the treatment of the infrared divergences with hard photon bremsstrahlung, it is more natural to consider photon emission from the proton instead of the quark. By this, we expect to reduce theoretical error down to the level of uncertainty of current electromagnetic form factor measurements. Finally, having momentum transfer dependence in radiative

54

corrections makes it possible to adapt our results to the current parity violating experiments.

4.2 Dirac and Pauli Coupling

In the approximation where the nucleon behaves as a point-like particle, vector boson couplings obey general rules of electroweak theory. Having left and right handed fermions, it is easy to use the following structure for the $\{Z - N\}$ type couplings:

$$\Gamma^\mu_{Z-N} = ie \left[g_L^{Z-N} \gamma^\mu \varpi_- + g_R^{Z-N} \gamma^\mu \varpi_+ \right], \tag{97}$$

where $\varpi_\pm = \frac{1 \pm \gamma_5}{2}$ are chirality projectors and $g_{L,R}^{Z-N}$ have meaning of the coupling strength for the left and right handed fermions, respectively. Substitution of $\varpi_\pm$ into Eq. (97) will give us vector and axial vector representation in the coupling Γ^μ_{Z-N}:

$$\Gamma^\mu_{Z-N} = ie \left[\frac{g_L^{Z-N} + g_R^{Z-N}}{2} \gamma^\mu + \frac{g_R^{Z-N} - g_L^{Z-N}}{2} \gamma^\mu \gamma_5 \right]. \tag{98}$$

It is obvious that equality of g_L^{Z-N} and g_R^{Z-N} will produce no difference whatsoever in the cross sections for left or right handed type particles, and the coupling Γ^μ_{Z-N} will contain only a vector part. On the other hand, the nonzero difference between g_R^{Z-N} and g_L^{Z-N} is directly responsible for the asymmetry; and Γ^μ_{Z-N} has axial vector part as well. Couplings of vector bosons to fermions derived from the neutral current part of the electroweak Lagrangian relate coupling strengths g_L^{Z-N} and g_R^{Z-N} to the electric and weak charges of the fermion in the following way (See Chapter 1):

$$\frac{g_L^{Z-N} + g_R^{Z-N}}{2} = \frac{1}{4} \frac{C_3 - 4s^2 Q}{c_w s_w},$$

$$\tag{99}$$

$$\frac{g_R^{Z-N} - g_L^{Z-N}}{2} = -\frac{1}{4}\frac{C_3}{c_w \, s_w}.$$

Here, C_3 and Q are the fermion weak and electric charges respectively, s_w and c_w are $\sin\theta_W$ and $\cos\theta_W$. In the case when a photon couples to the nucleon, $g_L^{\gamma-N} = g_R^{\gamma-N} = Q$ and $\Gamma_{\gamma-N}^\mu = ieQ\gamma^\mu$.

For a realistic nucleon, the couplings preserve their vector and vector-axial structure, but with the charges replaced by the corresponding form factors. The most general electromagnetic $\Gamma_{\gamma-N}^\mu$ coupling has two vector components responsible for static electric and magnetic interactions:

$$\Gamma_{\gamma-N}^\mu (q) = ie\left[F_1^N (q)\gamma^\mu + \frac{i}{2m_N}\sigma^{\mu\alpha}q_\alpha F_2^N (q)\right], \tag{100}$$

where $F_1^N (q)$ and $F_2^N (q)$ are the Dirac and Pauli form factors, respectively, and q_α is the four-momentum transferred to the nucleon. As for $\Gamma_{Z-N}^\mu (q)$, we have:

$$\Gamma_{Z-N}^\mu (q) = ie\left[f_1^N (q)\gamma^\mu + \frac{i}{2m_N}\sigma^{\mu\alpha}q_\alpha f_2^N (q) + g_1^N (q)\gamma^\mu\gamma_5\right], \tag{101}$$

with $f_1^N (q)$, $f_2^N (q)$ and $g_1^N (q)$ as weak electric, magnetic and axial-vector form factors. According to the first line of the Eq. (99), form factors $f_1^N (q)$ and $f_2^N (q)$ are expressed as:

$$f_{1,2}^N (q) = \frac{1}{4c_w s_w}\left(F_{1,2}^{V(N)} (q) - 4s_w^2 F_{1,2}^N (q)\right), \tag{102}$$

with $F_{1,2}^{V(p)} = -F_{1,2}^{V(n)} = F_{1,2}^p - F_{1,2}^n$. For $g_1^N (q)$ we have

$$g_1^N (q) = -\frac{1}{4c_w s_w}g_A^N (q), \tag{103}$$

56

where $g_A^p(q) = -g_A^n(q) = g_A(q)$ is a well known axial form factor. To simplify analytical expressions considerably, we will use the monopole structure for form factors

$$\left\{F_{1,2}^N, g_A^N\right\}(q) = \frac{\Lambda^2 \left\{F_{1,2}^N, g_A^N\right\}(0)}{\Lambda^2 - q^2}, \tag{104}$$

($\Lambda^2 = 0.83 m_N^2$), which is a quite reasonable approximation in our case. The value of the parameter Λ we use is found after the fit of the electromagnetic formfactors by monopole approximation in the low momentum transfer region.

Comparing Eq. (98) and Eq. (101), combined with Eq. (102) and Eq. (103), it is possible to write

$$\Gamma_{Z-N}^\mu(q) = ie\left[\frac{g_R^{Z-N}(q) + g_L^{Z-N}(q)}{2}\gamma^\mu + \frac{g_R^{Z-N}(q) - g_L^{Z-N}(q)}{2}\gamma^\mu\gamma_5 + \right.$$

$$\left. + \frac{i}{2m_N}\sigma^{\mu\alpha}q_\alpha f_2^N(q)\right] =$$

$$\tag{105}$$

$$= ie\left[g_L^{Z-N}(q)\gamma^\mu\varpi_- + g_R^{Z-N}(q)\gamma^\mu\varpi_+ + \frac{i}{2m_N}\sigma^{\mu\alpha}q_\alpha f_2^N(q)\right]$$

$$\Gamma_{\gamma-N}^\mu(q) = ie\left[\frac{g_L^{\gamma-N}(q) + g_R^{\gamma-N}(q)}{2}\gamma^\mu + \frac{i}{2m_N}\sigma^{\mu\alpha}q_\alpha F_2^N(q)\right] =$$

$$\tag{106}$$

$$= ie\left[g_L^{\gamma-N}(q)\gamma^\mu\varpi_- + g_R^{\gamma-N}(q)\gamma^\mu\varpi_+ + \frac{i}{2m_N}\sigma^{\mu\alpha}q_\alpha F_2^N(q)\right] \quad,$$

where

$$g_{L,R}^{Z-N}(q) \;=\; \frac{1}{4c_w s_w}\left(F_1^{V(N)}(0) - 4s^2 F_1^N(0) \pm g_A^N(0)\right)\frac{\Lambda^2}{\Lambda^2 - q^2}$$

(107)

$$g_{L,R}^{\gamma-N}(q) \;=\; g^{\gamma-N}(q) = F_1^N(0)\frac{\Lambda^2}{\Lambda^2 - q^2}.$$

In Eqs. (105) and (106), we have adopted the general structure of the coupling from Eq. (97), with coupling strengths $g_{L,R}^{Z-N}(q)$ and $g_{L,R}^{\gamma-N}(q)$ given by Eq. 107. Moreover, to represent splitting between strength and kinematical parts of the coupling, we introduce the following matrix representation of Eq. (105) and Eq. (106):

$$\Gamma(N, N, V_\mu) = \left(\; \gamma^\mu \varpi_-, \quad \gamma^\mu \varpi_+, \quad [\gamma^\mu, \slashed{A}]\,\varpi_-, \quad [\gamma^\mu, \slashed{A}]\,\varpi_+ \;\right)\overrightarrow{G}_{NNV}(q), \quad (108)$$

with $\overrightarrow{G}_{NNV}$ expressed as a 2×4 matrix

$$\overrightarrow{G}_{NNV} = ie\begin{pmatrix} g_L^{f-V}(q) & G_{1L}^{f-V} \\[1.5ex] g_R^{f-V}(q) & G_{1R}^{f-V} \\[1.5ex] -\frac{1}{4m_N}F_2^{V-N}(q) & G_{2L}^{f-V} \\[1.5ex] -\frac{1}{4m_N}F_2^{V-N}(q) & G_{2R}^{f-V} \end{pmatrix}. \quad (109)$$

The second column of $\overrightarrow{G}_{NNV}$ represents counterterms of the first order, which will be described later in this work. The Pauli form factor F_2^{V-N} has the following structure:

$$F_2^{Z-N}(q) \;=\; f_2^{Z-N}(q),$$

(110)

$$F_2^{\gamma-N}(q) \;=\; F_2^N(q).$$

58

4.3 Definition of Radiative Corrections

In analogy with one-quark corrections, we define the next to leading order hadronic radiative corrections using the electron-nucleon parity violating Hamiltonian in the following form:

$$H^{PV} = \frac{G_F}{\sqrt{2}} \left[C_{1N} \left(\overline{u}_e \gamma^\mu \gamma^5 u_e \right) \left(\overline{u}_N \gamma^\mu u_N \right) + C_{2N} \left(\overline{u}_e \gamma^\mu u_e \right) \left(\overline{u}_N \gamma^\mu \gamma^5 u_N \right) \right]. \tag{111}$$

Form factors C_{1N} and C_{2N} represent perturbative expansion resulting in

$$C_{\{1,2\}N} = \sum_i C^i_{\{1,2\}N} = C^0_{\{1,2\}N} + C^1_{\{1,2\}N} + O\left(\alpha^3 \right). \tag{112}$$

Superscript in $C^i_{\{1,2\}N}$ represents the order of the perturbation ("zero"- tree level, "one" - one loop level and so on). Here $C^1_{\{1,2\}N}$ can be defined as one-loop radiative corrections normalized to the Fermi constant $G_F = \frac{\alpha \pi}{\sqrt{2} m_W^2}$. One-loop corrections are generally split into three topological classes: box, self energy, and vertex (triangle) graphs. To preserve gauge invariance we have to include all the possible bosons of the Standard Model in these topological classes. Taking into account that in the t'Hooft-Feynman gauge the contribution coming from the Higgs scalar and gauge fixing fields is negligible, we choose to consider boxes, triangles and self energies with γ, Z, $W^\pm$ vector bosons only. Accordingly, we will give details on radiative corrections for every class, starting with an analytical example for the $\gamma - Z$ boxes.

4.4 Example of $\{\gamma - Z\}$ Box Diagram in $e - N$ Scattering

A reason to provide analytical details for $\{\gamma - Z\}$ box only is straightforward. First of all, precise formulae for an entire set of graphs are cumbersome, and it is not feasible to show them in the present work. Secondly, as will be seen later, this example will be used as a generalization of the computational model which was applied in this work toward calculations of weak charges and hadronic radiative corrections. According to the Feynman rules, the amplitude for a $\{\gamma - Z\}$ box can be written as (see Fig. (4)):

$$M^{\{\gamma - Z\}} \quad = \quad \frac{1}{16\pi^4} \int d^4q \left(i\overline{u}_e \Gamma^\mu_{Z-e} \frac{m_e + \slashed{k}_1 + \slashed{k}_2 - \slashed{q} - \slashed{p}_2}{(p_2 - k_1 - k_2 + q)^2 - m_e^2} \Gamma^\nu_{\gamma - e} u_e \right)$$

(113)

$$\left(i\overline{u}_N \Gamma^\mu_{Z-N} \frac{m_N + \slashed{q} + \slashed{p}_2}{(p_2 + q)^2 - m_N^2} \Gamma^\nu_{\gamma - N} u_N \right) \frac{1}{q^2} \frac{1}{(p_2 + q - k_2)^2 - m_Z^2}.$$

Here, the coupling Γ^μ_{Z-e} can be found in Eq. (98) and Eq. (99). Substituting Eq. (100) - Eq. (104) into amplitude in Eq. (113), and using the fact that in each nucleonic vertex couplings behave as a function of momentum transferred through a vertex, we can write

$$M^{\{\gamma - Z\}} = \frac{1}{16\pi^4} \int d^4q \, i\overline{u}_e \Gamma^\mu_{Z-e} \frac{m_e + \slashed{k}_1 + \slashed{k}_2 - \slashed{q} - \slashed{p}_2}{(p_2 - k_1 - k_2 + q)^2 - m_e^2} \Gamma^\nu_{\gamma - e} u_e \quad .$$

60
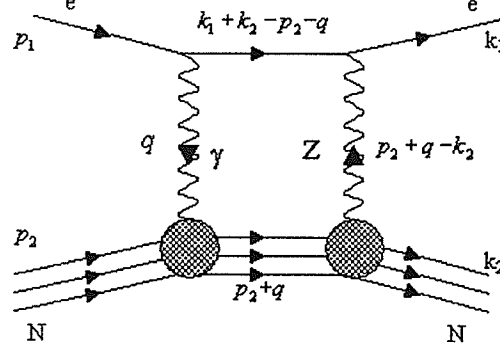
Figure 4: $\{\gamma - Z\}$ box in case of realistic $\{e - N\}$ scattering

$$i\bar{u}_N \left(-e^2\right) \left(\begin{array}{c} \left(F_1^{V(N)}(0) - 4s^2 F_1^N(0)\right)\gamma^\mu - \\ -\frac{1}{4m_N}\left(F_2^{V(N)}(0) - 4s^2 F_2^N(0)\right)[\gamma^\mu, (\not{k}_2 - \not{p}_2 - \not{q})] - g_A^N(0)\gamma^\mu\gamma_5 \end{array} \right) \cdot$$

(114)

$$\cdot \frac{m_N + \not{q} + \not{p}_2}{(p_2 + q)^2 - m_N^2}\left(F_1^N(0)\gamma^\nu - \frac{1}{4m_N}F_2^N(0)[\gamma^\nu, \not{q}]\right)u_N \quad \cdot$$

$$\cdot \frac{\Lambda^4}{4cs\left(\Lambda^2 - q^2\right)\left(\Lambda^2 - (k_2 - p_2 - q)^2\right)}\frac{1}{q^2}\frac{1}{(p_2 + q - k_2)^2 - m_Z^2} \quad \cdot$$

We should note that the latter expression is written for the $\{\gamma - Z\}$ box diagram only. To have a complete analysis, it is imperative to consider $\{Z - \gamma\}$, $\{\gamma - Z\}$ and $\{Z - \gamma\}$ crossed boxes as well. In addition, $\{Z - Z\}$ and $\{W - W\}$ box diagrams should be considered. To work out the integration in Eq. (114) we will split the nucleon current into four parts, then use the notation of Eq. (97). The nucleon

current from Eq. (114) now becomes

$$
J_N^{\mu\nu} \;=\; i\overline{u}_N\left(-e^2\right)\Phi\left(q\right)\cdot
$$

$$
\cdot
\begin{bmatrix}
g_L^{Z-N}\left(0\right)\gamma^\mu\varpi_- + g_R^{Z-N}\left(0\right)\gamma^\mu\varpi_+ - \\[4mm]
-\frac{1}{16\,c_w s_w\,m_N}\left(F_2^{V(N)}\left(0\right)-4s_w^2 F_2^N\left(0\right)\right)\left[\gamma^\mu,\left(\not{k}_2-\not{p}_2-\not{q}\right)\right]
\end{bmatrix}
\cdot
$$

(115)

$$
\cdot\frac{m_N+\not{q}+\not{p}_2}{\left(p_2+q\right)^2-m_N^2}\cdot
\begin{bmatrix}
g_L^{\gamma-N}\left(0\right)\gamma^\mu\varpi_- + g_R^{\gamma-N}\left(0\right)\gamma^\mu\varpi_+ - \\[6mm]
-\frac{1}{4m_N}F_2^N\left(0\right)\left[\gamma^\nu,\not{q}\right]
\end{bmatrix}
u_N,
$$

where $\Phi\left(q\right)=\frac{\Lambda^4}{\left(\Lambda^2-q^2\right)\left(\Lambda^2-(k_2-p_2-q)^2\right)}$. Expansion of $J_N^{\mu\nu}$ will lead to the following results with four parts of nucleon current:

$$
J_{N_1}^{\mu\nu} \;=\; i\overline{u}_N\left(-e^2\right)\Phi\left(q\right)\left[g_L^{Z-N}\left(0\right)\gamma^\mu\varpi_- + g_R^{Z-N}\left(0\right)\gamma^\mu\varpi_+\right]\cdot
$$

(116)

$$
\cdot\frac{m_N+\not{q}+\not{p}_2}{\left(p_2+q\right)^2-m_N^2}\cdot\left[g_L^{\gamma-N}\left(0\right)\gamma^\mu\varpi_- + g_R^{\gamma-N}\left(0\right)\gamma^\mu\varpi_+\right]u_N
$$

$$
J_{N_2}^{\mu\nu} \;=\; i\overline{u}_N\left(-e^2\right)\Phi\left(q\right)\left[g_L^{Z-N}\left(0\right)\gamma^\mu\varpi_- + g_R^{Z-N}\left(0\right)\gamma^\mu\varpi_+\right]
$$

(117)

$$
\cdot\frac{m_N+\not{q}+\not{p}_2}{\left(p_2+q\right)^2-m_N^2}\cdot\left[-\frac{1}{4m_N}F_2^N\left(0\right)\left[\gamma^\nu,\not{q}\right]\right]u_N
$$

$$
J_{N_3}^{\mu\nu} \;=\; i\overline{u}_N\left(-e^2\right)\Phi\left(q\right)\cdot
$$

$$\cdot \left[-\frac{1}{16\, cs\, m_N} \left(F_2^{V(N)}\left(0\right) - 4s^2 F_2^N\left(0\right) \right) \left[\gamma^\mu, \left(\not{k}_2 - \not{p}_2 - \not{q} \right) \right] \right] \cdot$$

$$(118)$$

$$\cdot \frac{m_N + \not{q} + \not{p}_2}{\left(p_2 + q\right)^2 - m_N^2} \cdot \left[g_L^{\gamma - N}\left(0\right) \gamma^\mu \varpi_- + g_R^{\gamma - N}\left(0\right) \gamma^\mu \varpi_+ \right] u_N$$

$$J_{N_4}^{\mu\nu} = i\overline{u}_N \left(-e^2 \right) \Phi\left(q\right) \cdot$$

$$\cdot \left[-\frac{1}{16\, c_w s_w\, m_N} \left(F_2^{V(N)}\left(0\right) - 4s_w^2 F_2^N\left(0\right) \right) \left[\gamma^\mu, \left(\not{k}_2 - \not{p}_2 - \not{q} \right) \right] \right] \cdot$$

$$(119)$$

$$\cdot \frac{m_N + \not{q} + \not{p}_2}{\left(p_2 + q\right)^2 - m_N^2} \cdot \left[-\frac{1}{4m_N} F_2^N\left(0\right) \left[\gamma^\nu, \not{q} \right] \right] u_N.$$

The fourth current carries a coupling between weak magnetic and electric magnetic fields of the nucleon, and has a negligible contribution. Nevertheless we take it into account in our actual calculations, although in this example it is not given. As for the first current, we can see coupling between weak static and electric static fields here. This current gives small but sizable contributions into the amplitude. The second and third currents are the most important, and represent couplings between weak static and electric magnetic, and weak magnetic and electric static fields, respectively. It is worthwhile to point out that only the second current contributes to the $\{e - n\}$ box amplitude, and, as result, the value of the $\{e - n\}$ radiative correction is directly proportional to the neutron's anomalous magnetic moment. Moreover, for the $\{e - n\}$ amplitude we will not have infrared divergences due to the absence of the electric static part in the coupling. The third current gives surprisingly the biggest contribution

into the $\{e - p\}$ box amplitude which makes weak magnetism dominant in this type of calculation.

4.4.1   Results

To integrate the amplitude according to Eq. (114), we will have to split it into four integrals. Each of them could be expanded into a linear combination of the "usual" four-point tensor integrals. Details are in the section called "Tensor Decomposition". Let us provide a simple example by taking into account the first current only. As we know, the general definition of four-point tensor integral is

$$T^4_{\mu_1 \dots \mu_k} \quad = \quad \frac{1}{i\pi^2} \int d^4 q \frac{q_{\mu_1} \dots q_{\mu k}}{\left((p_2 - k_1 - k_2 + q)^2 - m_e^2 \right) \left((p_2 + q)^2 - m_N^2 \right)} \cdot$$

$$\cdot \frac{1}{q^2} \cdot \frac{1}{(p_2 + q - k_2)^2 - m_Z^2} \cdot \tag{120}$$

By adding the monopole form factor approximation into the above definition, we will obtain a six-point tensor integral which could be reduced into a combination of four-point integrals by using following simple expansion:

$$\frac{1}{D_1 D_2} = \frac{1}{q^2} \cdot \frac{1}{(p_2 + q - k_2)^2 - m_Z^2} \cdot \frac{\Lambda^4}{(q^2 - \Lambda^2) \left((p_2 + q - k_2)^2 - \Lambda^2 \right)} = \tag{121}$$

$$\frac{\Lambda^2}{(\Lambda^2 - m_Z^2)} \left(\frac{1}{q^2 - \Lambda^2} - \frac{1}{q^2} \right) \cdot \left(\frac{1}{(p_2 + q - k_2)^2 - \Lambda^2} - \frac{1}{(p_2 + q - k_2)^2 - m_Z^2} \right) \cdot$$

Now, we put this expansion into Eq. (116)-Eq. (119) and evaluate each of the integrals with FormCalc language (FormCalc was developed by Thomas Hahn and modified by

64

the author of this thesis to include hadronic sector in the $e-N$ scattering. FormCalc is available from http://www.feynarts.de) by contracting indeces in the numerator and using dimensional reduction within tensor decomposition algorithms. The results are listed below.

First Current (static weak and static electric coupling only)   Before going into the analytical details, let us introduce the following notation for the variables of the four-point tensor coefficients. We set

$$D_{ij}\left\{m_e^2, s, m_N^2, t, m_N^2, m_e^2, 0, m_e^2, m_N^2, \Lambda^2\right\} \equiv D_{ij}\left\{0, \Lambda^2\right\},$$

(122)

$$D_{ij}\left\{m_e^2, s, m_N^2, t, m_N^2, m_e^2, \Lambda^2, m_e^2, m_N^2, \Lambda^2\right\} \equiv D_{ij}\left\{\Lambda^2, \Lambda^2\right\},$$

where $\{s, t, u\}$ are Mandelstam Lorentz invariant variables defined as follows:

$$s = (k_1 + k_2)^2,$$

$$t = (k_1 - k_3)^2,$$

(123)

$$u = (k_1 - k_4)^2.$$

Using the tensor coefficient reduction approach, we can now reduce D_{ij} functions into D_0, C_0 and B_0 scalar integrals. This step makes the final expressions very cumbersome. However, we only need to expand the IR divergent terms, which are represented by $D_0\{0, \Lambda^2\}$ scalar integral alone. The vector-axial part of the first

65

current is

$$M_1^{V-A} = \frac{\alpha^2 \Lambda^2 g^{\gamma-N}}{4 c_w s_w \left(\Lambda^2 - m_Z^2\right)} [\left(g_R^{Z-N} - g_L^{Z-N}\right) \left(m_e^2 + m_N^2 - S\right) \left(4 s_w^2 - 1\right) \cdot$$

$$\cdot \left(D_0 \left\{0, \Lambda^2\right\} - D_0 \left\{\Lambda^2, \Lambda^2\right\}\right) + 2 \left(2 g_L^{Z-N} \left(2 - 5 s^2\right) + g_R^{Z-N} \left(1 + 10 s_w^2\right)\right) \cdot$$

$$\cdot \left(D_{00} \left\{0, \Lambda^2\right\} - D_{00} \left\{\Lambda^2, \Lambda^2\right\}\right) + \left(4 s_w^2 - 1\right) \left(g_L^{Z-N} - g_R^{Z-N}\right) \left(m_N^2 - t - u\right)$$

$$\cdot \left(D_1 \left\{0, \Lambda^2\right\} - D_1 \left\{\Lambda^2, \Lambda^2\right\}\right) + \left(m_e^2 + m_N^2 - s\right) \begin{pmatrix} g_L^{Z-N} \left(3 - 10 s_w^2\right) + \\ +2 g_R^{Z-N} \left(5 s_w^2 - 1\right) \end{pmatrix} \cdot$$

(124)

$$\cdot D_{12} \left\{0, \Lambda^2\right\} + 2 \left(g_R^{Z-N} - g_L^{Z-N}\right) \left(2 m_e^2 + m_N^2 - s\right) \left(4 s_w^2 - 1\right) D_{13} \left\{0, \Lambda^2\right\} +$$

$$+ \left(g_R^{Z-N} - g_L^{Z-N}\right) \left(m_e^2 + 2 m_N^2 - s\right) \left(4 s_w^2 - 1\right) \left(D_2 \left\{0, \Lambda^2\right\} - D_2 \left\{\Lambda^2, \Lambda^2\right\}\right) +$$

$$+ 2 \left(g_R^{Z-N} - g_L^{Z-N}\right) \left(4 s_w^2 - 1\right) m_N^2 \left(D_{22} \left\{0, \Lambda^2\right\} - D_{22} \left\{\Lambda^2, \Lambda^2\right\}\right) +$$

$$+ 2 \left(g_R^{Z-N} - g_L^{Z-N}\right) \left(m_e^2 + 2 m_N^2 - s\right) \left(4 s_w^2 - 1\right) D_{23} \left\{0, \Lambda^2\right\} +$$

$$+2\left(g_R^{Z-N}-g_L^{Z-N}\right)\left(m_e^2+m_N^2-s\right)\left(4s_w^2-1\right)\left(D_3\left\{0,\Lambda^2\right\}+D_{33}\left\{0,\Lambda^2\right\}\right)]\cdot$$

$$\cdot\left(\overline{u}_e\gamma_\mu u_e\right)\left(\overline{u}_N\gamma_\mu\gamma_5 u_N\right)\qquad.$$

Here, $D_0\left\{0,\Lambda^2\right\}$ is the IR divergent term. As for the axial-vector part, we have

$$M_1^{A-V}=\frac{\alpha^2\Lambda^2 g^{\gamma-N}}{4c_w s_w\left(\Lambda^2-m_Z^2\right)}[\left(g_L^{Z-N}+g_R^{Z-N}\right)\left(m_e^2+m_N^2-s\right)\left(\begin{array}{c}D_0\left\{0,\Lambda^2\right\}-\\[4pt]-D_0\left\{\Lambda^2,\Lambda^2\right\}\end{array}\right)+$$

$$+2\left(g_L^{Z-N}\left(4-6s_w^2\right)+g_R^{Z-N}\left(1+6s_w^2\right)\right)\left(D_{00}\left\{0,\Lambda^2\right\}-D_{00}\left\{\Lambda^2,\Lambda^2\right\}\right)-$$

$$-\left(g_L^{Z-N}+g_R^{Z-N}\right)\left(m_N^2-t-u\right)D_1\left\{0,\Lambda^2\right\}+\left(m_e^2+m_N^2-s\right)\cdot$$

$$\tag{125}$$

$$\cdot\left(g_L^{Z-N}\left(3-2s_w^2\right)+2g_R^{Z-N}\left(1+s_w^2\right)\right)D_{12}\left\{0,\Lambda^2\right\}+2\left(g_L^{Z-N}+g_R^{Z-N}\right)\cdot$$

$$\cdot\left(2m_e^2+m_N^2-s\right)D_{13}\left\{0,\Lambda^2\right\}+\left(g_L^{Z-N}+g_R^{Z-N}\right)\left(m_e^2+2m_N^2-s\right)\cdot$$

$$\cdot\left(D_2\left\{0,\Lambda^2\right\}-D_2\left\{\Lambda^2,\Lambda^2\right\}\right)+2\left(g_L^{Z-N}+g_R^{Z-N}\right)m_N^2\left(\begin{array}{c}D_{22}\left\{0,\Lambda^2\right\}-\\[4pt]-D_{22}\left\{\Lambda^2,\Lambda^2\right\}\end{array}\right)$$

$$+2\left(g_L^{Z-N}+g_R^{Z-N}\right)\left(m_e^2+2m_N^2-s\right)\left(D_{23}\left\{0,\Lambda^2\right\}-D_{23}\left\{\Lambda^2,\Lambda^2\right\}\right)+$$

$$2 \left(g_L^{Z-N} + g_R^{Z-N} \right) \left(m_e^2 + m_N^2 - s \right) D_3 \left\{ 0, \Lambda^2 \right\}] \left(\overline{u}_e \gamma_\mu \gamma_5 u_e \right) \left(\overline{u}_N \gamma_\mu u_N \right) \qquad ,$$

where $g^{\gamma-N} = g^{\gamma-N}(0)$, $g_{L,R}^{Z-N} = g_{L,R}^{Z-N}(0)$. It is obvious that for the neutron the first current contribution is zero because $g^{\gamma-n} = 0$. We have kept only terms of $O\left(\alpha^2\right)$ to reduce the size of our expressions.

Second Current (static weak and electric magnetic coupling only) This part is the only contribution to the neutron's scattering amplitude. $F_2^N(0)$, the nucleon's anomalous magnetic moment, is equal to $F_2^n(0) = -1.91$ for the neutron, and $F_2^p(0) = 1.79$ for the proton. For both neutron and proton,

$$M_2^{V-A} = \frac{\alpha^2 \Lambda^2 F_2^N(0)}{16 c_w s_w \left(\Lambda^2 - m_Z^2 \right)} [2\Lambda^2 \left(g_R^{Z-N} - g_L^{Z-N} \right) \left(1 - 4s_w^2 \right) D_0 \left\{ \Lambda^2, \Lambda^2 \right\} +$$

$$+ 4 \left(g_R^{Z-N} \left(1 + 8s_w^2 \right) + g_L^{Z-N} \left(5 - 8s_w^2 \right) \right) \left(D_{00} \left\{ 0, \Lambda^2 \right\} - D_{00} \left\{ \Lambda^2, \Lambda^2 \right\} \right) +$$

$$+ 8 \left(g_L^{Z-N} - g_R^{Z-N} \right) \left(4s_w^2 - 1 \right) \left(m_N^2 - t - u \right) D_{13} \left\{ 0, \Lambda^2 \right\} -$$

$$- 3\Lambda^2 \left(g_L^{Z-N} - g_R^{Z-N} \right) \left(4s_w^2 - 1 \right) D_2 \left\{ \Lambda^2, \Lambda^2 \right\} +$$

$$(126)$$

$$+ \left(g_L^{Z-N} - g_R^{Z-N} \right) \left(4s_w^2 - 1 \right) \left(m_e^2 - m_N^2 - s \right) D_{22} \left\{ 0, \Lambda^2 \right\} +$$

$$+ \left(g_L^{Z-N} - g_R^{Z-N}\right)\left(4s_w^2 - 1\right)\left(3\left(s-u\right) - 8m_N^2\right)\left(D_{23}\left\{0,\Lambda^2\right\} - D_{23}\left\{\Lambda^2,\Lambda^2\right\}\right)]+$$

$$+2\left(g_L^{Z-N} - g_R^{Z-N}\right)\left(4s_w^2 - 1\right)\left(s-u\right)D_3\left\{0,\Lambda^2\right\}]\left(\overline{u}_e\gamma_\mu u_e\right)\left(\overline{u}_N\gamma_\mu\gamma_5 u_N\right).$$

As for the axial-vector part, here we have

$$M_2^{A-V} = \frac{\alpha^2\Lambda^2 F_2^N\left(0\right)}{16c_w s_w\left(\Lambda^2 - m_Z^2\right)}[2\Lambda^2\left(g_R^{Z-N} + g_L^{Z-N}\right)D_0\left\{\Lambda^2,\Lambda^2\right\}+$$

$$+4\left(g_R^{Z-N}\left(12s_w^2 - 1\right) + g_L^{Z-N}\left(5 - 12s_w^2\right)\right)\left(D_{00}\left\{0,\Lambda^2\right\} - D_{00}\left\{\Lambda^2,\Lambda^2\right\}\right)+$$

$$+4\left(g_L^{Z-N}\left(\begin{array}{c} m_e^2\left(3 - 4s_w^2\right) - \\ -4\left(m_N^2 - s\right)\left(s_w^2 - 1\right)\end{array}\right) + g_R^{Z-N}\left(\begin{array}{c} m_e^2\left(1 + 4s_w^2\right) + \\ +2\left(m_N^2 - s\right)\left(1 + 2s_w^2\right)\end{array}\right)\right)\cdot$$

$$\tag{127}$$

$$\cdot\left(D_{12}\left\{0,\Lambda^2\right\} - D_{12}\left\{\Lambda^2,\Lambda^2\right\}\right) + 3\Lambda^2\left(g_R^{Z-N} + g_L^{Z-N}\right)D_2\left\{\Lambda^2,\Lambda^2\right\}+$$

$$+\left(g_R^{Z-N} + g_L^{Z-N}\right)\left(s - m_e^2 - m_N^2\right)\left(D_{22}\left\{0,\Lambda^2\right\} - D_{22}\left\{\Lambda^2,\Lambda^2\right\}\right) + \left(g_R^{Z-N} + g_L^{Z-N}\right)\cdot$$

$$\cdot\left(4m_e^2 - 4s - 3t\right)\left(D_{23}\left\{0,\Lambda^2\right\} - D_{23}\left\{\Lambda^2,\Lambda^2\right\}\right) + 2\left(3\Lambda^2 + t\right)\cdot$$

$$\cdot \left(g_R^{Z-N} + g_L^{Z-N} \right) D_3 \left\{ \Lambda^2, \Lambda^2 \right\} + 2 \left(g_R^{Z-N} + g_L^{Z-N} \right) (u - s - 2t) \cdot$$

$$\cdot D_{33} \left\{ 0, \Lambda^2 \right\} \right] \left(\overline{u}_e \gamma_\mu \gamma_5 u_e \right) \left(\overline{u}_N \gamma_\mu u_N \right).$$

The second current amplitude has no infrared divergences in it, and that makes the neutron amplitude finite.

Third Current (weak magnetic and static electric coupling only)   The numerical analysis of the third current's amplitude shows that it gives a dominant contribution into proton's radiative correction. The following expressions show $\{V - A\}$ and $\{A - V\}$ amplitudes, respectively:

$$M_3^{V-A} = \frac{3\alpha^2 \Lambda^2 F_2^{weak(N)}(0) g^{\gamma - N}}{c_w s_w \left(\Lambda^2 - m_Z^2 \right)} \left(D_{00} \left\{ 0, \Lambda^2 \right\} - D_{00} \left\{ \Lambda^2, \Lambda^2 \right\} \right) \left(\overline{u}_e \gamma_\mu u_e \right) \left(\overline{u}_N \gamma_\mu \gamma_5 u_N \right),$$

(128)

and

$$M_3^{A-V} = \frac{\alpha^2 \Lambda^2 F_2^{weak(N)}(0) g^{\gamma - N}}{4 c_w s_w \left(\Lambda^2 - m_Z^2 \right)} [4 \left(m_e^2 + m_N^2 - s \right) \left(D_0 \left\{ 0, \Lambda^2 \right\} - D_0 \left\{ \Lambda^2, \Lambda^2 \right\} \right) +$$

$$+16 \left(D_{00} \left\{ 0, \Lambda^2 \right\} - D_{00} \left\{ \Lambda^2, \Lambda^2 \right\} \right) + 4 \left(2m_e^2 + m_N^2 - s \right) \left(D_1 \left\{ 0, \Lambda^2 \right\} - D_1 \left\{ \Lambda^2, \Lambda^2 \right\} \right) -$$

$$-4 \left(m_e^2 + m_N^2 - s \right) \left(D_{12} \left\{ 0, \Lambda^2 \right\} - D_{12} \left\{ \Lambda^2, \Lambda^2 \right\} \right) + 4 \left(3m_e^2 + m_N^2 - s \right) D_{13} \left\{ 0, \Lambda^2 \right\} +$$

$$+4 \left(m_e^2 + 2m_N^2 - s\right) D_2 \left\{0, \Lambda^2\right\} + \left(\Lambda^2 - 4m_e^2 - 8m_N^2 + 4s\right) D_2 \left\{\Lambda^2, \Lambda^2\right\} +$$

$$(129)$$

$$+ \left(m_e^2 - 5m_N^2 - s\right) \left(D_{22} \left\{0, \Lambda^2\right\} - D_{22} \left\{\Lambda^2, \Lambda^2\right\}\right) + \left(4m_e^2 + 8m_N^2 - 4s - t\right) \cdot$$

$$\cdot \left(D_{23} \left\{0, \Lambda^2\right\} - D_{23} \left\{\Lambda^2, \Lambda^2\right\}\right) + 8 \left(m_e^2 + m_N^2 - s\right) D_3 \left\{0, \Lambda^2\right\} +$$

$$+ 2 \left(\Lambda^2 - 4m_e^2 - 4m_N^2 + 4s\right) D_3 \left\{\Lambda^2, \Lambda^2\right\} + 2 \left(2m_e^2 + 2m_N^2 - 2s - t\right) \cdot$$

$$\cdot D_{33} \left\{0, \Lambda^2\right\}] \left(\overline{u}_e \gamma_\mu \gamma_5 u_e\right) \left(\overline{u}_N \gamma_\mu u_N\right)$$

Here,

$$F_2^{weak(N)}(0) = \frac{F_2^{V(N)}(0) - 4s_w^2 F_2^N(0)}{2}. \tag{130}$$

Comparing the strengths of the weak static and weak magnetic couplings for the proton's vector current, we can see that $\frac{\left(g_L^{Z-p}(0) + g_R^{Z-p}(0)\right)}{2} = \frac{1 - 4s_w^2}{4c_w s_w} = 0.085$ is almost twelve times smaller than $F_2^{weak(p)}(0) = 1.08$, which is a partial proof of the weak magnetism dominance in the $\{\gamma - Z\}$ box amplitude. The presence of infrared divergences in the proton's $\{\gamma - Z\}$ boxes makes it impossible to provide conclusive numerical analysis. Later, the proton's box diagrams will be combined with IR divergent vertex graphs, soft and hard-photon bremsstrahlung terms. As for the neutron, it is possible to compare results with Ref. [9] right now. If we take $G_F = 1.166 \cdot 10^{-5} \ GeV^{-2}$

71

in Eq. (111) and consider extrapolation to zero momentum transfer, use Eq. (111), Eq. (126), and Eq. (127), and include all of the $\{\gamma - Z\}$ boxes, we can compute the

following:

	Current results	Ref. [9]
$C_{1n}^{1(\gamma-Z \text{ boxes only})}$	-0.00273	-0.0032
$C_{2n}^{1(\gamma-Z \text{ boxes only})}$	-0.00219	-0.0025

The discrepancies are minimal and can be explained by the differences in the definitions of the Weinberg mixing angle and the fact that the monopole form factor approximation was used. The momentum transfer dependencies from which the zero momentum transfer extrapolation was taken are shown in Fig. (5) and Fig. (6). Numerical noise can be explained by the fact that box graphs have Landau singularities at small momentum transfer coming from the condition for the Gramm matrix $\det(X_{N-1})_{t\to 0} = 0$.

Although now we have $\{\gamma - Z\}$ box results for a realistic nucleon, it is still not sufficient for the definite determination of the weak charges of the proton and neutron. As was mentioned before, we need to include the rest of the graphs in the perturbative expansion. With the procedure used for the $\{\gamma - Z\}$ box at hand, it is rather computationally complex to use the proposed expansion technique (See Eqs. (116-119)). For the particular monopole form factor approximation, we may use Eq. (121) instead to create a rather simple representation of the tensor one-loop integrals (Eq. (120)).
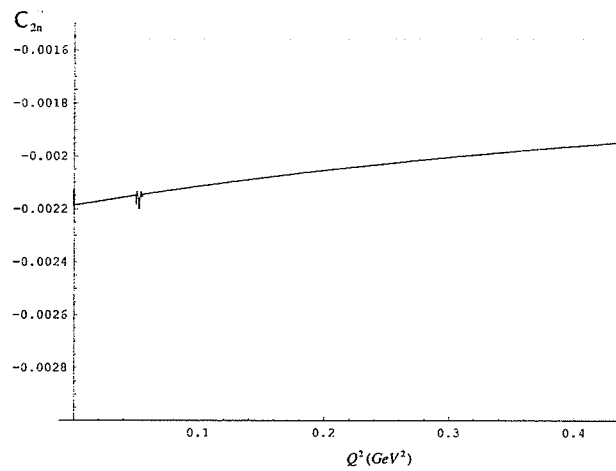
Figure 5: Axial part of the contribution to the neutron's weak charge coming from the $\{\gamma - Z\}$ boxes.
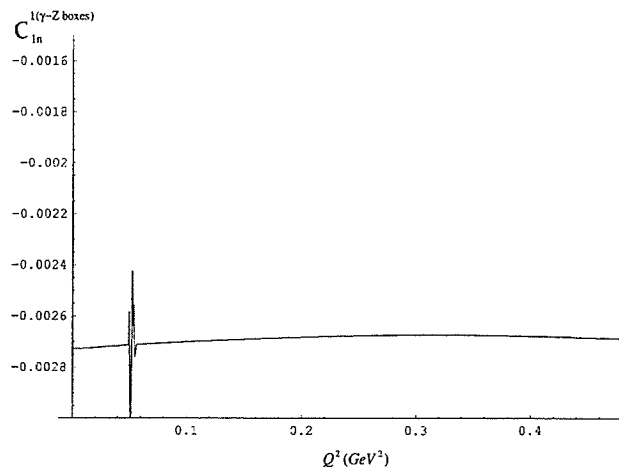
Figure 6: Vector part of the contribution to the neutron's weak charge coming from the $\{\gamma - Z\}$ boxes.
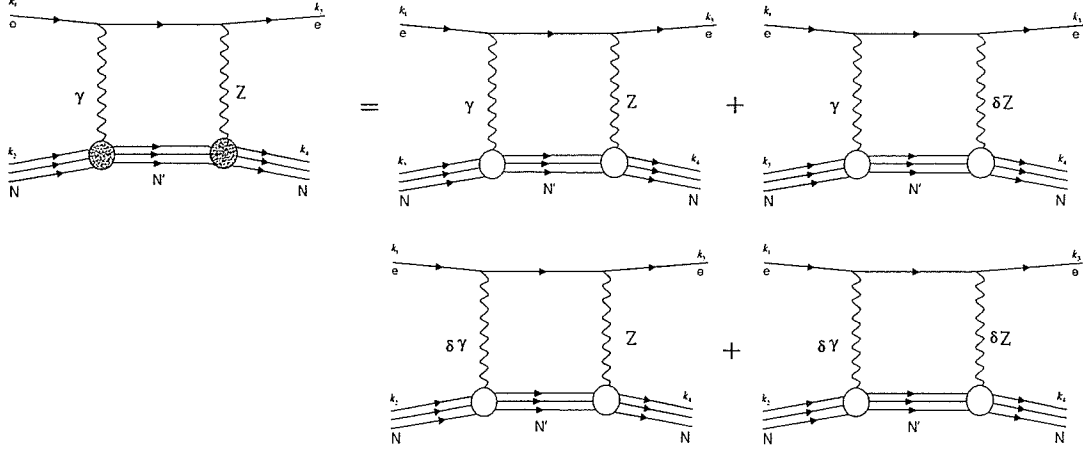
Figure 7: Expansion of the $\{\gamma - Z\}$ box in terms of $\{\delta\gamma, \delta Z\}$ particles.

Explicitly, in the right-hand side of Eq. (121) is written in the form

$$
\frac{1}{D_1 D_2} = \left(\begin{array}{c} \frac{\Lambda^2}{\left(\Lambda^2 - m_Z^2\right)} \frac{1}{q^2} \frac{1}{(p_2+q-k_2)^2 - m_Z^2} + \\ \\ \frac{-\Lambda^2}{\left(\Lambda^2 - m_Z^2\right)} \frac{1}{q^2-\Lambda^2} \frac{1}{(p_2+q-k_2)^2 - m_Z^2} \end{array} \right) + \left(\begin{array}{c} \frac{-\Lambda^2}{\left(\Lambda^2 - m_Z^2\right)} \frac{1}{q^2} \frac{1}{(p_2+q-k_2)^2 - \Lambda^2} + \\ \\ \frac{\Lambda^2}{\left(\Lambda^2 - m_Z^2\right)} \frac{1}{q^2-\Lambda^2} \frac{1}{(p_2+q-k_2)^2 - \Lambda^2} \end{array} \right) \tag{131}
$$

each of the four terms can be interpreted as giving a contribution identical to the contribution coming from the point-like nucleon with nonzero magnetic moment defined at tree level. Also, in this consideration, the couplings between nucleon and vector boson are adjusted by the factor $\pm\sqrt{\frac{\Lambda^2}{\left(\Lambda^2 - m_Z^2\right)}}$, and the structure of the second, third and fourth terms suggests the introduction of "new" vector boson particles $\{\delta\gamma, \delta Z\}$ with fixed masses equal to $m_{\{\delta\gamma,\delta Z\}} = \Lambda$. A diagrammatic representation of the proposed expansion is given by the set of Feynman graphs in Fig. (7). The

already developed and tested automated approach used in the one-quark radiative corrections (Ref. [7]) can be used here as well to complete the calculations of the radiative corrections and weak charges. In this case, however, to consider electron nucleon scattering, one should add additional massive vector boson into the Standard Model. In addition, the set of the Feynman rules (see section "Feynman Rules") will be modified in the following way:

1. Each coupling in the vertex $\{N - V - N\}$ has to be multiplied by $B^{\{\gamma, Z, W^{\pm}\}-N} = + \left(\dfrac{\Lambda^{2n}}{\prod_{i=1}^{n} \left(\Lambda^2 - m_{V_i}^2 \right)} \right)^{1/n}$ in the case of $V = \{\gamma, Z, W^{\pm}\}$ and by $B^{\{\delta\gamma, \delta Z, \delta W^{\pm}\}-N} = - \left(\dfrac{\Lambda^{2n}}{\prod_{i=1}^{n} \left(\Lambda^2 - m_{V_i}^2 \right)} \right)^{1/n}$ for $V = \{\delta\gamma, \delta Z, \delta W^{\pm}\}$. Here, m_{V_i} corresponds to the mass of the V_i taken from Table (2) (even in the case of $V = \{\delta\gamma, \delta Z, \delta W^{\pm}\}$, masses of the corresponding bosons are $\{0, M_Z, M_{W^{\pm}}\}$), and n is the total number of the couplings between vector bosons and the nucleon in the loop.

2. Propagators have the same structure, where for the case of $V = \{\delta\gamma, \delta Z, \delta W^{\pm}\}$ vector boson carry mass $m_{\{\delta\gamma, \delta Z, \delta W^{\pm}\}} = \Lambda$.

Also, as will be seen later, these Feynman rules are topology dependent, and for the vertex correction graphs rule number 1 will be modified. As for the boxes, we have all we need to complete the automated calculations using the *FormCalc* language. Parts of the code are presented in Appendix 1. The computed contribution to the PV amplitude coming from the boxes (36 in total) and the detailed analysis is presented

75
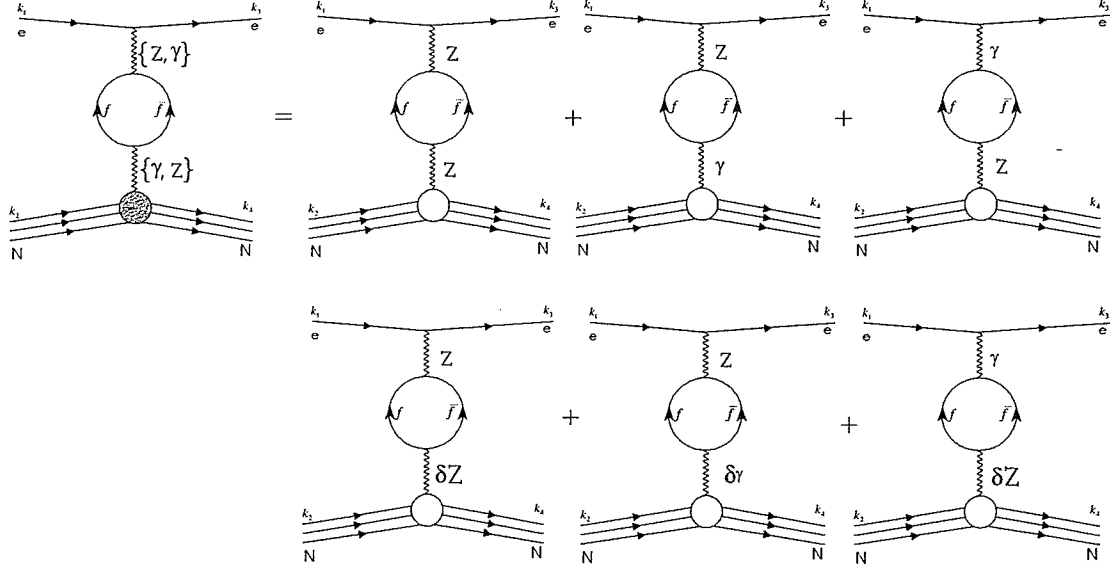
Figure 8: Self-energy graphs giving dominant contribution into PV $\{e - N\}$ amplitude.

in the "Results and Discussion" part of the thesis.

4.5 Self-Energy Graphs

In total, 116 self-energy graphs plus 6 counterterms contribute to the PV $\{e - N\}$ amplitude. This includes gauge and gauge-fixing fields, Higgs field, and virtual leptonic and quark pairs in creation-annihilation processes in the loops. Moreover, the vertex $\{N - V - N\}$ does not belong to the loop integrals and plays the role of a multiplication factor proportional to the coupling defined in Eq. (105) and Eq. (106). As an example, the parity-violating amplitude for $\{Z - \gamma\}$ and $\{Z - \delta\gamma\}$ mixing is

shown below:

$$\mathcal{M}^{\{Z-\gamma\}+\{Z-\delta\gamma\}} = \frac{3i}{16\pi^4} \int d^4q \, \bar{u}(k_3, m_e) \left(g_L^{e-Z} \gamma_\mu \varpi_- + g_R^{e-Z} \gamma_\mu \varpi_+ \right) u(k_1, m_e) \cdot$$

$$\bar{u}(k_4, m_N) \left(g_L^{N-\gamma}(0) \gamma_\nu \varpi_- + g_R^{N-\gamma}(0) \gamma_\nu \varpi_+ - \frac{1}{2} F_2^N(0) \left[\gamma_\nu, (\not{k}_3 - \not{k}_1) \right] \right) u(k_2, m_N) \cdot$$

$$\tag{132}$$

$$\sum_i Tr \left(\begin{array}{c} \frac{m_{f_i} - \not{q}}{q^2 - m_{f_i}^2}, \frac{m_{f_i} + (\not{k}_3 - \not{k}_1 - \not{q})}{(k_3 - k_1 - q)^2 - m_{f_i}^2}, \left(g_L^{f_i-Z} \gamma_\alpha \varpi_- + g_R^{f_i-Z} \gamma_\alpha \varpi_+ \right), \\ \\ \left(g_L^{f_i-\gamma} \gamma_\rho \varpi_- + g_R^{f_i-\gamma} \gamma_\rho \varpi_+ \right) \end{array} \right) \cdot$$

$$\frac{g_{\mu\alpha}}{(k_3 - k_1)^2} \frac{g_{\nu\rho}}{(k_3 - k_1)^2 - m_Z^2} \frac{\Lambda^2}{\Lambda^2 - (k_4 - k_2)^2}.$$

A tensor integral like that in the equation above can be evaluated using tensor decomposition and tensor reduction techniques, leaving the final result as a combination of one and two point scalar integrals which were computed using Gauss integration subroutines. Accordingly, the counterterms should be introduced to cancel ultraviolet divergences, so for Eq. (132) we have:

$$\delta\mathcal{M}^{\{Z-\gamma\}+\{Z-\delta\gamma\}} = i \, \bar{u}(k_3, m_e) \left(g_L^{e-Z} \gamma_\alpha \varpi_- + g_R^{e-Z} \gamma_\alpha \varpi_+ \right) u(k_1, m_e) \cdot$$

$$\bar{u}(k_4, m_N) \left(g_L^{N-\gamma}(0) \gamma_\rho \varpi_- + g_R^{N-\gamma}(0) \gamma_\rho \varpi_+ - \frac{1}{2} F_2^N(0) \left[\gamma_\rho, (\not{k}_3 - \not{k}_1) \right] \right) u(k_2, m_N) \cdot$$

$$\tag{133}$$

$$\begin{pmatrix} \frac{1}{2}i\,\delta Z^{ZA}\,g_{\mu\nu}\,m_Z^2 + \frac{i}{2}\left(\delta Z^{ZA} + \delta Z^{AZ}\right)(k_3 - k_1)_\mu(k_3 - k_1)_\nu + \\ \\ +\frac{i}{2}\left(\delta Z^{ZA} + \delta Z^{AZ}\right)g_{\mu\nu}\,(k_3 - k_1)^2 \end{pmatrix}.$$

$$\frac{g_{\mu\alpha}}{(k_3 - k_1)^2}\frac{g_{\nu\rho}}{(k_3 - k_1)^2 - m_Z^2}\frac{\Lambda^2}{\Lambda^2 - (k_4 - k_2)^2}.$$

Here, δZ^{ZA} and δZ^{AZ} are the $\{\gamma - Z\}$ mixing field renormalization constants represented by the set of Eq. (89-90) according to the constrained differential renormalization scheme described above. The assumption made about "free" quarks in the self-energy loops places certain constraints here. Free quarks are not detected, and we should consider the gluon couplings between them. This leads to a contribution coming from the sector of the color interactions. It is possible to bypass these complications by replacing quarks with pions and their resonances, or use "free" quarks but with adjusted effective masses. Here we used the second approach with the effective mass of the quarks coming from a fit of hadronic vacuum polarization to the measurements of QED cross section of the process $e^+e^- \rightarrow$ hadrons normalized to the QED $e^+e^- \rightarrow \mu^+\mu^-$ cross section. The real part of the renormalized hadronic vacuum polarization satisfies the dispersion relation:

$$\triangle\alpha_{hadr}^\gamma\,(s) = -Re\,\widehat{\Pi}_{had}^\gamma\,(s) = \frac{\alpha}{3\pi}s\int_{4m_\pi^2}^\infty \frac{R^\gamma\,(s')}{s'\,(s' - s)}ds', \tag{134}$$
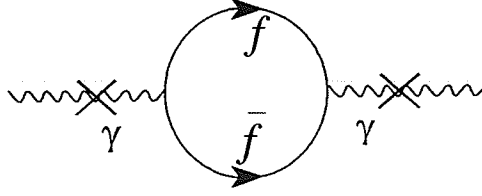
Figure 9: Truncated Self-Energy graph in hadronic vacuum polarization.

with

$$R^\gamma (s) = \frac{\sigma \left(e^+ e^- \to \text{hadrons}\right)}{\sigma \left(e^+ e^- \to \mu^+ \mu^-\right)} \tag{135}$$

being a very well known experimental quantity and used as an input.

Hadronic vacuum polarization $\widehat{\Pi}^\gamma_{had}(s)$ is related to the truncated $\{\gamma - \gamma\}$ renormalized self-energy (See Fig. (9)) by the following expression:

$$\widehat{\sum}^\gamma_{ferm}(s) = s\,\widehat{\Pi}^\gamma_{had}(s) + i\,Im\left(\widehat{\sum}^\gamma_{ferm}(s)\right), \tag{136}$$

which can be easily evaluated by employing the free quark approximation. An updated value of the dispersion integral, along with a logarithmic parametrization, can be taken from Ref. [36]. A new reported value coming from the light quark contribution at $s = m_Z^2$ is $\triangle \alpha^{\gamma(5)}_{hadr}(m_Z^2) = -0.02761$. This value can be reproduced by Eq. (136) using the following masses of the light quarks: $m_u = m_d = 53\,MeV$ (corresponds to $\triangle \alpha^{\gamma(5)}_{hadr}(m_Z^2) = -0.027609$). Clearly, the values of the light quark masses at low-Q scattering processes should be adjusted by using the latter approach, but with $\triangle \alpha^{\gamma(5)}_{hadr}(s)$ calculated at the c.m.s. energy in the region of $\sqrt{s} < 4.0$ (GeV). The

79

$\sqrt{\mathbf{s}}\,(GeV)$	A	B	C
$0.0 - 0.7$	0.0	0.0023092	3.9925370
$0.7 - 2.0$	0.0	0.0022333	4.2191779
$2.0 - 4.0$	0.0	0.0024402	3.2496684
$4.0 - 10.0$	0.0	0.0027340	2.0995092
$10.0 - m_Z$	0.0010485	0.0029431	1.0
$m_Z - 10000.0$	0.0012234	0.0029237	1.0
$10000.0 - 100000.0$	0.0016894	0.0028984	1.0

Table 4: Parametrization coefficients. Results taken from Ref. [36]

simple logarithmic parametrization can be used here to extract quark masses at low momentum transfer:

$$\triangle \alpha_{hadr}^{\gamma(5)}\left(s\right) = A + B \ln \left(1 + C \cdot s\right), \tag{137}$$

with A, B and C parameters taken from the Table 4.

For low-momentum transfer experiments, the c.m.s. energy is $\sqrt{s} < 4.0\ (GeV)$, which gives, $m_u = m_d \simeq 45\,MeV$.

4.6 Vertex Corrections Graphs

The vertex correction ("penguin" graph) contributions can be split into two classes. In the first class, where the electron vertex is at one-loop level, the amplitude is calculated according to the set of Feynman graphs shown in Fig. (10), plus the coun-
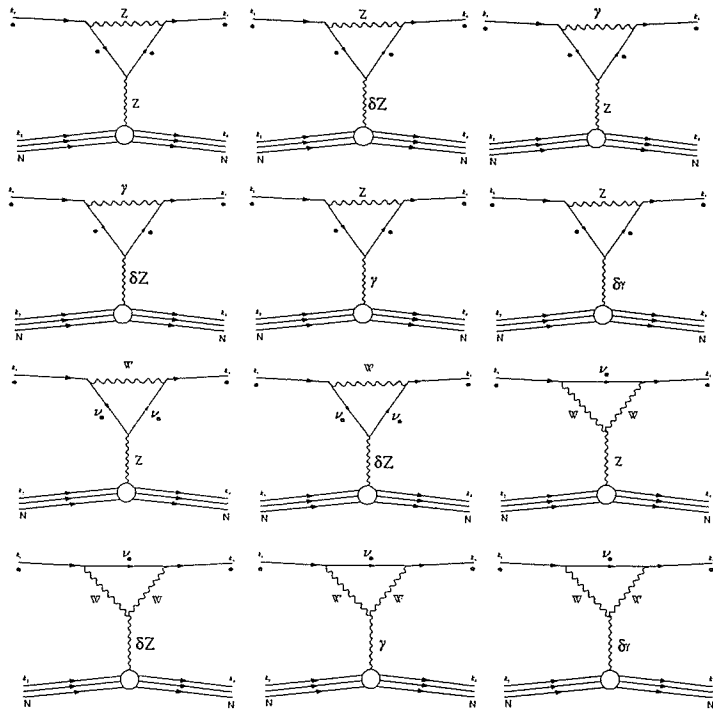
Figure 10: Electron vertex corrections contribution
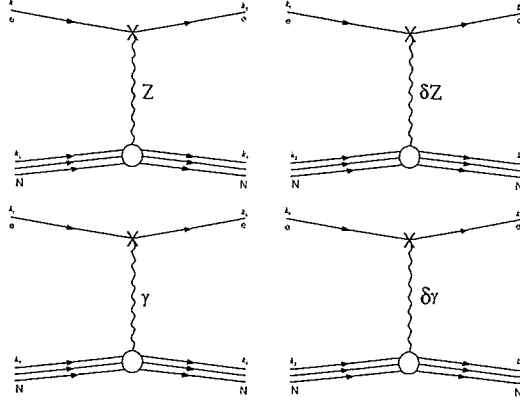
Figure 11: Counterterm in electron vertex corrections

terterms graphs from Fig. (11).

As in the case of the self-energy graphs, the hadronic vertex does not belong to the loop integrals, and therefore the PV amplitude was constructed according to the SM Feynman rules taken from the section "Feynman Rules" with counterterms computed according to Eq. (48) and Eq. (49). Moreover, the electron vertex corrections will have an infrared divergence at $q \to 0$ and will be treated by the soft-photon bremsstrahlung contribution considered later in this work.

The second class of the triangle graphs are nucleonic vertex corrections. In this case, the Feynman rules described above have to be modified due to specifics of the topology of the triangle graphs. To work out the set of Feynman rules for the triangle topology, it is sufficient to consider the example in Fig. (12).
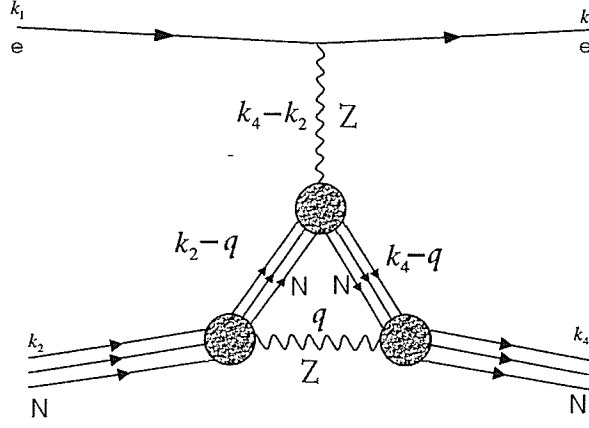
Figure 12: Nucleonic vertex correction graph (shaded bubble corresponds to the real nucleon)

For the graph in Fig. (12), the amplitude denominator has the structure

$$\frac{1}{D_1 D_2 D_3 D_4} = \frac{1}{(k_4 - q)^2 - m_N^2} \frac{1}{(k_2 - q)^2 - m_N^2} \frac{1}{(k_4 - k_2)^2 - m_Z^2} \cdot$$

(138)

$$\frac{\Lambda^2}{(k_4 - k_2)^2 - \Lambda^2} \frac{1}{q^2 - m_Z^2} \frac{\Lambda^4}{(q^2 - \Lambda^2)^2},$$

which can be easily expanded into

$$\frac{1}{D_1 D_2 D_3 D_4} = \frac{1}{(k_4 - q)^2 - m_N^2} \frac{1}{(k_2 - q)^2 - m_N^2} \cdot$$

$$\left(\frac{B^{Z-N}}{(k_4 - k_2)^2 - m_Z^2} + \frac{B^{\delta Z-N}}{(k_4 - k_2)^2 - \Lambda^2} \right) \cdot$$

(139)

$$\lim_{\{\Lambda_1, \Lambda_2\} \to \Lambda} \left(\frac{\left(C^{Z-N} \right)^2}{q^2 - m_Z^2} + \frac{\left(C^{\delta_1 Z-N} \right)^2}{q^2 - \Lambda_1^2} + \frac{\left(C^{\delta_2 Z-N} \right)^2}{q^2 - \Lambda_2^2} \right) \cdot$$
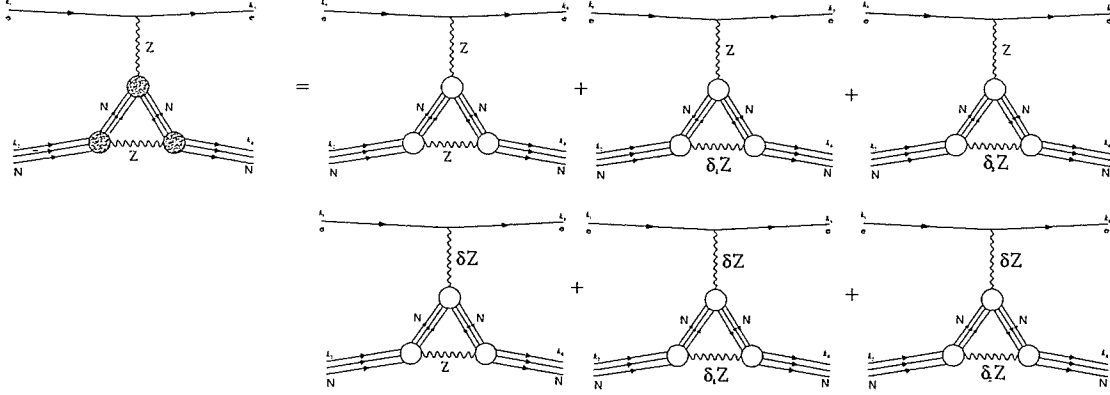
Figure 13: Nucleon vertex expansion in the terms of $\{Z, \delta_1 Z, \delta_2 Z\}$ particles.

Here, the coefficients B^{Z-N} and $B^{\delta Z-N}$ are defined according to the Feynman rules ($n = 1$) described previously. $C^{Z-N}, C^{\delta_1 Z-\Lambda_1}$, and $C^{\delta_2 Z-\Lambda_2}$ can be calculated using the following formulae:

$$\left(C^{Z-N} \right)^2 = \frac{\Lambda^4}{\left(m_Z^2 - \Lambda_1^2 \right) \left(m_Z^2 - \Lambda_2^2 \right)},$$

$$\left(C^{\delta_1 Z-N} \right)^2 = -\frac{\Lambda^4}{m_Z^2 - \Lambda_1^2} \frac{1}{\Lambda_1^2 - \Lambda_2^2},$$

$$\left(C^{\delta_2 Z-N} \right)^2 = -\frac{\Lambda^4}{m_Z^2 - \Lambda_1^2} \left(\frac{1}{m_Z^2 - \Lambda_2^2} - \frac{1}{\Lambda_1^2 - \Lambda_2^2} \right).$$

$$(140)$$

Expansion of the amplitude denominator in Eq. (139) has a simple graphical representation (See Fig. (13)). The latter expansion suggests, in this particular case of the triangle topology, introducing a set of virtual particles $\delta_1 Z$ and $\delta_2 Z$ as a part of SM

in the next to leading order corrections. It is straightforward now to give a set of additional Feynman rules:

1. In the case where a vector boson couples to a nucleon through self-energy interaction, each coupling in the vertex $\{N - V - N\}$ has to be multiplied by

$$C^{\{\gamma, Z, W^\pm\}-N} = \left(\frac{\Lambda^{2n}}{\left(m_{V_i}^2 - \Lambda_1^2\right)\left(m_{V_i}^2 - \Lambda_2^2\right)} \right)^{1/n} \text{ for } V = \{\gamma, Z, W^\pm\}, \text{ by } C^{\{\delta_1\gamma, \delta_1 Z, \delta_1 W^\pm\}-N} =$$

$$i\left(\frac{\Lambda^{2n}}{\left(m_Z^2 - \Lambda_1^2\right)\left(\Lambda_1^2 - \Lambda_2^2\right)} \right)^{1/n} \text{ for } V = \{\delta_1\gamma, \delta_1 Z, \delta_1 W^\pm\}, \text{ and by } C^{\{\delta_2\gamma, \delta_2 Z, \delta_2 W^\pm\}-N} =$$

$$i\left(\frac{\Lambda^{2n}}{\left(m_Z^2 - \Lambda_1^2\right)} \left(\frac{1}{m_Z^2 - \Lambda_2^2} - \frac{1}{\Lambda_1^2 - \Lambda_2^2} \right) \right)^{1/n} \text{ for } V = \{\delta_2\gamma, \delta_2 Z, \delta_2 W^\pm\}. \text{ Here, } m_{V_i} \text{ corresponds to the mass of the } V_i \text{ taken from Table (2) (here, even in the case}$$

of $V = \{\delta_1\gamma, \delta_1 Z, \delta_1 W^\pm\}$ or $V = \{\delta_2\gamma, \delta_2 Z, \delta_2 W^\pm\}$, masses of corresponding bosons are $\{0, M_Z, M_{W^\pm}\}$), and n is the total number of couplings between vector bosons (the vector boson should be part of the loop) and the nucleon in the loop ($n = 2$ in the triangle graphs case).

2. Propagators have the same structure, where for the case of $V = \{\delta_1\gamma, \delta_1 Z, \delta_1 W^\pm\}$ vector bosons carry mass $m_{\{\delta_1\gamma, \delta_1 Z, \delta_1 W^\pm\}} = \Lambda_1$, and for $V = \{\delta_2\gamma, \delta_2 Z, \delta_2 W^\pm\}$ the masses are $m_{\{\delta_2\gamma, \delta_2 Z, \delta_2 W^\pm\}} = \Lambda_2$.

3. Particles $\{\delta_1\gamma, \delta_1 Z, \delta_1 W^\pm\}$ and $\{\delta_2\gamma, \delta_2 Z, \delta_2 W^\pm\}$ do not couple to any other particles except the nucleon. Couplings of the type $\{W^\pm - \{\gamma, Z\} - W^\pm\}$, $\{W^\pm - \{\gamma, Z\} - \delta W^\pm\}$ and $\{\delta W^\pm - \{\gamma, Z\} - W^\pm\}$ are the same as in the case of the couplings of the three vector bosons $V_\mu(k_1) - V_\nu(k_2) - V_\alpha(k_3)$ defined

85

in the Standard Model.

Although ultraviolet divergences are absent in the nucleonic vertex corrections due to the additional terms proportional to $\frac{\Lambda^2}{q^2-\Lambda^2}$ in the coupling, it is still necessary to compute the counterterm amplitude. The coupling defined in Eq. (109) has a counterterm part at the one-loop level represented by the column matrix $\begin{pmatrix} G_{1L}^{f-V} \\ G_{1R}^{f-V} \\ G_{2L}^{f-V} \\ G_{2R}^{f-V} \end{pmatrix}$,

which can be replaced by

$$\begin{pmatrix} G_{1L}^{f-V} \\ G_{1R}^{f-V} \\ G_{2L}^{f-V} \\ G_{2R}^{f-V} \end{pmatrix} = \begin{pmatrix} g_L^{f-Z}\,\mathrm{Re}[\delta\,f_L^N] \\ g_R^{f-Z}\,\mathrm{Re}[\delta\,f_R^N] \\ -\frac{1}{4m_N}F_2^{V-N}\,(q)\,\mathrm{Re}[\delta\,f_L^N] \\ -\frac{1}{4m_N}F_2^{V-N}\,(q)\,\mathrm{Re}[\delta\,f_R^N] \end{pmatrix}. \tag{141}$$

Here, we have used the fact that at $\{N-V-N\}$ vertex, parts of the counterterm coupling related to the $\delta Z'_{V_i,V_j}$ mixing are defined by

$$(\delta Z')^{V_i,V_j} = \left[\left(C^{\{\gamma,Z,W^{\pm}\}-N}\right)^2 \delta Z^{V_i,V_j} + \left(C^{\{\delta_1\gamma,\delta_1 Z,\delta_1 W^{\pm}\}-N}\right)^2 \delta Z^{\delta_1 V_i,V_j} + \right.$$
$$\left. + \left(C^{\{\delta_2\gamma,\delta_2 Z,\delta_2 W^{\pm}\}-N}\right)^2 \delta Z^{\delta_2 V_i,V_j} \right] = \tag{142}$$
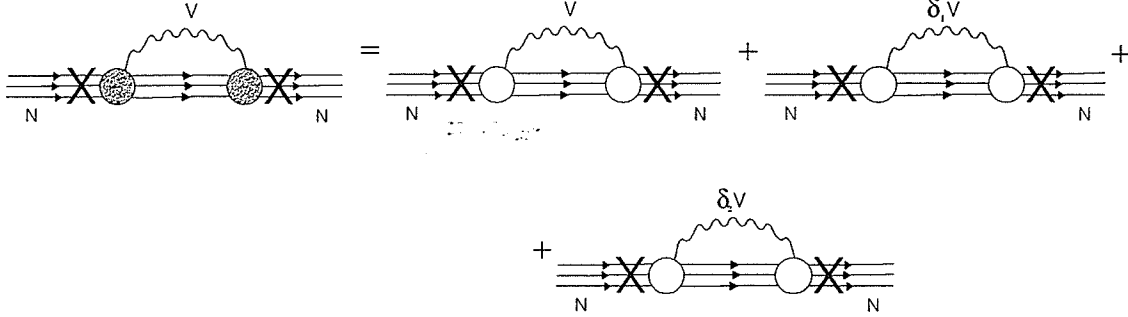
Figure 14: Nucleonic field renormalization expansion.

$$= \pm 2 \left[\begin{array}{c} \left(C^{\{\gamma, Z, W^\pm\} - N} \right)^2 + \left(C^{\{\delta_1 \gamma, \delta_1 Z, \delta_1 W^\pm\} - N} \right)^2 + \\ \\ + \left(C^{\{\delta_2 \gamma, \delta_2 Z, \delta_2 W^\pm\} - N} \right)^2 \end{array} \right] \text{Re} \left(\frac{\Sigma_\perp^{V_i, V_j} \left(m_{V_j}^2 \right)}{m_{V_j}^2} \right).$$

This can be justified by the fact that all of the vector bosons field renormalization constants are defined by the truncated self-energy graphs at $k^2 = m_{V_i}^2$ and that all of them will have the same contribution. A property $\left(C^{\{\gamma, Z, W^\pm\} - N} \right)^2 +$ $\left(C^{\{\delta_1 \gamma, \delta_1 Z, \delta_1 W^\pm\} - N} \right)^2 + \left(C^{\{\delta_2 \gamma, \delta_2 Z, \delta_2 W^\pm\} - N} \right)^2 = 0$ will leave the counterterm amplitude only with the nucleonic field renormalization constants computed through the expansion given by Fig. (14). As well as in the case of electron vertex corrections, the nucleon vertex will have an infrared divergence at the pole $q \to 0$. A detailed discussion of the treatment of this type of divergence is given in the next section.

5 Bremsstrahlung Effects

The contribution of soft-photon emission to the asymmetry was calculated in Ref. [7],

giving final results that are free of infrared divergences. However, even after remov-

ing IR divergences through soft-photon emission corrections, calculated one-quark

radiative corrections show a logarithmic dependence on the detector's photon accep-

tance parameter ΔE. Elimination of this dependence can be achieved by adding

the hard-photon bremsstrahlung[3] (HPB) term. For one-quark radiative corrections,

the HPB term is hard to account for due to the poorly known quark dynamics. In

the case of the HPB computation for electron-proton scattering, we can avoid the

theoretical problem of having to know detailed quark dynamics by representing cu-

mulative quark dynamics directly through an experimentally determined set of form

factors. Using the monopole approximation, we modify general electroweak couplings

by inserting appropriate form factors into vertices and construct a HPB factor as a

function of Mandelstam invariants. For each set of experimental constraints, integra-

tion over emitted photon phase space can be performed numerically. We provide ab

initio numerical results for SAMPLE (Ref. [10]), (Ref. [11]), HAPPEX (Ref. [12]), G0

(Ref. [13]), A4 (Ref. [14]), and Q-Weak (Ref. [15]) experiments.

The present chapter on bremsstrahlung effects can be considered as methodologi-

---

[3] Although SPB and HPB are parts of the same photon emission process, in the SPB approximation momentum of the emitted photon is negligibly small to account in the numerator algebra. Generally, we can approximate SPB as $2 \to 2$ process, which is not possible for HPB emission.

cal, where electron-proton scattering is considered as an example. The same technique of treating IR divergences can be expanded to many other processes. We describe both hard- and soft-photon emission treatment, starting with the latter.

5.1 Soft-Photon Bremsstrahlung

The independence of the soft-photon emission amplitude from the magnetic part of the hadronic current, and more generally from any form factors in photon-nucleon coupling, makes the soft-photon approximation universal and applicable for almost any radiative process. The diagrams responsible for cancellation of IR divergences in one-loop parity violating radiative corrections are shown in Fig. (15).

Generally, bremsstrahlung diagrams can be described as $(2 \rightarrow 3)$ processes in which the integration over the emitted photon's phase space should be performed. If the momentum of the emitted photon is small enough to be neglected in the numerator algebra, we can present the bremsstrahlung cross section as a soft-photon factor multiplied by the tree level cross section of $(2 \rightarrow 2)$ process.

Let us consider a corresponding example. The scattering amplitude for the first diagram of Fig. (15) has the following structure:

$$M_1 = \langle \overline{u}(m_e, k_3) | \, \Gamma_{Z-e}^{\nu} \, | u(m_e, k_1) \rangle \cdot$$

$$\tag{143}$$

$$\langle \overline{u}(m_N, k_4) | \, \Gamma_{Z-N}^{\mu}(q) \frac{\not{k}_2 - \not{k}_5 + m_N}{(k_2 - k_5)^2 - m_N^2} \Gamma_{\gamma-N}^{\alpha}(k_5) \, | u(m_N, k_2) \rangle \cdot$$

89
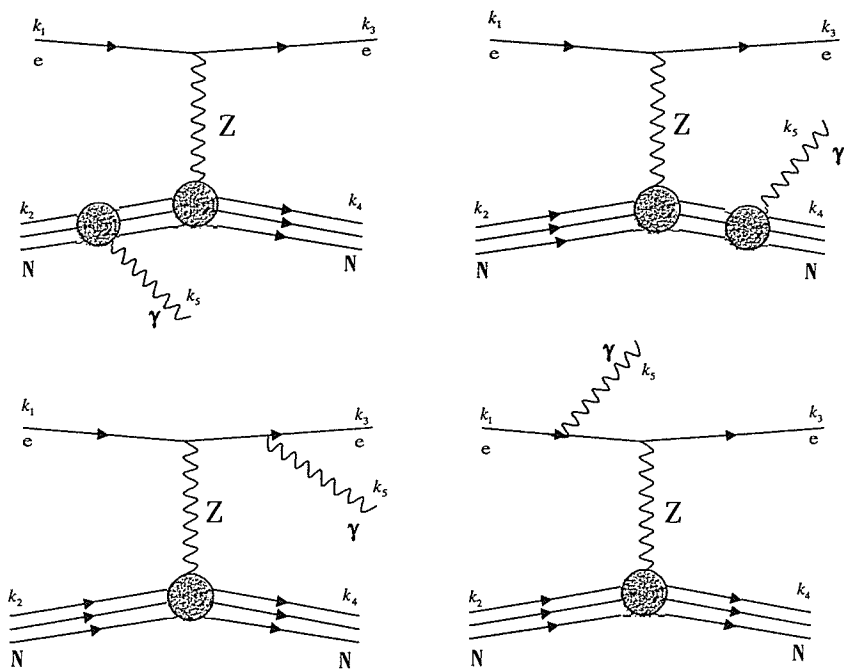
Figure 15: Photo emission diagrams

$$\frac{g_{\mu\nu}}{(k_4 - k_2 + k_5)^2 - m_Z^2} \varepsilon_\alpha^*(k_5),$$

where the photon polarization vector enters as $\varepsilon_\alpha(k_5)$; Γ_{Z-e}^ν, Γ_{Z-N}^μ and $\Gamma_{\gamma-N}^\alpha$ are the couplings of electron with Z boson, nucleon with Z boson, and photon with nucleon, respectively, defined as

$$\Gamma_{Z-e}^\nu \quad = \quad ie\left[-\frac{1 - 2s^2}{2c_w\,s_w}\gamma^\nu\varpi_- + \frac{s_w}{c_w}\gamma^\nu\varpi_+\right],$$

$$\Gamma_{Z-N}^\mu(q) \quad = \quad ie\left[f_1^N(q)\gamma^\mu + \frac{i}{2m_N}\sigma^{\mu\rho}q_\rho\,f_2^N(q) + g_1^N(q)\gamma^\mu\gamma_5\right], \qquad (144)$$

$$\Gamma_{\gamma-N}^\alpha(k_5) \quad = \quad ieQ\left[F_1^N(k_5)\gamma^\alpha + \frac{i}{2m_N}\sigma^{\alpha\rho}(-k_5)_\rho F_2^N(k_5)\right].$$

For the form factors $f_{1,2}^N(q)$, $F_{1,2}^N(k_5)$, and $g_1^N(q)$ we have used

$$f_{1,2}^N(q) \quad = \quad \frac{1}{4s_w\,c_w}\left(F_{1,2}^{V(N)}(0) - 4s_w^2 F_{1,2}^N(0)\right)\frac{\Lambda^2}{\Lambda^2 - q^2},$$

$$F_{1,2}^N(k_5) \quad = \quad F_{1,2}^N(0)\frac{\Lambda^2}{\Lambda^2 - k_5^2} = F_{1,2}^N(0),$$

$$\tag{145}$$

$$F_{1,2}^{V(n)}(0) \quad = \quad F_{1,2}^n(0) - F_{1,2}^p(0), \quad F_{1,2}^{V(p)}(0) = F_{1,2}^p(0) - F_{1,2}^n(0),$$

$$g_1^N(q) \quad = \quad -\frac{g_A^N(0)}{4s_w\,c_w}\frac{\Lambda^2}{\Lambda^2 - q^2},$$

with $F_{1,2}^N(0)$ and $g_A^N(0)$ defined as the nucleon's Dirac, Pauli, and axial form factors at zero momentum transfer, respectively.

In the soft-photon emission approximation the coupling $\Gamma_{\gamma-N}^\alpha(k_5)$ becomes equal to $ieQ\gamma^\alpha$. The numerator of the nucleon's propagator $\not{k}_2 - \not{k}_5 + m_N$ can be replaced by $\not{k}_2 + m_N$, and $(k_2 - k_5)^2 - m_N^2$ can be easily simplified into $-2(k_2 \cdot k_5)$. Using the Dirac equation for free spinors, we have

$$\frac{\not{k}_2 + m_N}{-2(k_2 \cdot k_5)} ieQ\gamma^\alpha \left| u(m_N, k_2) \right\rangle \varepsilon_\alpha^*(k_5) = -ieQ \frac{\not{k}_2 \gamma^\alpha + \gamma^\alpha \not{k}_2}{2(k_2 \cdot k_5)} \left| u(m_N, k_2) \right\rangle \varepsilon_\alpha^*(k_5) =$$

(146)

$$= -ieQ \frac{(k_2 \cdot \varepsilon^*(k_5))}{(k_2 \cdot k_5)} \left| u(m_N, k_2) \right\rangle .$$

Now we can present the soft-photon amplitude in the following form:

$$M_1^{soft} = \left\langle \overline{u}(m_e, k_3) \right| \Gamma_{Z-e}^\nu \left| u(m_e, k_1) \right\rangle \left\langle \overline{u}(m_N, k_4) \right| \Gamma_{Z-N}^\mu(q) \left| u(m_N, k_2) \right\rangle$$

(147)

$$\frac{g_{\mu\nu}}{(k_4 - k_2 + k_5)^2 - m_Z^2} \left(-ieQ \frac{(k_2 \cdot \varepsilon^*(k_5))}{(k_2 \cdot k_5)} \right) =$$

$$= M_0 \left(-ieQ \frac{(k_2 \cdot \varepsilon^*(k_5))}{(k_2 \cdot k_5)} \right) .$$

Here, M_0 is a tree level amplitude of $(2 \rightarrow 2)$ process. Eq. (147) can be used for the other photon emission diagrams with a different factor $\left(\pm ieQ_i \frac{(k_i \cdot \varepsilon^*(k_5))}{(k_i \cdot k_5)} \right)$. As one can see, M_1^{soft} does not depend on the magnetic part. This is a very important result.

The independence of soft-photon emission amplitude from the magnetic part, and generally from any form factors in photon-nucleon coupling, makes the soft-photon approximation universal and applicable for almost any radiative process.

We can sum over all four graphs in Fig. (15) and square the total amplitude to get the following:

$$\left| M_1^{soft} \right|^2 = |M_0|^2\, e^2 \left| \frac{(k_1 \cdot \varepsilon^*(k_5))}{(k_1 \cdot k_5)} - Q\frac{(k_2 \cdot \varepsilon^*(k_5))}{(k_2 \cdot k_5)} - \frac{(k_3 \cdot \varepsilon^*(k_5))}{(k_3 \cdot k_5)} + Q\frac{(k_4 \cdot \varepsilon^*(k_5))}{(k_4 \cdot k_5)} \right|^2 .$$

(148)

The photon couples to a current which is conserved: $k^\mu M_\mu = 0$. This fact, and the summation over all photon polarizations, gives us the possibility to replace $\sum_\varepsilon (k_i)^\mu (k_j)^\nu \varepsilon_\mu^* \varepsilon_\nu$ with $-g_{\mu\nu}(k_i)^\mu(k_j)^\nu = -(k_i \cdot k_j)$. The last step is to integrate over the emitted photon phase space $d\Gamma_{k_5} = \frac{d^3 k_5}{(2\pi^3)\, 2k_5^0}$ and regularize the infrared divergence by assigning to the photon a small rest mass λ. This dependence on the rest mass of the photon will be canceled when added to the IR divergent radiative corrections, and the final radiative corrections will be free of IR divergences. The resulting soft-photon emission differential cross section is expressed as

$$d\sigma_{soft} = (d\sigma_0)_{(2\to 2)} \left(-\frac{\alpha^2}{2\pi^2}\right) \int_{|k_5| \le \Delta E} \frac{d^3 k_5}{2\sqrt{k_5^2 + \lambda^2}} \left(\begin{array}{c} \frac{k_1}{(k_1 \cdot k_5)} - Q\frac{k_2}{(k_2 \cdot k_5)} - \\[2ex] \frac{k_3}{(k_3 \cdot k_5)} + Q\frac{k_4}{(k_4 \cdot k_5)} \end{array} \right)^2 =$$

$$= (d\sigma_0)_{(2\to 2)} \left(-\frac{\alpha^2}{2\pi^2}\right) \left(2m_e^2\, I(k_1, k_1) - (2m_e^2 - t)\, I(k_1, k_3) + 2Q^2 m_N^2\, I(k_2, k_2) - \right.$$

93

$$Q^2(2m_N^2 - t)\, I\,(k_2, k_4) - 2Q\,(u - m_e^2 - m_N^2)\, I\,(k_1, k_4) - 2(s - m_e^2 - m_N^2)\, I\,(k_1, k_2))$$

$$= \ (d\sigma_0)_{(2\to2)} \cdot \delta_{soft}. \tag{149}$$

Here, ΔE is the maximum possible energy of the emitted photon where the soft-photon approximation is still valid. Numerical analysis leads to the condition $\lambda < \Delta E \le 10^{-3} E_{cms}$.

$I\,(k_i, k_j) = \int_{|k_5| \le \Delta E} \frac{d^3 k_5}{2\sqrt{k_5^2 + \lambda^2}} \frac{1}{(k_i \cdot k_5)(k_j \cdot k_5)}$ is the soft-photon emission integral evaluated earlier by Ref. [37], and is equal to

$$I\,(k_i, k_j) = \frac{2\pi\alpha_{ij}}{\alpha_{ij}^2 m_i^2 - m_j^2} \left[\begin{array}{c} \frac{1}{2}Ln\left(\frac{\alpha_{ij}^2 m_i^2}{m_j^2}\right) Ln\left(\frac{4\Delta E^2}{\lambda^2}\right) + \frac{1}{4}Ln^2\left(\frac{E_i - |k|_i}{E_i + |k|_i}\right) - \frac{1}{4}Ln^2\left(\frac{E_j - |k|_j}{E_j + |k|_j}\right) + \\[2ex] Li_2\left(1 - \frac{\alpha_{ij}}{v_{ij}}\left(E_i + |k|_i\right)\right) + Li_2\left(1 - \frac{\alpha_{ij}}{v_{ij}}\left(E_i - |k|_i\right)\right) - \\[2ex] Li_2\left(1 - \frac{1}{v_{ij}}\left(E_j + |k|_j\right)\right) - Li_2\left(1 - \frac{1}{v_{ij}}\left(E_j - |k|_j\right)\right), \end{array} \right]$$
$$\tag{150}$$

where $v_{ij} = \frac{\alpha_{ij}^2 m_i^2 - m_j^2}{2\alpha_{ij} E_i - E_j}$, and E_i, $|k|_j$ are the fermion's energy and spatial momentum in the center of mass reference frame, respectively. The parameter α_{ij} can be extracted from Table (5) . We expect the dependence on ΔE to be canceled as a result of adding the soft- and hard-photon emission differential cross sections. It is worthwhile to mention here that $d\sigma_{soft}$ is proportional to $(d\sigma_0)_{(2\to2)}$ which makes it possible to

94

i	j	m_i	m_j	α_{ij}
1	1	m_e	m_e	1
2	2	m_q	m_q	1
1	3	m_e	m_e	$1 - \frac{t}{2m_e^2} + \frac{\sqrt{t^2-4tm_e^2}}{2m_e^2}$
2	4	m_q	m_q	$1 - \frac{t}{2m_f^2} + \frac{\sqrt{t^2-4tm_f^2}}{2m_f^2}$
1	4	m_e	m_q	$\frac{m_e^2+m_f^2-u+\sqrt{\left(u-m_e^2-m_f^2\right)^2-4m_e^2m_f^2}}{2m_e^2}$
1	2	m_e	m_q	$\frac{s-m_e^2-m_f^2+\sqrt{\left(m_e^2+m_f^2-s\right)^2-4m_e^2m_f^2}}{2m_e^2}$

Table 5: Soft-photon emission integral parameters of Eq.(149)

insert the soft-photon factor δ_{soft} into radiative corrections and to treat them from IR divergences:

$$\tilde{R}_V \equiv R_V + \frac{1}{2}\delta_{soft}, \tag{151}$$

$$\tilde{R}_A \equiv R_A + \frac{1}{2}\delta_{soft}.$$

Here R_V and R_A correspond to the radiative corrections defined as

$$R_V = \frac{C_{1N}^1}{C_{1N}^0}$$

$$\tag{152}$$

$$R_A = \frac{C_{2N}^1}{C_{2N}^0}.$$

However, in the case of hard-photon emission, parametrization in this simple way is not possible, which makes it harder to get rid of radiative corrections of the photon

95

detector acceptance ΔE.

5.2 Hard-Photon Bremsstrahlung

This section gives details on the evaluation of the hard-photon bremsstrahlung differential cross section. The results are expressed in a form convenient for further analysis.

5.2.1 Electron-Nucleon Scattering

In the case where the momentum of the photon ($k_5^0 > \Delta E$) can no longer be neglected in the numerator algebra, we have to account for all the differences between hard- and soft-photon emission. Besides the fact that the hard-photon amplitude will have k_5 in the numerator, calculations for the differential cross section will have to include matrix elements with different helicity. These matrix elements come from the use of the momentum conservation law for $(2 \rightarrow 3)$ process. Thus, the helicity matrix elements will depend on the extended set of Mandelstam variables:

$$
\begin{aligned}
s &= (k_1 + k_2)^2, \ s' = (k_3 + k_4)^2, \\
t &= (k_1 - k_3)^2, \ t' = (k_2 - k_4)^2, \\
u &= (k_1 - k_4)^2, \ u' = (k_2 - k_3)^2.
\end{aligned}
\tag{153}
$$

96

Let us start with the total amplitude for the set of the graphs in Fig. (15):

$$
M_{tot}^{2\to3} = \left(\begin{array}{c} \langle \overline{u}_e(k_3) | \, \Gamma_{Z-e}^{\nu} \, | u_e(k_1) \rangle \cdot \\[2ex] \cdot \langle \overline{u}_N(k_4) | \, \Gamma_{Z-N}^{\mu}(t) \frac{\not{k}_2 - \not{k}_5 + m_N}{(k_2-k_5)^2 - m_N^2} \Gamma_{\gamma-N}^{\alpha}(k_5) \, | u_N(k_2) \rangle \end{array} \right) \frac{g_{\mu\nu}}{t - m_Z^2} \varepsilon_{\alpha}^{*}(k_5)
$$
$$
+
$$
$$
\left(\begin{array}{c} \langle \overline{u}_e(k_3) | \, \Gamma_{Z-e}^{\nu} \, | u_e(k_1) \rangle \cdot \\[2ex] \cdot \langle \overline{u}_N(k_4) | \, \Gamma_{\gamma-N}^{\alpha}(k_5) \frac{\not{k}_4 + \not{k}_5 + m_N}{(k_4+k_5)^2 - m_N^2} \Gamma_{Z-N}^{\mu}(t) \, | u_N(k_2) \rangle \end{array} \right) \frac{g_{\mu\nu}}{t - m_Z^2} \varepsilon_{\alpha}^{*}(k_5)
$$
$$
+ \qquad\qquad (154)
$$
$$
\left(\begin{array}{c} \langle \overline{u}_e(k_3) | \, \Gamma_{\gamma-e}^{\alpha} \frac{\not{k}_3 + \not{k}_5 + m_e}{(k_3+k_5)^2 - m_e^2} \Gamma_{Z-e}^{\nu} \, | u_e(k_1) \rangle \cdot \\[2ex] \cdot \langle \overline{u}_N(k_4) | \, \Gamma_{Z-N}^{\mu}(t') \, | u_N(k_2) \rangle \end{array} \right) \frac{g_{\mu\nu}}{t' - m_Z^2} \varepsilon_{\alpha}^{*}(k_5)
$$
$$
+
$$
$$
\left(\begin{array}{c} \langle \overline{u}_e(k_3) | \, \Gamma_{Z-e}^{\nu} \frac{\not{k}_1 - \not{k}_5 + m_e}{(k_1-k_5)^2 - m_e^2} \Gamma_{\gamma-e}^{\alpha} \, | u_e(k_1) \rangle \cdot \\[2ex] \cdot \langle \overline{u}_N(k_4) | \, \Gamma_{Z-N}^{\mu}(t') \, | u_N(k_2) \rangle \end{array} \right) \frac{g_{\mu\nu}}{t' - m_Z^2} \varepsilon_{\alpha}^{*}(k_5).
$$

Here, $t' - m_Z^2$ can be replaced by $t - m_Z^2$ due to the fact that $\{t, t'\} \ll m_Z^2$. The evaluation of the total amplitude squared is somewhat cumbersome because it includes calculations of 3136 helicity matrix elements. To avoid complications in the HPB differential cross section, we decided to split the amplitude into two terms: $M_{tot}^{2\to3} = M_0^{2\to3} + M_1^{2\to3}$. Here, $M_0^{2\to3}$ is the total amplitude without dependence on

97

the momentum of the emitted photon in the numerator, and $M_1^{2\to3}$ is everything that

is left up to order $O(k_5)$. Now, the squared amplitude has a very simple form:

$$\left|M_{tot}^{2\to3}\right|^2 = \left|M_0^{2\to3}\right|^2 + 2\left(M_0^{2\to3}\right)^*\left(M_1^{2\to3}\right) + \left|M_1^{2\to3}\right|^2. \qquad (155)$$

The first term of Eq. (155) can be obtained from

$$M_0^{2\to3} = \Lambda^2 M_0' \left(\frac{(k_1\varepsilon^*(k_5))}{(k_1k_5)(\Lambda^2-t')} - Q\frac{(k_2\varepsilon^*(k_5))}{(k_2k_5)(\Lambda^2-t)} - \frac{(k_3\varepsilon^*(k_5))}{(k_3k_5)(\Lambda^2-t')} + Q\frac{(k_4\varepsilon^*(k_5))}{(k_4k_5)(\Lambda^2-t)}\right), \qquad (156)$$

where

$$M_0' = (ie)\,\langle\overline{u}(m_e,k_3)|\,\Gamma_{Z-e}^\nu\,|u(m_e,k_1)\rangle\,\langle\overline{u}(m_N,k_4)|\,\left(\Gamma_{Z-N}^\mu\right)'\,|u(m_N,k_2)\rangle\,\frac{g_{\mu\nu}}{t-m_Z^2}. \qquad (157)$$

The term $\left(\Gamma_{Z-N}^\mu\right)'$ represents a coupling which was modified in a way so it would no

longer have a dependency on the monopole term $\frac{\Lambda^2}{(\Lambda^2-t)}$, and no longer contain the

momentum of the photon in its magnetic part:

$$\left(\Gamma_{Z-N}^\mu\right)' = ie\left[\mathfrak{f}_1^N\gamma^\mu + \frac{i}{2m_N}\sigma^{\mu\rho}(k_4-k_2)_\rho\,\mathfrak{f}_2^N + \mathfrak{g}_1^N\gamma^\mu\gamma_5\right]. \qquad (158)$$

In Eq. (157) and Eq. (156), the coupling $\Gamma_{\gamma-\{e,N\}}^\alpha$ was replaced by $(ieQ)\,\gamma^\alpha$. As for

$\left\{\mathfrak{f}_{1,2}^N,\,\mathfrak{g}_1^N\right\}$, we use Eq. (145) but without the monopole term[4] $\frac{\Lambda^2}{(\Lambda^2-t)}$. It is straight-

forward to see that after the integration over the phase space of the emitted photon

only the amplitude $M_0^{2\to3}$ squared will have a logarithmic dependence on the pho-

ton detector acceptance parameter ΔE. Therefore, $M_0^{2\to3}$ squared, when combined

[4] Alternatively we can define terms $\left\{\mathfrak{f}_{1,2}^N,\,\mathfrak{g}_1^N\right\}$ as formfactors $\left\{f_{1,2}^N(0),\,g_1^N(0)\right\}$ at the zero momentum transfer.

with the soft-photon bremsstrahlung differential cross section, will be responsible for cancellation of the $\log(4\Delta E^2)$ term .

Further numerical analysis shows that the second and third terms of Eq. (155) have no dependence on ΔE. They both are small compared to the first term when the energy of incident electrons is less than 6 GeV. For energies $E_{lab} > 6$ GeV, the second and third terms become non-negligible in the HPB cross section.

We can write the term $|M_0^{2\to3}|^2$ of Eq. (155) in the following form:

$$\left|M_0^{2\to3}\right|^2_{L,R} = -\left|M_0'\right|^2_{L,R}\cdot\delta_{HPB},$$

$$\delta_{HPB} = \frac{\Lambda^4}{(\Lambda^2 - t')^2}\left(m_e^2\left(\frac{1}{(k_1k_5)^2} + \frac{1}{(k_3k_5)^2}\right) - \frac{2m_e^2 - t}{(k_1k_5)(k_3k_5)}\right) +$$

$$(159)$$

$$\frac{Q^2\Lambda^4}{(\Lambda^2 - t)^2}\left(m_N^2\left(\frac{1}{(k_2k_5)^2} + \frac{1}{(k_4k_5)^2}\right) - \frac{2m_N^2 - t'}{(k_2k_5)(k_4k_5)}\right) + \frac{Q\,\Lambda^4}{(\Lambda^2 - t)(\Lambda^2 - t')}\cdot$$

$$\cdot\left(\frac{m_e^2 + m_N^2 - u}{(k_1k_5)(k_4k_5)} - \frac{s - m_e^2 - m_N^2}{(k_1k_5)(k_2k_5)} - \frac{s' - m_e^2 - m_N^2}{(k_3k_5)(k_4k_5)} + \frac{m_e^2 + m_N^2 - u'}{(k_2k_5)(k_3k_5)}\right).$$

The scalar products (k_ik_5) are the Lorentz invariants and can be replaced with the Mandelstam variables as

$$(k_1k_5) = -m_e^2 - m_N^2 + \frac{(s + t + u)}{2},$$

99

$$(k_2 k_5) = -m_e^2 - m_N^2 + \frac{(s + t' + u')}{2},$$

(160)

$$(k_3 k_5) = m_e^2 + m_N^2 - \frac{(s' + t + u')}{2},$$

$$(k_4 k_5) = m_e^2 + m_N^2 - \frac{(s' + t' + u)}{2}.$$

As for $|M_0'|_{L,R}^2$, in the case of the left-handed incident electrons, we have

$$|M_0'|_L^2 = \frac{4\alpha^3 \pi^3 (1 - 2s_w^2)^2}{c_w^2 \, s_w^2 \, (t - m_Z^2)^2} \left(\mathfrak{f}_2^N\right)^2 \left[\frac{\left(\mathfrak{f}_2^N\right)^2}{4m_N^2} (16 m_N^6 - 8 m_N^4 (s + s' + u + u') + \right.$$

$$4 m_N^2 (s + u)(s' + u') + t'(us' - ss' + tt' + su' - uu')) +$$

(161)

$$g_R^{Z-N} \mathfrak{f}_2^N (4 m_N^4 - 4 m_N^2 (u + u') - ss' + tt' + s'u + su' + 3uu') +$$

$$2 \left(g_L^{Z-N}\right)^2 (m_N^2 - s)(m_N^2 - s') + 2 \left(g_R^{Z-N}\right)^2 (m_N^2 - u)(m_N^2 - u') +$$

$$g_L^{Z-N} (4 g_R^{Z-N} m_N^2 \, t + \mathfrak{f}_2^N (4 m_N^4 - 4 m_N^2 (s + s') + 3ss' + tt' + s'u + su' - uu'))],$$

and for the right-handed incident electrons

$$|M_0'|_R^2 = \frac{16\alpha^3 \pi^3 s_w^2}{c_w^2 \, (t - m_Z^2)^2} \left[\frac{\left(\mathfrak{f}_2^N\right)^2}{4m_N^2} (16 m_N^6 - 8 m_N^4 (s + s' + u + u') + \right.$$

100

$$4m_N^2(s+u)(s'+u') + t'(us' - ss' + tt' + su' - uu')) +$$

$$g_R^{Z-N} f_2^N (4m_N^4 - 4m_N^2(s+s') - uu' + tt' + s'u + su' + 3ss') +$$

$$(162)$$

$$2\left(g_R^{Z-N}\right)^2 (m_N^2 - s)(m_N^2 - s') + 2\left(g_L^{Z-N}\right)^2 (m_N^2 - u)(m_N^2 - u') +$$

$$g_L^{Z-N}(4g_R^{Z-N} m_N^2\ t + f_2^N(4m_N^4 - 4m_N^2(u + u') + 3uu' + tt' + s'u + su' - ss'))].$$

For simplicity, we have introduced a set of coupling constants $g_{L,R}^{Z-N}$ defined as

$$g_{R,L}^{Z-N}\ =\ f_1^N \pm \mathfrak{g}_1^N,$$

$$(163)$$

$$\left(\Gamma_{Z-N}^\mu\right)'\ =\ ie\left[g_R^{Z-N}\gamma^\mu\varpi_+ + g_L^{Z-N}\gamma^\mu\varpi_- + \frac{i}{2m_N}\sigma^{\mu\rho}(k_4 - k_2)_\rho\ f_2^N\right],\quad (164)$$

where $\varpi_\pm = \frac{1\pm\gamma_5}{2}$ are the chirality projector operators (see Eq. (44) and the discussion below).

The amplitude $M_1^{2\to3}$ entering expression Eq. (155) has eight terms. Each term is responsible for a different type of product of static or magnetic parts of the $(Z - N)$ coupling. Explicitly, we have :

$$M_1^{2\to3} = \frac{g_{\mu\nu}}{t - m_Z^2}\varepsilon_\alpha^*(k_5) \cdot R$$

101

$$R = \langle \overline{u}_e(k_3) | \, \Gamma^\nu_{Z-e} \, | u_e(k_1) \rangle \, \langle \overline{u}_N(k_4) | \left(\Gamma^\mu_{Z-N} \right)' \frac{(- \slashed{k}_5)}{(k_2 - k_5)^2 - m_N^2} \, (ieQ) \, \gamma^\alpha \, | u_N(k_2) \rangle \, \frac{\Lambda^2}{\Lambda^2 - t}$$

$$+$$

$$\langle \overline{u}_e(k_3) | \, \Gamma^\nu_{Z-e} \, | u_e(k_1) \rangle \, \langle \overline{u}_N(k_4) | \, (ieQ) \, \gamma^\alpha \frac{\slashed{k}_5}{(k_4 + k_5)^2 - m_N^2} \left(\Gamma^\mu_{Z-N} \right)' | u_N(k_2) \rangle \, \frac{\Lambda^2}{\Lambda^2 - t}$$

$$+$$

$$\langle \overline{u}_e(k_3) | \, \Gamma^\alpha_{\gamma-e} \frac{\slashed{k}_5}{(k_3 + k_5)^2 - m_e^2} \Gamma^\nu_{Z-e} \, | u_e(k_1) \rangle \, \langle \overline{u}_N(k_4) | \left(\Gamma^\mu_{Z-N} \right)' | u_N(k_2) \rangle \, \frac{\Lambda^2}{\Lambda^2 - t'}$$

$$+ \tag{165}$$

$$\langle \overline{u}_e(k_3) | \, \Gamma^\nu_{Z-e} \frac{(- \slashed{k}_5)}{(k_1 - k_5)^2 - m_e^2} \Gamma^\alpha_{\gamma-e} \, | u_e(k_1) \rangle \, \langle \overline{u}_N(k_4) | \left(\Gamma^\mu_{Z-N} \right)' | u_N(k_2) \rangle \, \frac{\Lambda^2}{\Lambda^2 - t'}$$

$$+$$

$$\left(\begin{array}{c} \langle \overline{u}_e(k_3) | \, \Gamma^\nu_{Z-e} \, | u_e(k_1) \rangle \cdot \\[2ex] \cdot \langle \overline{u}_N(k_4) | \, (-e) \frac{\sigma^{\mu\rho} f_2^N}{2m_N} \, (k_5)_\rho \frac{\slashed{k}_2 + m_N}{(k_2 - k_5)^2 - m_N^2} \, (ieQ) \, \gamma^\alpha \, | u_N(k_2) \rangle \end{array} \right) \frac{\Lambda^2}{\Lambda^2 - t}$$

$$+$$

$$\left(\begin{array}{c} \langle \overline{u}_e(k_3) | \, \Gamma^\nu_{Z-e} \, | u_e(k_1) \rangle \cdot \\[2ex] \cdot \langle \overline{u}_N(k_4) | \, (ieQ) \, \gamma^\alpha \frac{\slashed{k}_4 + m_N}{(k_4 + k_5)^2 - m_N^2} \, (-e) \frac{\sigma^{\mu\rho} f_2^N}{2m_N} \, (k_5)_\rho \, | u_N(k_2) \rangle \end{array} \right) \frac{\Lambda^2}{\Lambda^2 - t}$$

$$+$$

$$\left(\begin{array}{c} \langle \overline{u}_e(k_3) | \, \Gamma^\nu_{Z-e} \, | u_e(k_1) \rangle \cdot \\[2ex] \cdot \langle \overline{u}_N(k_4) | \left(\Gamma^\mu_{Z-N} \right)' \frac{\slashed{k}_2 + m_N}{(k_2 - k_5)^2 - m_N^2} \, (eQ) \frac{\sigma^{\alpha\rho} F_2^N}{2m_N} \, (k_5)_\rho \, | u_N(k_2) \rangle \end{array} \right) \frac{\Lambda^2}{\Lambda^2 - t}$$

$+$

$$\left(\begin{array}{c} \langle \overline{u}_e(k_3)| \, \Gamma^\nu_{Z-e} \, |u_e(k_1)\rangle \cdot \\ \\ \langle \overline{u}_N(k_4)| \, (eQ) \, \frac{\sigma^{\alpha\rho} F_2^N}{2m_N} \, (k_5)_\rho \, \frac{\slashed{k}_4 + m_N}{(k_4+k_5)^2 - m_N^2} \left(\Gamma^\mu_{Z-N} \right)' \, |u_N(k_2)\rangle \end{array} \right) \frac{\Lambda^2}{\Lambda^2 - t}$$

The second and third parts of Eq. (155) are too lengthy to show them here explicitly.

We have them analytically expressed in a *Mathematica* file available upon request.

5.2.2 Electron-Quark Scattering

The case of electron-quark scattering is much simpler than the more general electron-nucleon scattering, and can be easily derived. First of all, there is no magnetic part in the coupling. Second, the monopole form factor approximation is no longer required.

Now we have

$$\Gamma^\mu_{Z-q} \;\; = \;\; ie \left[g_R^{Z-q} \gamma^\mu \varpi_+ + g_L^{Z-q} \gamma^\mu \varpi_- \right],$$

$$(166)$$

$$\Gamma^\alpha_{\gamma-q} \;\; = \;\; ieQ\gamma^\alpha,$$

where

$$g_L^{Z-q} \;\; = \;\; \frac{T_3^q - Q\, s_w^2}{s_w\, c_w},$$

$$(167)$$

$$g_R^{Z-q} \;\; = \;\; -Q\frac{s_w}{c_w}.$$

103

Here, T_3^q, Q are quark's isospin and charge, respectively. The amplitude $M_0^{2\to3}$ becomes

$$M_0^{2\to3} = M_0' \left(\frac{(k_1\varepsilon^*(k_5))}{(k_1 k_5)} - Q\frac{(k_2\varepsilon^*(k_5))}{(k_2 k_5)} - \frac{(k_3\varepsilon^*(k_5))}{(k_3 k_5)} + Q\frac{(k_4\varepsilon^*(k_5))}{(k_4 k_5)} \right),$$

(168)

$$M_0' = (ie) \langle \overline{u}(m_e,k_3)| \Gamma_{Z-e}^{\nu} |u(m_e,k_1)\rangle \langle \overline{u}(m_q,k_4)| \Gamma_{Z-q}^{\mu} |u(m_q,k_2)\rangle \frac{g_{\mu\nu}}{t - m_Z^2}.$$

The first term of Eq. (155) for polarized incident electrons can be expressed as

$$\left| M_0^{2\to3} \right|^2_{L,R} = - |M_0'|^2_{L,R} \cdot \delta_{HPB},$$

$$\delta_{HPB} = \left(m_e^2 \left(\frac{1}{(k_1 k_5)^2} + \frac{1}{(k_3 k_5)^2} \right) - \frac{2m_e^2 - t}{(k_1 k_5)(k_3 k_5)} \right) +$$

(169)

$$Q^2 \left(m_q^2 \left(\frac{1}{(k_2 k_5)^2} + \frac{1}{(k_4 k_5)^2} \right) - \frac{2m_q^2 - t'}{(k_2 k_5)(k_4 k_5)} \right) +$$

$$Q \left(\frac{m_e^2 + m_q^2 - u}{(k_1 k_5)(k_4 k_5)} - \frac{s - m_e^2 - m_q^2}{(k_1 k_5)(k_2 k_5)} - \frac{s' - m_e^2 - m_q^2}{(k_3 k_5)(k_4 k_5)} + \frac{m_e^2 + m_q^2 - u'}{(k_2 k_5)(k_3 k_5)} \right),$$

and $|M_0'|^2_{L,R}$ is

$$|M_0'|^2_L = \frac{8\alpha^3\pi^3 (1 - 2s_w^2)^2}{c_w^2 s_w^2 (t - m_Z^2)^2} \left[\begin{array}{c} \left(g_L^{Z-q} \right)^2 (m_N^2 - s)(m_N^2 - s') + \\ + \left(g_R^{Z-q} \right)^2 (m_N^2 - u)(m_N^2 - u') + \\ 2g_L^{Z-q} g_R^{Z-q} m_q^2 \, t \end{array} \right],$$

(170)

104

$$|M_0'|_R^2 = \frac{32\alpha^3\pi^3\,s_w^2}{c_w^2\,(t-m_Z^2)^2}\left[\begin{array}{c}\left(g_R^{Z-q}\right)^2(m_N^2-s)(m_N^2-s')+\\[4pt] +\left(g_L^{Z-q}\right)^2(m_N^2-u)(m_N^2-u')+\\[4pt] 2g_L^{Z-q}\,g_R^{Z-q}m_q^2\,t\end{array}\right].$$

The amplitude $M_1^{2\to3}$ will have only four parts with the following structure:

$$M_1^{2\to3} = \frac{g_{\mu\nu}}{t-m_Z^2}\varepsilon_\alpha^*(k_5)\cdot R,$$

$$
\begin{aligned}
R =\ & \langle\overline{u}_e(k_3)|\,\Gamma_{Z-e}^\nu\,|u_e(k_1)\rangle\,\langle\overline{u}_q(k_4)|\,\Gamma_{Z-q}^\mu\frac{(-\slashed{k}_5)}{(k_2-k_5)^2-m_q^2}\,(ieQ)\,\gamma^\alpha\,|u_q(k_2)\rangle\\[8pt]
& +\\[6pt]
& \langle\overline{u}_e(k_3)|\,\Gamma_{Z-e}^\nu\,|u_e(k_1)\rangle\,\langle\overline{u}_q(k_4)|\,(ieQ)\,\gamma^\alpha\frac{\slashed{k}_5}{(k_4+k_5)^2-m_N^2}\Gamma_{Z-q}^\mu\,|u_q(k_2)\rangle\\[8pt]
& +\\[6pt]
& \langle\overline{u}_e(k_3)|\,\Gamma_{\gamma-e}^\alpha\frac{\slashed{k}_5}{(k_3+k_5)^2-m_e^2}\Gamma_{Z-e}^\nu\,|u_e(k_1)\rangle\,\langle\overline{u}_q(k_4)|\,\Gamma_{Z-q}^\mu\,|u_q(k_2)\rangle\\[8pt]
& + \hspace{7cm}(171)\\[6pt]
& \langle\overline{u}_e(k_3)|\,\Gamma_{Z-e}^\nu\frac{(-\slashed{k}_5)}{(k_1-k_5)^2-m_e^2}\Gamma_{\gamma-e}^\alpha\,|u_e(k_1)\rangle\,\langle\overline{u}_q(k_4)|\,\Gamma_{Z-q}^\mu\,|u_q(k_2)\rangle.
\end{aligned}
$$

Now we can give some details on the $2\left(M_0^{2\to3}\right)^*\left(M_1^{2\to3}\right)$ and $|M_1^{2\to3}|^2$ terms. The electron mass enters into calculations of helicity matrix elements as a small parameter. Using this fact, for $2\left(M_0^{2\to3}\right)^*\left(M_1^{2\to3}\right)$ we derive:

$$2\left(M_0^{2\to3}\right)^*\left(M_1^{2\to3}\right)_{L,R} = \sum_{i=1}^{4}\left[\frac{\mathfrak{M}_i\,(k_1)_{L,R}}{(k_1k_5)}-\frac{Q\mathfrak{M}_i\,(k_2)_{L,R}}{(k_2k_5)}-\frac{\mathfrak{M}_i\,(k_3)_{L,R}}{(k_3k_5)}+\frac{Q\mathfrak{M}_i\,(k_4)_{L,R}}{(k_4k_5)}\right].$$

$$(172)$$

Expressions for $\mathfrak{M}_i(k_j)$ are explicitly listed below. For $k_j = k_1$, we have

$$\sum_{i=1}^{4} \mathfrak{M}_i(k_1)_L = -\frac{8\alpha^3\pi^3(1-2s_w^2)^2}{c_w^2 s_w^2 (t-m_Z^2)^2} \cdot$$

$$[\left(g_L^{Z-q}\right)^2 (m_q^2 - s)(m_q^2 - s') + 2g_L^{Z-q} g_R^{Z-q} m_q^2 t + \left(g_R^{Z-q}\right)^2 (m_q^2 - u)(m_q^2 - u') -$$

$$\frac{Q}{(s+t'+u'-2m_q^2-2m_e^2)} \left(\left(g_L^{Z-q}\right)^2 (m_q^2-s)(m_q^2-s')\varpi_{11} + \left(g_R^{Z-q}\right)^2 (m_q^2-u)\varpi_{21}\right) +$$

$$\frac{Q}{(s'+t'+u-2m_q^2-2m_e^2)} \left(\left(g_L^{Z-q}\right)^2 (m_q^2-s)\varpi_{31} + \left(g_R^{Z-q}\right)^2 (m_q^2-u)(m_q^2-u')\omega_{11}\right) +$$

$$\frac{1}{(s'+t+u'-2m_q^2-2m_e^2)} \left(\begin{array}{c} \left(g_L^{Z-q}\right)^2 (m_q^2-s)\varpi_{31} - 2g_L^{Z-q} g_R^{Z-q} m_q^2 t\varpi_{11}+ \\ \\ + \left(g_R^{Z-q}\right)^2 (m_q^2-u)\varpi_{21} \end{array}\right)],$$

(173)

where coefficients ω_{ij} are

$$\omega_{11} = (2m_q^2 - s - t - u),$$

$$\varpi_{21} = (2m_q^4 - m_q^2(s' - t + 2s + u') + s(s' + u') - t(t' + u')),$$

$$\varpi_{31} = (2m_q^4 - m_q^2(s' - t + 2u + u') - tt' + s'(u - t) + uu').$$

For $k_j = k_2$,

$$\sum_{i=1}^{4} \mathfrak{M}_i(k_2)_L = -\frac{8\alpha^3\pi^3(1-2s_w^2)^2}{c_w^2 s_w^2 (t-m_Z^2)^2} \cdot$$

106

$$[\frac{Q}{(s'+t'+u-2m_q^2-2m_e^2)}\left(\left(g_L^{Z-q}\right)^2(m_q^2-s)\omega_{12}+\left(g_R^{Z-q}\right)^2(m_q^2-u')\omega_{22}\right)+$$

$$\frac{1}{(s+t+u-2m_q^2-2m_e^2)}\left(\begin{array}{c}\left(g_L^{Z-q}\right)^2(m_q^2-s')\omega_{32}+2g_L^{Z-q}g_R^{Z-q}m_q^2\,\varpi_{42}-\\[2ex]-\left(g_R^{Z-q}\right)^2(m_q^2-u')\omega_{22}\end{array}\right)+$$

$$(174)$$

$$\frac{1}{(s'+t+u'-2m_q^2-2m_e^2)}\left(\begin{array}{c}\left(g_L^{Z-q}\right)^2(m_q^2-s)\omega_{12}+2g_L^{Z-q}g_R^{Z-q}m_q^2\,\varpi_{42}-\\[2ex]-\left(g_R^{Z-q}\right)^2(m_q^2-u)\omega_{52}\end{array}\right)+$$

$$\frac{Q}{(s+t'+u'-2m_q^2-2m_e^2)}\left(\left(g_L^{Z-q}\right)^2(m_q^2-s')\omega_{32}+\left(g_R^{Z-q}\right)^2(m_q^2-u)\omega_{52}\right)],$$

with

$$\omega_{12} = (2m_q^4-m_q^2(s'-u+2t+t')+tt'+s'(t'-u')-uu'),$$

$$\omega_{22} = (2m_q^4+m_q^2(s'-2t-t'-u)-s(s'+u)+t'(t+u)),$$

$$\omega_{32} = (6m_q^4-m_q^2(5s+2t+t'+2u+u')+s(s+t'+u')),$$

$$\varpi_{42} = (m_q^2(s+s'-u-u')-s(s'+t)+u'(t+u)),$$

$$\omega_{52} = (6m_q^4-m_q^2(5u'+2t+t'+2s'+s)+u'(s+t'+u')).$$

When $k_j=k_3$, $\mathfrak{M}_i(k_j)$ is given by

$$\sum_{i=1}^{4} \mathfrak{M}_i \, (k_3)_L = -\frac{8\alpha^3 \pi^3 \left(1 - 2s_w^2\right)^2}{c_w^2 \, s_w^2 \, \left(t - m_Z^2\right)^2} \cdot$$

$$[\left(g_L^{Z-q}\right)^2 (m_q^2 - s)(m_q^2 - s') + 2g_L^{Z-q} \, g_R^{Z-q} m_q^2 \, t + \left(g_R^{Z-q}\right)^2 (m_q^2 - u)(m_q^2 - u') -$$

$$\frac{Q}{(s' + t' + u - 2m_q^2 - 2m_e^2)} \left(\left(g_L^{Z-q}\right)^2 (m_q^2 - s)(m_q^2 - s')\varpi_{13} + \left(g_R^{Z-q}\right)^2 (m_q^2 - u')\varpi_{23} \right) +$$

$$\frac{Q}{(s + t' + u' - 2m_q^2 - 2m_e^2)} \left(\left(g_L^{Z-q}\right)^2 (m_q^2 - s')\varpi_{33} + \left(g_R^{Z-q}\right)^2 (m_q^2 - u)(m_q^2 - u')\omega_{13} \right) +$$

$$(175)$$

$$\frac{1}{(s + t + u - 2m_q^2 - 2m_e^2)} \begin{pmatrix} \left(g_L^{Z-q}\right)^2 (m_q^2 - s')\varpi_{33} - 2g_L^{Z-q} \, g_R^{Z-q} m_q^2 \, t\varpi_{13} + \\ \\ + \left(g_R^{Z-q}\right)^2 (m_q^2 - u)\varpi_{23} \end{pmatrix}],$$

where

$$\omega_{13} = (2m_q^2 - s' - t - u'),$$

$$\omega_{23} = (2m_q^4 - m_q^2(s' + 2s' - t + u) + ss' - tt' + u(s' - t)),$$

$$\omega_{33} = (2m_q^4 - m_q^2(s - t + u + 2u') + uu' - tt' + s(u' - t)).$$

And, finally, for $k_j = k_4$ we have

$$\sum_{i=1}^{4} \mathfrak{M}_i \, (k_4)_L = -\frac{8\alpha^3 \pi^3 \left(1 - 2s_w^2\right)^2}{c_w^2 \, s_w^2 \, \left(t - m_Z^2\right)^2} \cdot$$

$$[\frac{Q}{(s+t'+u'-2m_q^2-2m_e^2)}\left(\left(g_L^{Z-q}\right)^2(m_q^2-s')\omega_{14}+\left(g_R^{Z-q}\right)^2(m_q^2-u)\omega_{24}\right)+$$

$$\frac{1}{(s+t+u-2m_q^2-2m_e^2)}\left(\begin{array}{c}\left(g_L^{Z-q}\right)^2(m_q^2-s')\omega_{14}+2g_L^{Z-q}g_R^{Z-q}m_q^2\varpi_{44}-\\\\-\left(g_R^{Z-q}\right)^2(m_q^2-u')\omega_{34}\end{array}\right)+$$

$$\tag{176}$$

$$\frac{1}{(s'+t+u'-2m_q^2-2m_e^2)}\left(\begin{array}{c}\left(g_L^{Z-q}\right)^2(m_q^2-s)\omega_{54}+2g_L^{Z-q}g_R^{Z-q}m_q^2\varpi_{44}-\\\\-\left(g_R^{Z-q}\right)^2(m_q^2-u)\omega_{24}\end{array}\right)+$$

$$\frac{Q}{(s'+t'+u-2m_q^2-2m_e^2)}\left(\left(g_L^{Z-q}\right)^2(m_q^2-s)\omega_{54}+\left(g_R^{Z-q}\right)^2(m_q^2-u')\omega_{34}\right)],$$

with

$$\omega_{14}=(2m_q^4-m_q^2(s+2t+t'-u)+tt'+s(t'-u)-uu'),$$

$$\omega_{24}=(2m_q^4+m_q^2(s-2t-t'-u)-s'(s+u')+t'(t+u')),$$

$$\omega_{34}=(6m_q^4-m_q^2(5u+2t+t'+2s+s')+u(s'+t'+u)),$$

$$\varpi_{44}=(m_q^2(s+s'-u-u')-s'(s+t)+u(t+u')),$$

$$\omega_{54}=(6m_q^4-m_q^2(5s'+2t+t'+2u'+u)+s'(s'+t'+u)).$$

To get the right-handed matrix elements $\sum_{i=1}^{4} \mathfrak{M}_i (k_j)_R$, all we have to do is to replace the coupling constants $g_{L,R}^{Z-q}$ by $g_{R,L}^{Z-q}$, and the coefficient $\frac{8\alpha^3\pi^3\left(1-2s_w^2\right)^2}{c_w^2 s_w^2 \left(t-m_Z^2\right)^2}$ by $\frac{32\alpha^3\pi^3 s_w^2}{c_w^2 \left(t-m_Z^2\right)^2}$. As for the rest, the expressions for $\sum_{i=1}^{4} \mathfrak{M}_i (k_j)_L$ and $\sum_{i=1}^{4} \mathfrak{M}_i (k_j)_R$ are identical.

Let us continue with the last term of Eq. (155) $\left|M_1^{2\to3}\right|^2$. It is given simply by

$$\left|M_1^{2\to3}\right|^2 = \sum_{i=1}^{4} \sum_{j=i}^{4} (\mathfrak{M}_{ij})_L \tag{177}$$

with the following four sums.

The first sum is

$$\sum_{j=i}^{4} (\mathfrak{M}_{1j})_L = \frac{8\alpha^3\pi^3 Q \left(1 - 2s_W^2\right)^2}{c_w^2 s_w^2 \ \left(t - m_Z^2\right)^2 \left(s' + t' + u - 2m_q^2 - 2m_e^2\right)} \ .$$

$$[Q\left(\left(g_L^{Z-q}\right)^2 (m_q^2 - s)\omega_{13} + \left(g_R^{Z-q}\right)^2 (m_q^2 - u')\omega_{11}\right) +$$

$$\frac{1}{\left(s + t + u - 2m_q^2 - 2m_e^2\right)} \left(\begin{array}{c} \left(g_L^{Z-q}\right)^2 \Phi_{11} - 2g_L^{Z-q} g_R^{Z-q} m_q^2 \ \varpi_{11}\omega_{13} + \\ \\ +2\left(g_R^{Z-q}\right)^2 (m_q^2 - u')\omega_{11}\varpi_{13} \end{array} \right) -$$

$$\tag{178}$$

$$\frac{1}{\left(s' + t + u' - 2m_q^2 - 2m_e^2\right)} \left(\begin{array}{c} 2\left(g_L^{Z-q}\right)^2 (m_q^2 - s)\Phi_{12}\varpi_{13} - \\ \\ -2g_L^{Z-q} g_R^{Z-q} m_q^2 \ \varpi_{11}\omega_{13} - \left(g_R^{Z-q}\right)^2 \Phi_{13} \end{array} \right) +$$

$$\frac{Q}{\left(s + t' + u' - 2m_q^2 - 2m_e^2\right)} \left(\left(g_L^{Z-q}\right)^2 \Phi_{11} - 4g_L^{Z-q} g_R^{Z-q} m_q^2 \ \varpi_{11}\omega_{13} - \left(g_R^{Z-q}\right)^2 \Phi_{13}\right)],$$

where

$$\Phi_{11} = (m_q^4(8t - 4(u + u')) + m_q^2(-2t^2 - 6t't - ut + u^2 + u'^2 + t'u + t'u' + 6uu' +$$

$$s(-3t - t' + 3u + u') + s'(-3t - t' + u + 3u')) +$$

$$s(2tt' + s'(t + t' - u - u') - 2uu') + (2s' + t + t' + u + u')(tt' - uu')),$$

$$\Phi_{12} = (2m_q^2 - s' - t' - u),$$

$$\Phi_{13} = (4m_q^4(s + s' - 2t) - m_q^2(s^2 + (6s' - t + t' + 3u + u')s + s'^2 -$$

$$2t^2 - 6tt' - 3tu - t'u - 3tu' - t'u' + s'(t' - t + u + 3u')) - tt'^2 +$$

$$s^2s' - t^2t' - s'tt' - 2tt'u - 2tt'u' + s'uu' - tuu' - t'uu' +$$

$$s(s'^2 + (t + t' + 2(u + u'))s' - tt' + uu')).$$

The second sum is

$$\sum_{j=i}^{4} \left(\mathfrak{M}_{2j}\right)_L = \frac{8\alpha^3\pi^3 Q \left(1 - 2s_w^2\right)^2}{c_w^2\, s_w^2\, \left(t - m_Z^2\right)^2 \left(s + t' + u' - 2m_q^2 - 2m_e^2\right)} \cdot$$

$$\left[Q\left(\left(g_L^{Z-q}\right)^2 (m_q^2 - s')\omega_{11} + \left(g_R^{Z-q}\right)^2 (m_q^2 - u)\omega_{13} \right) + \right.$$

$$\frac{1}{\left(s' + t + u' - 2m_q^2 - 2m_e^2\right)} \left(\begin{array}{c} \left(g_L^{Z-q}\right)^2 \Phi_{11} - 2g_L^{Z-q}\, g_R^{Z-q} m_q^2\, \varpi_{11}\omega_{13} + \\ \\ +2\left(g_R^{Z-q}\right)^2 (m_q^2 - u)\Phi_{21}\varpi_{13} \end{array} \right) -$$

$$\left. \frac{1}{\left(s + t + u - 2m_q^2 - 2m_e^2\right)} \left(\begin{array}{c} 2\left(g_L^{Z-q}\right)^2 (m_q^2 - s')\Phi_{21}\varpi_{11} - \\ \\ -2g_L^{Z-q}\, g_R^{Z-q} m_q^2\, \varpi_{11}\omega_{13} - \left(g_R^{Z-q}\right)^2 \Phi_{13} \end{array} \right) \right], \quad (179)$$

with

$$\Phi_{21} = (2m_q^2 - s - t' - u').$$

The third sum is given by

$$\sum_{j=i}^{4} \left(\mathfrak{M}_{3j}\right)_L = \frac{8\alpha^3\pi^3 \left(1 - 2s_w^2\right)^2}{c_w^2\, s_w^2\, \left(t - m_Z^2\right)^2 \left(s' + t + u' - 2m_q^2 - 2m_e^2\right)} \cdot$$

$$\quad (180)$$

$$\left[\left(g_L^{Z-q}\right)^2 (m_q^2 - s)\Phi_{12} - 2g_L^{Z-q}\, g_R^{Z-q} m_q^2\, \varpi_{11} + \left(g_R^{Z-q}\right)^2 (m_q^2 - u)\Phi_{12} + \right.$$

$$\frac{1}{(s+t+u-2m_q^2-2m_e^2)} \left(\left(g_L^{Z-q}\right)^2 \Phi_{11} - \left(g_R^{Z-q}\right)^2 \Phi_{13}\right)] \qquad .$$

And, finally, the fourth sum is equal to

$$\sum_{j=i}^4 \left(\mathfrak{M}_{4j}\right)_L = \frac{8\alpha^3\pi^3 \left(1-2s_w^2\right)^2}{c_w^2\, s_w^2\, \left(t-m_Z^2\right)^2 \left(s+t+u-2m_q^2-2m_e^2\right)}. \tag{181}$$

$$\left[\left(g_L^{Z-q}\right)^2 (m_q^2-s')\Phi_{21} - 2g_L^{Z-q}\, g_R^{Z-q} m_q^2\, \varpi_{13} + \left(g_R^{Z-q}\right)^2 (m_q^2-u)\Phi_{12}\right] \qquad .$$

Similarly, to get the matrix elements for the right-handed incident electrons, we have

to replace $g_{L,R}^{Z-q}$ by $g_{R,L}^{Z-q}$, and coefficient $\frac{8\alpha^3\pi^3\left(1-2s_w^2\right)^2}{c_w^2 s_w^2 \left(t-m_Z^2\right)^2}$ by $\frac{32\alpha^3\pi^3 s_w^2}{c_w^2 \left(t-m_Z^2\right)^2}$. Now we are ready

to proceed to the next section, where we shall give the details on the parametrization

of the emitted photon's phase space and calculations of the differential cross section.

5.3 HPB Differential Cross Section

The parameterization of the phase space for a $\{2 \to 3\}$ process has been chosen according to Fig. (16). Here, the angle θ is a scattering angle and ξ corresponds to the

angle between emitted photon and scattered electron. The momenta are represented

as

$$\begin{aligned}
k_1 &= \{E_1, 0, 0, p_{in}\}, \\
k_2 &= \{E_2, 0, 0, -p_{in}\}, \\
k_3 &= \left\{k_3^0, \left|\vec{k_3}\right| \vec{e_3}\right\}, \\
k_4 &= \left\{k_4^0, \vec{k_4}\right\},
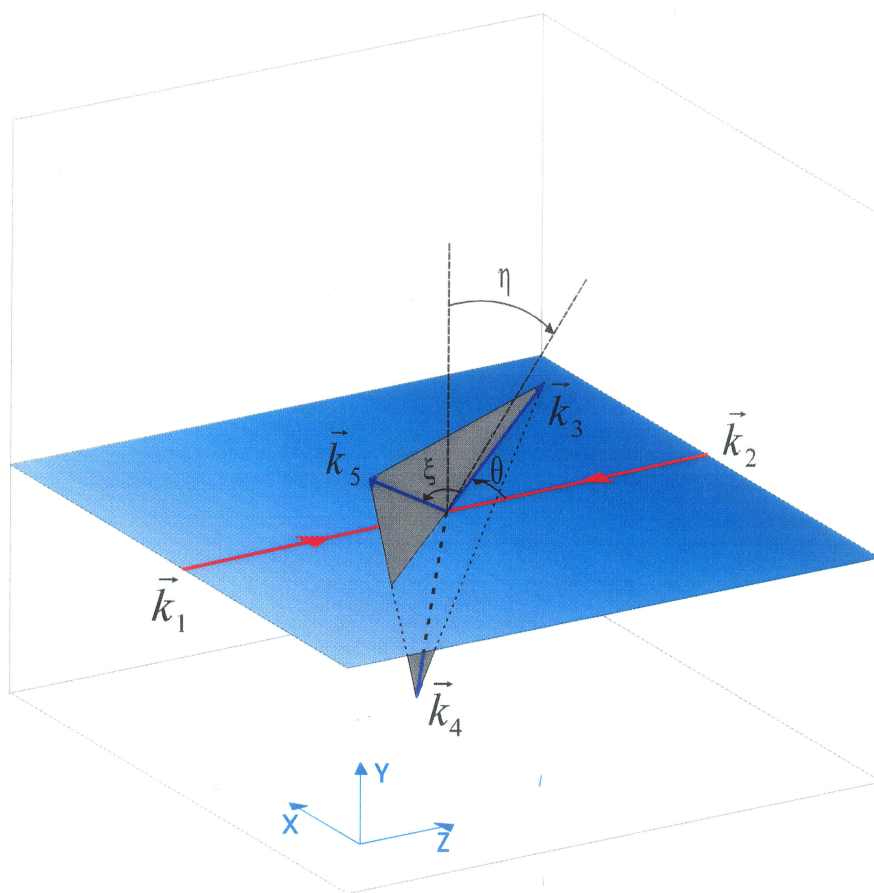\end{aligned} \tag{182}$$

Figure 16: Momenta for $(2 \to 3)$ process in the center of mass reference frame.

$$k_5 = \left\{ k_5^0, \left| \vec{k_5} \right| \vec{e_5} \right\},$$

where the unit vectors are

$$\vec{e_3} = \begin{pmatrix} \sin(\theta) \\ 0 \\ \cos(\theta) \end{pmatrix},$$

(183)

$$\vec{e_5} = \begin{pmatrix} \cos(\theta) \cos(\eta) \sin(\xi) + \sin(\theta) \cos(\xi) \\ \sin(\eta) \sin(\xi) \\ \cos(\theta) \cos(\xi) - \sin(\theta) \cos(\eta) \sin(\xi) \end{pmatrix}.$$

For on-shell particles, the incident momentum p_{in} can be found as

$$p_{in} = \sqrt{E_1 - m_e^2},$$

(184)

with

$$E_1 = \frac{E_{CMS} + m_e^2 - m_{q,N}^2}{2E_{CMS}}.$$

(185)

Here, E_{CMS} is center of mass energy and $m_{q,N}$ is a mass of the target particle (quark or nucleon). Center of mass energy can be determined as follows:

$$E_{CMS} = \sqrt{m_e^2 + m_{q,N}^2 + 2E_{lab} \, m_N \, x}.$$

(186)

When we consider $\{e - q\}$ scattering, $m_{q,N} = m_q$, and the parameter x represents the fraction of the nucleon's energy carried by a quark. For the case of $\{e - q\}$

115

scattering, the parameter x was chosen to be equal to $\frac{1}{6}$. It is believed what three constituent quarks contribute $\frac{1}{2}$ to the mass of the nucleon. Rest of the mass of the nucleon is made up from the contribution coming from the quark antiqurak sea. Having three quarks in the nucleon it is possible to assume what single quark contributes $\frac{1}{6}$ to the total mass. If we consider electron scattering on the nucleon as a whole, x is equal to 1.

Momentum k_4 is determined by the four-momentum conservation law in the CMS frame:

$$\sqrt{s} = k_1^0 + k_2^0 = k_3^0 + k_4^0 + k_5^0, \tag{187}$$

and

$$\vec{k_3} + \vec{k_4} + \vec{k_5} = 0. \tag{188}$$

The HPB differential cross section reads as follows

$$d\sigma = \frac{|M_{tot}^{2\to3}|^2}{\Phi} d\Gamma^3, \tag{189}$$

where Φ is a flux factor and given by

$$\Phi = 4p_{in}\sqrt{s}.$$

The $\{2 \to 3\}$ process phase-space element $d\Gamma^3$ is

$$d\Gamma^3 = \frac{d^3k_3}{(2\pi)^3 2k_3^0} \frac{d^3k_4}{(2\pi)^3 2k_4^0} \frac{d^3k_5}{(2\pi)^3 2k_5^0} (2\pi)^4 \delta^{(4)} (k_1 + k_2 - k_3 - k_4 - k_5). \tag{190}$$

Using

$$\frac{d^3k_i}{2k_i^0} = d^4k_i\delta\left(k_i^2 - m_i^2\right) = \frac{\left|\vec{k_i}\right|}{2}dk_i^0 d\Omega_i,$$

and the fact that the photon is a massless boson, i.e $\left|\vec{k_5}\right| = k_5^0$, we can write

$$d\Gamma^3 = \frac{\left|\vec{k_3}\right| k_5^0}{4\left(2\pi\right)^5}dk_3^0 d\Omega_3 dk_5^0 d\Omega_5 \delta\left(k_4^2 - m_{q,N}^2\right)d^4k_4\delta^{(4)}\left(k_1 + k_2 - k_3 - k_4 - k_5\right). \quad (191)$$

Employing the delta function $\delta^{(4)}(...)$ to eliminate the integration over momentum k_4, we arrive at

$$d\Gamma^3 = \frac{\left|\vec{k_3}\right|\left|\vec{k_5}\right|}{4\left(2\pi\right)^5}dk_3^0 d\Omega_3 dk_5^0 d\Omega_5 \delta\left(k_4^2 - m_{q,N}^2\right), \quad (192)$$

with $d\Omega_3 = d\cos\theta\,d\phi$ and $d\Omega_5 = d\cos\xi\,d\eta$. The remaining delta function $\delta\left(k_4^2 - m_{q,N}^2\right)$ will be used to eliminate the integration over the scattered electron's energy k_3^0.

We need to do some modifications first:

$$k_4^2 - m_{q,N}^2 = \left(k_4^0\right)^2 - \left|\vec{k_4}\right|^2 - m_{q,N}^2 = \left(\sqrt{s} - k_3^0 - k_5^0\right)^2 - \left|\vec{k_3}\right|^2 - \left|\vec{k_5}\right|^2 - 2\left|\vec{k_3}\right|\left|\vec{k_5}\right|\cos\xi - m_{q,N}^2.$$

$$(193)$$

Now, using

$$\left(k_i^0\right)^2 = \left|\vec{k_i}\right|^2 + m_i^2, \quad (194)$$

we arrive at

$$k_4^2 - m_{q,N}^2 = s - 2\sqrt{s}k_5^0 + m_e^2 - m_{q,N}^2 - 2k_3^0\left(\sqrt{s} - k_5^0\right) - 2\left|\vec{k_3}\right|k_5^0\cos\xi. \quad (195)$$

The electron's mass can be considered as a small parameter with respect to k_3^0. In

117

this case, we can replace $\left|\vec{k_3}\right|$ by k_3^0, thus

$$\left|\vec{k_3}\right| \simeq k_3^0 - \frac{m_e^2}{2k_3^0}. \tag{196}$$

Substitution of Eq. (196) into Eq. (195) leads to the following:

$$k_4^2 - m_{q,N}^2 = \left(s - 2\sqrt{s}k_5^0 + m_e^2 - m_{q,N}^2\right) - 2k_3^0\left(\sqrt{s} - k_5^0 + k_5^0\cos\xi\right) + \frac{m_e^2 k_5^0 \cos\xi}{k_3^0}. \tag{197}$$

The property of the delta function $\delta\left[g\left(k_3^0\right)\right] = \sum_i \frac{\delta\left(k_3^0 - r_i\right)}{|g'(r_i)|}$ (r_i is i-th root of the equation $k_4^2 - m_{q,N}^2 = 0$, solved with respect to k_3^0) makes it possible to replace $\delta\left(k_4^2 - m_{q,N}^2\right)$ by

$$\delta\left(k_4^2 - m_{q,N}^2\right) = \frac{1}{2\left(\sqrt{s} + k_5^0\left(\cos\left(\xi\right) - 1\right)\right) + \frac{m_e^2 k_5^0 \cos(\xi)}{r^2}}\delta\left(k_3^0 - r\right), \tag{198}$$

where

$$r = \frac{\left(s - 2\sqrt{s}k_5^0 + m_e^2 - m_{q,N}^2\right)}{2\left(\sqrt{s} + k_5^0\left(\cos\left(\xi\right) - 1\right)\right)} + \frac{m_e^2 k_5^0 \cos\left(\xi\right)}{\left(s - 2\sqrt{s}k_5^0 + m_e^2 - m_{q,N}^2\right)}.$$

The delta function $\delta\left(k_3^0 - r\right)$ will eliminate integration over k_3^0 leaving $k_3^0 = r$. Integration over the emitted photon's phase space $dk_5^0 d\Omega_5$ can be performed numerically using the cuts on the photon's energy k_5^0 :

$$\left(k_5^0\right)_{\min} = \Delta E,$$

$$\tag{199}$$

$$\left(k_5^0\right)_{\max} = \frac{\sqrt{s}}{2} - \frac{\left(m_e + m_{q,N}\right)^2}{2\sqrt{s}}.$$

118

Finally, Eq. (189) becomes

$$d\sigma_{R,L}^{HPB} = \frac{1}{4\,(2\pi)^5}\frac{1}{\Phi}\left(\iiint \frac{\left|\vec{k_3}\right|\,k_5^0\,\left|M_{tot}^{2\to3}\right|_{R,L}^2\,dk_5^0\,d\Omega_5}{2\left(\sqrt{s}+k_5^0\left(\cos\left(\xi\right)-1\right)\right)+\frac{m_e^2 k_5^0\cos(\xi)}{\left(k_3^0\right)^2}}\right)d\Omega_3, \qquad (200)$$

leaving the final differential cross section differential with respect to the scattered electron's solid angle $d\Omega_3$.

The asymmetry in parity-violating scattering is defined as

$$A_{RL} = \frac{d\sigma_R^{tot} - d\sigma_L^{tot}}{d\sigma_R^{tot} + d\sigma_L^{tot}}, \qquad (201)$$

where

$$d\sigma_{R,L}^{tot} = \frac{1}{4\,(2\pi)^2}\frac{1}{\Phi}\frac{\left|\vec{k_3}\right|}{\sqrt{s}}\left|M_0^{2\to2} + M_{one-loop}^{2\to2}\right|_{R,L}^2 d\Omega_3. \qquad (202)$$

The contribution of the soft- and hard-photon bremsstrahlung modifies the differential cross sections in Eq. (201) according to the following:

$$d\tilde{\sigma}_{R,L}^{tot} = d\sigma_{R,L}^{tot} + \left(d\sigma_0^{2\to2}\right)_{R,L}\cdot\delta_{soft} + d\sigma_{R,L}^{HPB}. \qquad (203)$$

In order to combine HPB differential cross section with the soft-photon emission contribution, and all this with previously calculated radiative corrections (Ref. [7]), we propose the following parametrization for the HPB differential cross section:

$$d\tilde{\sigma}_{R,L}^{HPB} = \left(d\sigma_0^{2\to2}\right)_{R,L}\cdot\frac{d\sigma_R^{HPB} - d\sigma_L^{HPB}}{\left(d\sigma_0^{2\to2}\right)_R - \left(d\sigma_0^{2\to2}\right)_L} = \left(d\sigma_0^{2\to2}\right)_{R,L}\cdot\tilde{\delta}_{HPB}. \qquad (204)$$

As can be easily seen, the substitution of Eq. (204) into the expression for asymmetry Eq. (201) will leave terms related to the HPB in the usual form $\left(d\sigma_R^{HPB} - d\sigma_L^{HPB}\right)$.

119

It is worth noting that the term $(d\sigma_R^{tot} + d\sigma_L^{tot})$ has a dominant contribution from the parity-conserved part of the differential cross section. Because of that, the denominator of Eq. (201) is left without parity-violating soft- and hard-photon bremsstrahlung terms.

One of the most important results of this work is that the combination of soft and HPB terms with radiative corrections can be written as follows

$$\widetilde{R}_{V,A}^p = R_{V,A}^p + \frac{1}{2}\left(\delta_{soft} + \widetilde{\delta}_{HPB}\right), \qquad (205)$$

i.e. all of the effects can be accounted for and put together on the level of radiative corrections.

For the case of $\{e - N\}$ scattering, we will show the contribution from soft and HPB terms, taking into account only the IR finite part of the soft-photon bremsstrahlung. We can do so because IR divergences are canceled when $\{e - N\}$ radiative corrections are added. As for $\{e - q\}$ scattering, after computing the total radiative corrections, we will demonstrate explicitly that the final result is indeed free of IR divergences as well as of a logarithmic dependence on ΔE parameter.

5.4   Numerical Results

Before going into the numerical details which involve various parity-violating experiments, let us first demonstrate that, indeed, we do not have ΔE dependence in the term $\frac{1}{2}\left(\delta_{soft} + \widetilde{\delta}_{HPB}\right)$ for an arbitrarily chosen kinematical point. We take
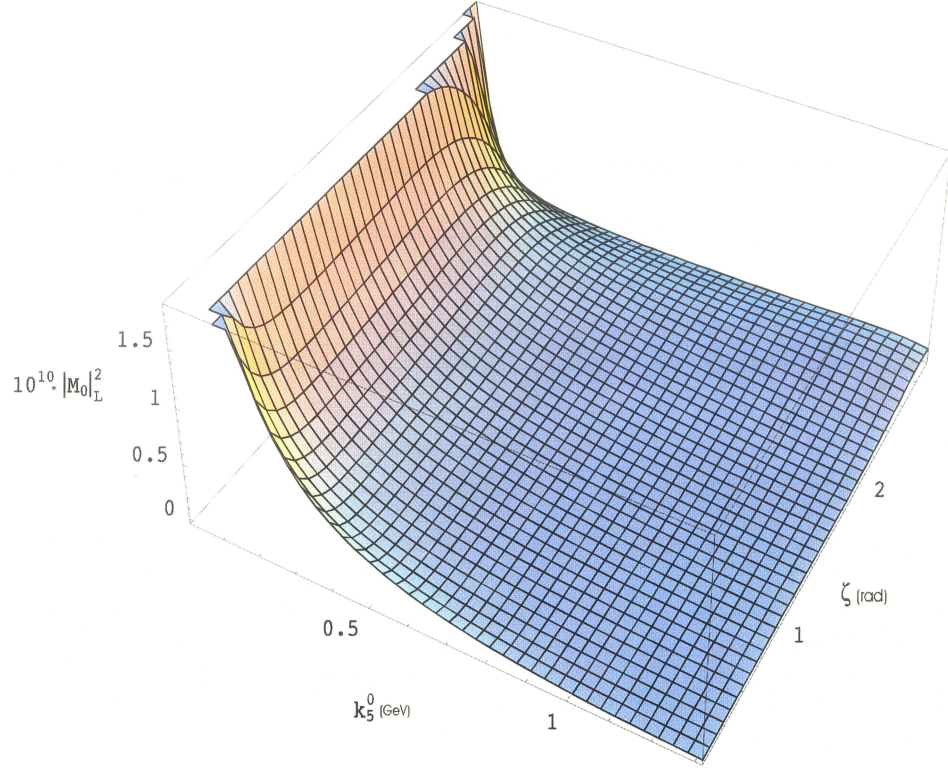
Figure 17: Term associated with $|M_0|^2_L$ in the HPB differential cross section for electron proton scattering as a function of $\{k_5^0, \xi\}$ ($E_{lab} = 5.0$ GeV, $\theta = 140.0^o$).

$E_{lab} = 5.0$ GeV and $\theta = 140^o$. Before the integration of Eq. (200) over the emitted photon's phase space, it is interesting to illustrate the expression in parenthesis of Eq. (200) graphically, studying the general behavior of terms associated with $|M_0^{2\rightarrow3}|^2$, $2\,(M_0^{2\rightarrow3})^*\,(M_1^{2\rightarrow3})$ and $|M_1^{2\rightarrow3}|^2$ as a function of $\{k_5^0, \xi\}$ (See Fig.(17), (18) and (19)). Of all the terms, it is obvious that only the integrated $|M_0^{2\rightarrow3}|^2$ will have a logarithmic dependence on photon detector acceptance and make a dominant contribution to HPB at this energy. During the numerical integration, we have used the
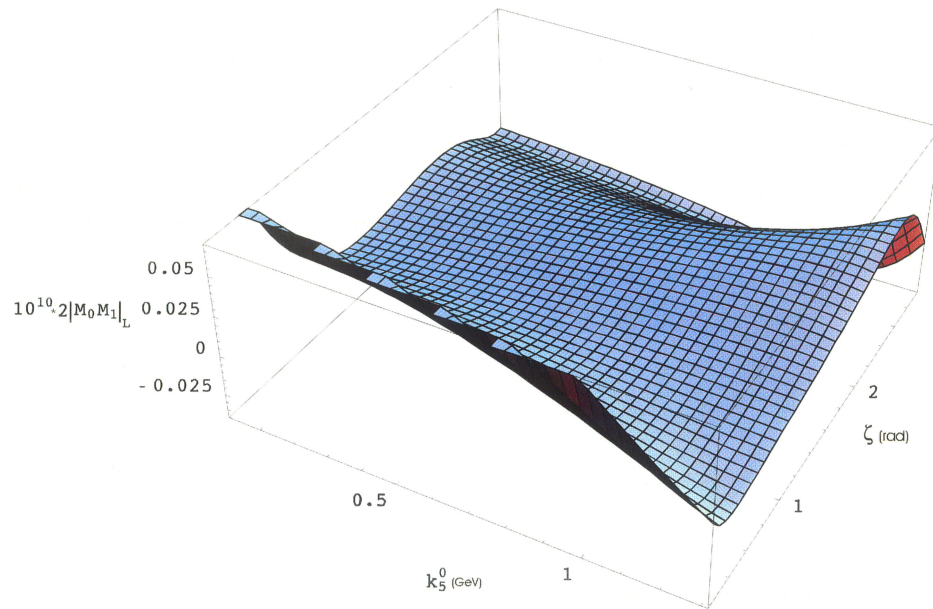
Figure 18: Term associated with $2\,|M_0 M_1|_L$ in the HPB differential cross section for electron proton scattering as a function of $\{k_5^0, \xi\}$ $(E_{lab} = 5.0 \text{ GeV}, \theta = 140.0^o)$
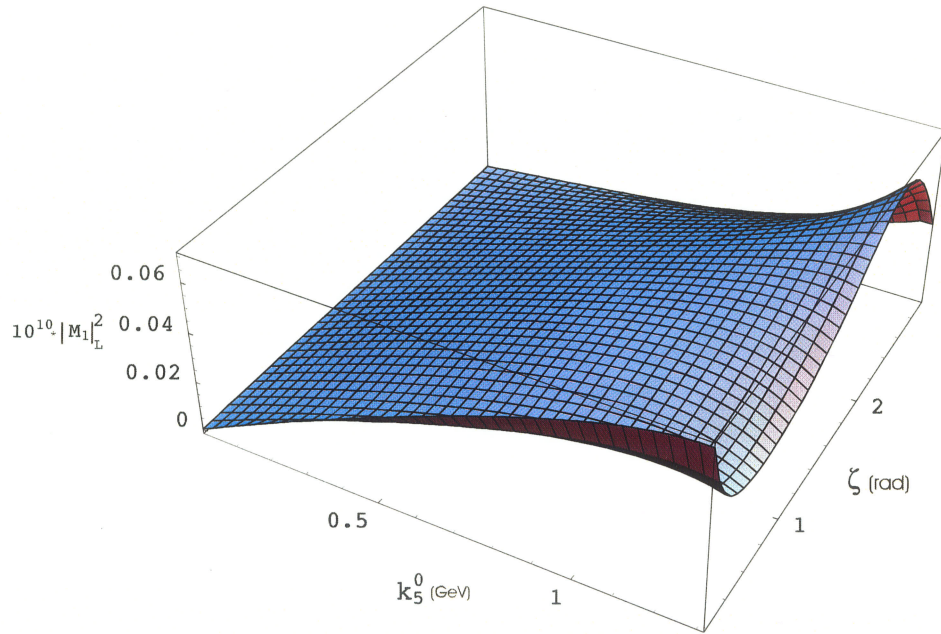
Figure 19: Term associated with $|M_1|^2_L$ in the HPB differential cross section for electron proton scattering as a function of $\{k_5^0, \xi\}$ ($E_{lab} = 5.0$ GeV, $\theta = 140.0^o$)

$\Delta E \ (\sqrt{s})$	$\frac{1}{2} \left(\delta_{soft} + \widetilde{\delta}_{HPB} \right)$
10^{-3}	-0.15032
10^{-4}	-0.15035
10^{-5}	-0.15035
10^{-6}	-0.15035
10^{-7}	-0.15036

Table 6: Dependence on the photon detector acceptance (electron nucleon scattering case ($E_{lab} = 5.0$ GeV, $\theta = 140.0^{o}$))

adaptive Genz-Malik algorithm which is implemented in the *Mathematica* program. For electron-proton scattering, the term $\frac{1}{2} \left(\delta_{soft} + \widetilde{\delta}_{HPB} \right)$ for different values of ΔE is shown in Table (6). We see that the variation of $\frac{1}{2} \left(\delta_{soft} + \widetilde{\delta}_{HPB} \right)$ is within 0.03% of that coming from the numerical "noise" due to the integration. As for electron-quark scattering, Table (7) gives convincing evidence that the final results are independent of the introduced photon's energy cutoff.

Various experiments in parity-violating electron scattering can be used as a base for our numerical calculations. We will include SAMPLE (Ref. [10]), (Ref. [11]), HAPPEX (Ref. [12]), G0 (Ref. [13]), A4 (Ref[14]), and Q-Weak (Ref. [15]). In Table (8) we give total radiative corrections with the soft- and hard-photon bremsstrahlung taken into account. One-quark radiative corrections now will be modified by the soft- and hard-photon emission terms for the electron-quark scattering case. We take ΔE

124

$\Delta E\ (\sqrt{s})$	$\frac{1}{2}\left(\delta_{soft}+\widetilde{\delta}_{HPB}\right)\ (eu)$	$\frac{1}{2}\left(\delta_{soft}+\widetilde{\delta}_{HPB}\right)\ (ed)$	$\frac{1}{2}\left(\delta_{soft}+\widetilde{\delta}_{HPB}\right)\ (es)$
10^{-3}	-0.20461	-0.17176	-0.16842
10^{-4}	-0.20472	-0.17182	-0.16849
10^{-5}	-0.20473	-0.17183	-0.16850
10^{-6}	-0.20473	-0.17183	-0.16850
10^{-7}	-0.20474	-0.17183	-0.16850

Table 7: Dependence on the photon detector acceptance (electron-quark scattering case ($E_{lab} = 5.0$ GeV, $\theta = 140.0°$))

$= 10^{-4}\sqrt{s}$ simply because there is no need to show again that there is no dependence on the ΔE parameter.

Combination of the above leads to the nucleonic radiative corrections listed in Table (9).

The HPB parity-violating differential cross sections for the electron-proton scattering case, including tree level PV and IR finite soft-photon emission terms ($d\sigma_{R,L}^{tot} = (d\sigma_0^{2\to2})_{R,L}(1 + \delta_{one-loop} + \delta_{soft}) + d\sigma_{R,L}^{HPB} = (d\sigma_0^{2\to2})_{R,L}\,\delta_{one-loop} + \eta_{R,L}$), can be found in Table (10).

125

$\mathbf{R}_{VA}^{ff'}$	SAM. I	SAM. II	HAP. I	HAP. II	G0(a)	A4(a)	Q-Weak
R_{VA}^{eu}	−0.335	−0.333	−0.368	−0.371	−0.335	−0.351	−0.360
R_{VA}^{ed}	−0.545	−0.552	−0.543	−0.544	−0.545	−0.550	−0.552
R_{VA}^{es}	−0.596	−0.607	−0.593	−0.597	−0.588	−0.597	−0.602
R_{AV}^{eu}	−0.071	−0.069	−0.073	−0.072	−0.070	−0.071	−0.069
R_{AV}^{ed}	−0.024	−0.025	−0.036	−0.033	−0.031	−0.036	−0.033
R_{AV}^{es}	−0.030	−0.031	−0.036	−0.033	−0.032	−0.035	−0.031

Table 8: Modified by HPB one-quark radiative corrections

	$T = 0$	$T = 1$	$isosinglet$	p	n
R_V	0.040	−0.042	−0.017	−0.366	−0.0055
R_A	−0.210	−0.440	−0.817	−0.650	−0.231

Table 9: Modified by HPB and combined radiative corrections (SAMPLE I experiment).

$\eta_{R,L}$ $(10^{-14}mb)$	SMPL I	SMPL II	HPX I	HPX II	G0(a)	A4(a)	Q-Weak
η_R	0.048	0.034	3.613	4.183	0.061	0.553	1.295
η_L	0.251	0.114	6.036	6.644	0.573	1.267	2.086

Table 10: Combined HPB and soft-photon differential cross sections in e-p scattering

6 Discussion and Analysis

The application of the methods described above for $\{e - N\}$ scattering can be seen in calculations of the weak charges of the nuclei. Consider the parity-violating Hamiltonian in Eq. (111). Here, for a heavy nucleus we have a coherent effect for $V(N) \otimes A(e)$:

$$(\overline{u}_N \gamma^\mu u_N) \rightarrow \rho_{nuc}(r)\, \delta_{\mu,0}. \tag{206}$$

The contribution coming from $V(e) \otimes A(N)$ is small as it depends on unpaired valence nucleons. The latter will determine the Hamiltonian for the electron parity-violating interaction with the nucleus in the following form:

$$H(r) = \frac{G_\mu}{2\sqrt{2}} Q_{weak} \gamma_5 \rho_{nuc}(r). \tag{207}$$

A relation between the weak charge Q_{weak} and form factors $\{C_{1p}, C_{1n}\}$ is straightforward:

$$Q^p_{weak} = 2C_{1p},$$

$$\tag{208}$$

$$Q^n_{weak} = 2C_{1n}.$$

If we take into account only the leading order of the interaction, the weak charge of the proton and neutron have the simple definitions:
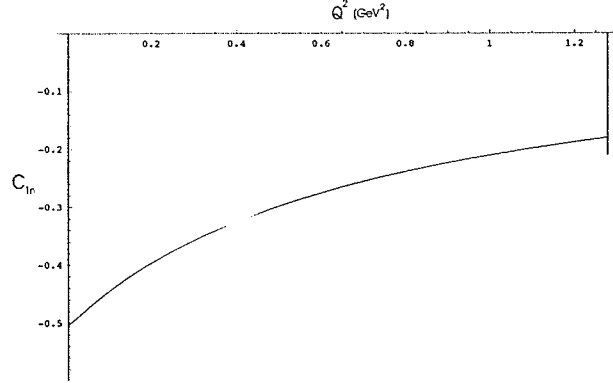
$$Q^{p(0)}_{weak} = 1 - 4s_w^2,$$

127

Figure 20: Momentum transfer dependence of C_{1n} neutron vector formfactor.

$$(209)$$

$$Q_{weak}^{n(0)} = -1,$$

and for the nucleus

$$Q_{weak} = Z \cdot Q_{weak}^{p} + N \cdot Q_{weak}^{n} , \qquad (210)$$

where Q_{weak}^{p}, Q_{weak}^{n} are the weak charges of the proton and neutron including next to leading order radiative corrections.

Extrapolation of the $\{C_{1n}, C_{2n}\}$ and $\{C_{1p} C_{2p}\}$ to zero momentum transfer (see Fig. (20) and Fig. (21)), and combining with the HPB contribution, gives the following numerical results:

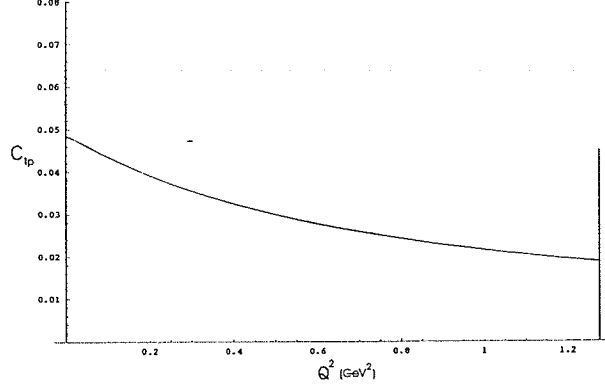$$C_{1p} = 0.0481 \pm 0.0005,$$

$$C_{2p} = 0.060 \pm 0.010,$$

128

Figure 21: Momentum transfer dependence of C_{1p} proton vector formfactor.

$$\tag{211}$$

$$C_{1n} = -0.5017 \pm 0.0020,$$

$$C_{2n} = -0.058 \pm 0.010.$$

We believe it is useful to give some details on the angular dependence of C_{1n} and C_{1p} (see Fig. (22) and Fig. (23). Here, the numerical noise at forward angles is associated with Landau singularities, and was incorporated into the theoretical error estimation.

Some of the existing measurement results are obtained from atomic parity violation (APV), deep inelastic neutrino-nucleus scattering (NuTeV), and from Z^0 pole asymmetries (LEP+SLC). The available results from atomic parity-violating experiments for the weak charges of Cs_{55}^{133}, Tl_{81}^{205} and Bi_{83}^{209} can be used as an experimental
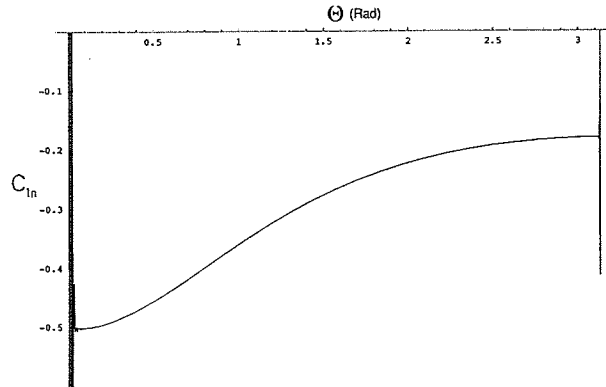
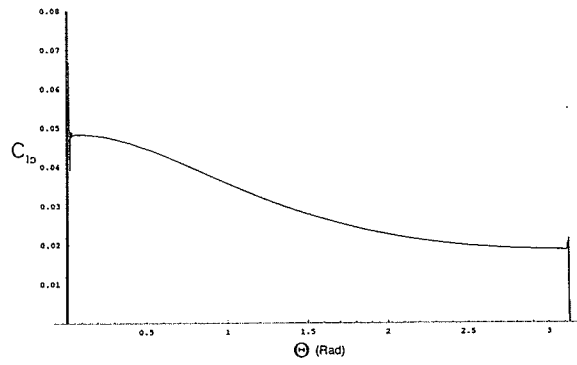Figure 22: Angular dependence of the C_{1n} vector form factor

Figure 23: Angular dependence of the C_{1p} vector formfactor

130

test of the theoretical predictions:

$$Cs_{55}^{133}(\text{exp}) = -72.65 \pm 0.28 \pm 0.34,$$

$$(212)$$

$$Tl_{81}^{205}(\text{exp}) = -114.8 \pm 1.2 \pm 3.4,$$

$$Bi_{83}^{209}(\text{exp}) = -140 \pm 40.$$

Here, the errors are statistical, systematic and coming from an uncertainty of the atomic-physics theory, respectively. For example, in the case of Cs_{55}^{133}, one should observe $7s$ (*excited*) $\to$ $6s$ (*ground*) parity-violating electric dipole transitions in order to extract the weak charge of Cs_{55}^{133}. This requires an accurate knowledge of the atomic wave functions. Using Eq. (211), Eq. (208) and Eq. (210) we compute the following results for the corresponding nuclear weak charges:

$$Cs_{55}^{133}(\text{theor}) = -72.97 \pm 0.26,$$

$$(213)$$

$$Tl_{81}^{205}(\text{theor}) = -116.8 \pm 0.4,$$

$$Bi_{83}^{209}(\text{theor}) = -118.4 \pm 0.4.$$

The model predictions are in good agreement with the available experimental

results. However, to make more definitive conclusions about the validity of the proposed computational model, we have to reduce the experimental errors for precision measurements of the weak charge of the nucleon. This type of measurement is proposed by the Q-Weak collaboration. The general purpose of the Q-Weak experiment is to search for new physics at 4.6 TeV scale to challenge predictions of the Standard Model. More precisely, Q-Weak is designed to measure the weak charge of the proton. The Standard Model evolution predicts a shift of $\Delta \sin^2 \theta_W = +0.007$ at low Q^2 with respect to the Z^0 pole best fit value of 0.23113 ± 0.00015. The weak mixing angle at the energy scale close to the Z^0 pole was measured very precisely. A precision experimental study of the evolution of $\sin^2 \theta_W$ to lower energies still has to be carried out. The asymmetry measurements proposed for Q-Weak experiment will go as low as 0.1 GeV.

At tree level, Eq. (209) has a definite prediction in the electroweak Standard Model. Any significant deviation of $\sin^2 \theta_W$ from the Standard Model prediction at low Q^2 would be a signal of new physics. The proton's weak charge Q^p_{weak} is also a well-defined experimental observable. At $Q^2 \to 0$ and $\theta \to 0$ the asymmetry can be parameterized as

$$\mathcal{A} = \left[\frac{-G_F Q^2}{4\sqrt{2}\pi\alpha} \right] [Q^2 Q^p_{weak} + Q^4 B(Q^2)],$$

where $B(Q^2)$ is a function of Sachs electromagnetic form factors $G^\gamma_{E,M}$ related to the

132

Dirac and Pauli formfactors by the following expressions.

$$G_E^\gamma = F_1(q) + \frac{t}{4m_N^2} F_2(q), \quad G_M^\gamma = F_1(q) + F_2(q) \tag{214}$$

At JLab, the Q-Weak collaborators [15] propose a new precision measurement of parity-violating electron scattering on the proton at very low Q^2 and forward angles. According to [15], "A unique opportunity exists to carry out the first precision measurement of the proton's weak charge, $Q_{weak}^p = 1 - 4\sin^2\theta_W$ building on technical advances that have been made in JLab's parity violation program."

The parity-violating asymmetry in elastic $e - p$ scattering at $Q^2 = 0.028$ GeV^2 will be measured employing 180 μA of 80% polarized beam of $E_{beam} = 1.165$ GeV on a 35 cm liquid hydrogen target. This 2200 hour measurement will allow one to determine the proton's weak charge with $\simeq 4\%$ combined statistical and systematic errors. The electrons are collimated to $\theta_e = 9° \pm 2°$. The production is expected to make multiple runs from 2007 to 2009.

As for our computational model, several directions for improvement can be pursued in the near future. In the Pauli and Dirac couplings, electric and magnetic form factors will give a better fit of the experimental results for the electromagnetic (EM) form factor measurements if we use the dipole approximation. Using the identity

$$\left(\frac{-\Lambda^2}{k^2 - \Lambda^2} \right)^m = \frac{(-\Lambda^2)^{m-1}}{(m-1)!} \frac{\partial^{m-1}}{\partial (\Lambda^2)^{m-1}} \left(\frac{1}{k^2 - \Lambda^2} \right), \tag{215}$$

we can achieve the dipole approximation ($m = 2$) by differentiating form factors C_{1p}

133

and C_{1n} with respect to Λ^2. Although analytical expressions for the C_{1p} and C_{1n} have been derived, it is easier to carry out differentiation using numerical techniques. The latter will require additional CPU power, and one possibility is to use parallelization techniques available through Beowulf clusters.

Also, in the current work, we have only included the static part $\left(\gamma^\mu \gamma_5 g_1^N(q)\right)$ of the $\langle N \left| j^{\mu 5a} \right| N \rangle$ nucleon axial matrix elements. Extension of the $\langle N \left| j^{\mu 5a} \right| N \rangle$ as

$$\langle N \left| j^{\mu 5a} \right| N \rangle = \overline{u}_N \left(\gamma^\mu \gamma_5 g_1^N(q) + \frac{i\sigma^{\mu\alpha}}{2m_N} q_\alpha \gamma_5 F_2^5(q) \right) u_N \tag{216}$$

along with the strange electric and strange magnetic form factors in the vector and axial parts of the nucleon matrix elements should give us more complete description of the parity-violating electron-nucleon interaction.

In general, we are highly satisfied with the unique and innovative computational model developed in this work. Our numerical results are in a very good agreement with the experimental data; our analytical and programming routines show a considerable promise for extension, and future plans are well defined.

7 Appendix

The following appendix gives partial details on the code developed in this thesis. The first part explains model definitions and the second gives details on the $\{\gamma - Z\}$ box code.

7.1 *Mathematica* Code for Model Definitions

Prior to execution of the code for the one-loop calculations, model files along with an unevaluated amplitude should be defined. Below is an example of definitions in the model file.

7.1.1 *Definition of the nucleon and vector bosons propagators*

General fermion propagator:

> *(external propagator takes the form either Majorana or Dirac spinors)*
>
> *(internal propagator takes the form as defined by the Feynman rules in this work)*
>
> AnalyticalPropagator[External][s1 F[j1, mom]] ==
>
> NonCommutative[If[SelfConjugate[F[j1]], MajoranaSpinor,
>
> DiracSpinor][-mom, Mass[F[j1]]]],
>
> AnalyticalPropagator[Internal][s1 F[j1, mom]] ==
>
> NonCommutative[DiracSlash[-mom] + Mass[F[j1]]] *
>
> I PropagatorDenominator[mom, Mass[F[j1]]],

General vector boson external propagator: (external propagator is represented by polarization vector of the vector boson (used in the HPB calculations))

AnalyticalPropagator[External][s1 V[j1, mom, li2]] ==

PolarizationVector[V[j1], mom, li2],

General vector boson internal propagator: (internal propagator defined by the Feynman rules of SM)

AnalyticalPropagator[Internal][s1V[j1,mom,li1->li2]]==

-I*PropagatorDenominator[mom,Mass[V[j1]]]*

(MetricTensor[li1,li2]-(1-GaugeXi[V[j1]])*

FourVector[mom,li1]FourVector[mom,li2]*

PropagatorDenominator[mom,Sqrt[GaugeXi[V[j1]]]Mass[V[j1]]])

7.1.2 Structure of the $\{V - N - V\}$ coupling

AnalyticalCoupling[s1 F[j1, mom1], s2 F[j2, mom2],

s3 V[j3, mom3, li3]] == G[-1][s1 F[j1], s2 F[j2], s3 V[j3]] .

NonCommutative[DiracMatrix[li3], ChiralityProjector[-1]],

NonCommutative[DiracMatrix[li3], ChiralityProjector[+1]],

(NonCommutative[DiracMatrix[li3], DiracSlash[- mom2 - mom1]] -

NonCommutative[DiracSlash[- mom2 - mom1], DiracMatrix[li3]]) *

NonCommutative[ChiralityProjector[-1]], (NonCommutative[DiracMatrix[li3],

DiracSlash[- mom2 - mom1]] - NonCommutative[DiracSlash[- mom2 -

136

mom1],

DiracMatrix[li3]]) * NonCommutative[ChiralityProjector[+1]] ,

7.1.3 *Definitions for neutron and proton*

(*Neutron:I_3=-1/2,Q=0*)

F[5] == {

SelfConjugate -> False,

Indices -> Index[neutron],

Mass -> Mprot,

QuantumNumbers -> 0 Charge,

MatrixTraceFactor -> 1,

PropagatorLabel -> ComposedChar["n", Index[neutron]],

PropagatorType -> Straight,

PropagatorArrow -> Forward },

(*Proton:I_3=1/2,Q=1*)

F[6] == {

SelfConjugate -> False,

Indices -> Index[proton],

Mass -> Mprot,

QuantumNumbers -> 1 Charge,

MatrixTraceFactor -> 1,

PropagatorLabel -> ComposedChar["p", Index[proton]],

PropagatorType -> Straight,

PropagatorArrow -> Forward },

7.1.4 Coupling $\{F - V - F\}$

(Case of $\{p - \gamma - p\}$ coupling)

C[-F[6, j1], F[6, j2], V[1]] ==

I EL * CNP[1] *

{ {-FermionCharge[5] IndexDelta[j1, j2],

 -FermionCharge[5] * dZfL1cc[6, j1, j2]},

{-FermionCharge[5] IndexDelta[j1, j2],

-FermionCharge[5] * dZfR1cc[6, j1, j2]},

{F2P/2 IndexDelta[j1, j2],

F2P/2 IndexDelta[j1, j2] dZfL1cc[6, j1, j2]},

{F2P/2 IndexDelta[j1, j2],

F2P/2 IndexDelta[j1, j2] dZfR1cc[6, j1, j2]} },

(Case of $\{p - Z - p\}$ coupling)

C[-F[6, j1], F[6, j2], V[2]] == I EL * CNP[2] *

{ {GLZP IndexDelta[j1, j2],

GLZP dZfL1cc[6, j1, j2]},

{GRZP IndexDelta[j1, j2],

GRZP dZfR1cc[6, j1, j2]},

{ -F2WEAKP/2 IndexDelta[j1, j2],

-F2WEAKP/2 dZfL1cc[6, j1, j2] IndexDelta[j1, j2]},

{ -F2WEAKP/2 IndexDelta[j1, j2],

-F2WEAKP/2 dZfR1cc[6, j1, j2] IndexDelta[j1, j2]} } ,

7.2 Details on $\{\gamma - Z\}$ box in the case $e - n$ scattering

Below, is the *Mathematica* code for $\{\gamma - Z\}$ box. Due to the extremely lengthy

expressions involved in the output of the following program only input parts of the

cells are presented.

(Loading packages)

<< "FeynArts'"

<< "/data/FormCalcNew/FormCalc.m"

num = Simplify

SetOptions[InsertFields, InsertionLevel -> Particles]

(Small electron mass approximation)

Small[ME] := 0

SetOptions[CalcFeynAmp, OnShell -> True, Dimension -> 4, MomSim-

plify -> True, EditCode -> False]

GLGN = GN; GRGN = GN; CNP[1] = 1; CNP[2] = 1; CNPB[1] = 1;

CNPB[2] = 1;

*(Passing amplitude **GZenboxonlyfrommodel.amp** to the "Form")*

res0 = CalcFeynAmp[<< "/data/FormCalc/GZenboxonlyfrommodel.amp",

VADecompose -> True] //. Abbr[]

(Taking only parity-violating part of amplitude)

axialenself = Coefficient[res0, Mat[DiracChain[Spinor[k[3], ME, 1], Lor[1],

Spinor[k[1], ME, 1]]* DiracChain[Spinor[k[4], MN, 1], 5, Lor[1], Spinor[k[2],

MN, 1]]]]

axialneself = Coefficient[res0, Mat[DiracChain[Spinor[k[4], MN, 1], Lor[1],

Spinor[k[2], MN, 1]]* DiracChain[Spinor[k[3], ME, 1], 5, Lor[1], Spinor[k[1],

ME, 1]]]]

axialneself1 = Coefficient[res0, Mat[DiracChain[Spinor[k[3], ME, 1], 5,

k[2], Spinor[k[1], ME, 1]]* DiracChain[Spinor[k[4], MN, 1], Spinor[k[2],

MN, 1]]]]

axialenself1 = Coefficient[res0, Mat[DiracChain[Spinor[k[4], MN, 1], 5,

Spinor[k[2], MN, 1]]* DiracChain[Spinor[k[3], ME, 1], k[2], Spinor[k[1],

ME, 1]]]]

(Expanding abbreviations)

MLE2[1] := ME2; MLE2[2] := MM2; MLE2[3] := ML2; MQU2[1] :=

MU2; MQU2[2] := MC2; MQU2[3] := MT2; MQD2[1] := MD2; MQD2[2]

:= MS2; MQD2[3] := MB2; MLE[1] := ME; MLE[2] := MM ; MLE[3] :=

ML; MQU[1] := MU; MQU[2] := MC; MQU[3] := MT; MQD[1] := MD;

MQD[2] := MS; MQD[3] := MB;

(Tree level definition of the mixing angle)

SW2 := (MZ2 - MW2)/MZ2

CW2 := MW2/MZ2

(On-shell definitions)

Pair[k[1], k[1]] := ME2

Pair[k[2], k[2]] := MN2

Pair[k[3], k[3]] := Pair[k[1], k[1]]

Pair[k[4], k[4]] := Pair[k[2], k[2]]

Mass2[1] := ME2

Mass2[2] := MN2

(Mandelstam variables)

p2 := (ecms^2+ Mass2[2] - Mass2[1])^2/(4*ecms^2) - Mass2[2]

el := Sqrt[p2 + Mass2[1]] ef := Sqrt[p2 + Mass2[2]]

S := 2*p2 + Mass2[1] + Mass2[2] + 2*el*ef

T := -2*p2*(1 - Cos[theta])

U := Mass2[1] + Mass2[2] - 2*el*ef - 2*p2*Cos[theta]

(Loading integration package)

Install["LoopTools"]

(Numerical values of the masses)

ME := 0.510998902/10^3; MU := 47/10^3; MD := 47/10^3; MM := 105.658357/10^3; ML := 1777.03/10^3; MC := 1.25; MB := 4.2; MT := 174.3; MS := 0.125; Alfa := 1/137.0359895; Alfa2 := Alfa^2; MZ := 91.1882; MW := 80.419; MH := 100.;

MH2 := MH*MH; MM2 := MM*MM; ML2 := ML*ML; MC2 := MC*MC; MB2 := MB*MB; MT2 := MT*MT; MS2 := MS*MS; MZ2 := MZ*MZ; MW2 := MW*MW; MD2 := MD*MD; MU2 := MU*MU; ME2 := ME*ME; MN2 := MN*MN;

MN := 0.93972

f := 1

(Centre of the mass energy definition)

ecms := (ME2 + MN2 + 2*Elab*(MN/f)* (1 - ((Elab^2-ME2)^(1/2)*((MN/f)^2-MN2)^(1/2)*Cos[angle])/ (Elab*(MN/f))))^(1/2)

Den[a,b]:= 1/(a - b)

GN:=0

(Fermi constant (tree level definition))

Gf := (Pi*Alfa)/(SW2*MW2*Sqrt[2])

(Numerical values of the electric and magnetic form factors at zero momentum transfer)

142

NAB := Sqrt[0.83*MN2]

NAB1 := 1.0000001*NAB

F1neutron := 0

F1proton := 1

F2neutron := -1.91

F2proton := 2.79 - 1

F1Vneutron := F1neutron - F1proton

F2Vneutron := F2neutron - F2proton

G1neutron := -1.25

GLGN := F1neutron

GRGN := F1neutron

F2N := F2neutron/2/MN

F2WEAKN := (F2Vneutron - 4*SW2*F2neutron)/(2*MN)/4/SW/CW

GLZN := (F1Vneutron - 4*SW2*F1neutron + G1neutron)/(4*SW*CW)

GRZN := (F1Vneutron - 4*SW2*F1neutron - G1neutron)/(4*SW*CW)

en := axialenself

ne := axialneself

(Energy and scattering angle values at close to zero momentum transfer (smallest moment transfer without Landau singularities))

Elab := 0.5

theta := (Pi/180)*9

SetLambda[10^0]

SetMudim[10^0]

(Monopole formfactor approximation)

BOX2 := (1/(NAB^2- MZ2))*NAB^2

(Getting final numericall results)

(en + MN*axialenself1)*(Sqrt[2]/Gf/2)

(ne + MN*axialneself1)*(Sqrt[2]/Gf/2)

References

[1] D.H. Beck. *Phys. Rev.*, D39:3248, 1989.

[2] M.J. Musolf. Ph.d. thesis. *Princeton University*, 1989.

[3] M.J. Musolf and B.R. Holstein. *Phys. Lett.*, B242:461, 1990.

[4] M.J. Musolf and B.R. Holstein. *Phys. Rev.*, 43:2956, 1991.

[5] M. J. Musolf and M. Burkardt. *Z. Phys.*, C61:433, 1994.

[6] S.-L. Zhu, S.J. Puglia, B.R. Holstein and M.J. Ramsey-Musolf. *Phys. Rev.*, D62:033008, 2000.

[7] S. Barkanova, A. Aleksejevs, P. Blunden. Radiative corrections and parity-violating electron-nucleon scattering. *Jefferson Laboratory preprint #JLAB-THY-02-59, also at http://xxx.lanl.gov/abs/nucl-th/0212105*, page 21, 2002.

[8] W. J. Marciano, A. Sirlin. *Phys. Rev.*, D29:75, 1984.

[9] W. J. Marciano, A. Sirlin. Some general properties of the $o(\alpha)$ corrections to parity violation in atoms. *Phys. Rev. D*, 29:75-88, 1983.

[10] B.A. Mueller *et al.*, Phys. Rev. Lett. **78** 1997

D.T. Spayde *et al.* Phys. Rev. Lett. **84** 2000

R. Hasty *et al.* Science **290** 2117 2000.

[11] SAMPLE *et al.*, Collaboration: T. M. Ito. *preprint nucl-ex/0310001*, 2003.

[12] K.A. Aniol *et al. Phys. Lett.*, B509:211, 2001.

[13] G0 Web Page. *http://www.npl.uiuc.edu/exp/G0/G0Main.html.*

[14] A4 at Mainz Proposal at. *http://www.kph.uni-mainz.de/A4/Welcome.html.*

[15] J. Bowman, R. Carlini, J. Finn, V. A. Kowalski, S. Page. "The Q(Weak) experiment: A search for physics at the TeV scale via a measurement of the proton's weak charge". *Jefferson Lab Experiment -E02020. Proposal to PAC 21 at http://www.jlab.org/qweak/.*

[16] S. Weinberg Phys. Rev. Lett. 19 19 1967.

A. Salam "Elementary Particle Theory" P. 367 1968.

S. L. Glashow, Nucl. Phys. B 22 579 1961.

[17] W. F. L. Hollik. *DESY 88-188, ISSN 0418-9833.*

[18] G 't Hooft. *Nucl. Phys.*, B33:173, 1971.

[19] D.E. Groom *et al. Eur. Phys. J.*, C15:1, 2000.

[20] J. F. Donoghue, E. GolowichB, R. Holstein. Dynamics of the standard model. *Cambrige University Press*, 1996.

[21] B. Bauss *et al.* "The ATLAS experiment at CERN". *at http://www.physik.uni-mainz.de/Forschungsbericht/ETAP/sec_atlas.html.*

[22] J.B. Bjorken, S.D. Drell. "Relativistic quantum fields". *McGraw-Hill, New York,* 1965.

[23] C. Itzykson, J. Zuber. "Quantum field theory". *McGraw-Hill, New York,* 1980.

[24] L. D. Faddeev, V. N. Popov. *Phys. Lett.,* B25:29, 1967.

[25] M. Bohm, H. Speisberger, W. Hollik. *Fort. Phys.,* 34:688, 1986.

[26] Michio Kaku. "Quantum field theory". *Oxford University Press,* 1993.

[27] T. Hahn and M. Perez-Victoria. *Comp. Phys. Comm.,* 118:153, 1999.

[28] W. Siegel. *Phys. Lett.,* B84:193, 1979.

[29] T. Hahn. Ph.d. thesis. *University of Karlsruhe,* 1997.

[30] G. Passarino and M. Veltman. *Nucl. Phys.,* B160:151, 1979.

[31] M. E. Peskin, D. V. Schroeder. "An introduction to quantum field theory". *Westview Press,* 1995.

[32] F. del Aguila *et al. Nucl. Phys.,* B537:561, 1999.

[33] Aoki K. *et al. Prog. Theor. Phys., Suppl.,* 73:1, 1982.

[34] F. Del Aguila, A. Culatti, R. Munoz Tapia and M. Perez-Victoria. *Phys. Lett.*, B419:263, 1998.

[35] J. C. Ward. *Phys. Rev.*, 78:182, 1950.

[36] H. Burkhardt, B. Pietrzyk. Update of the hadronic contribution to the QED vacuum polarization. *Phys. Lett.*, B513:46–52, 2001.

[37] G. T Hooft and M. Veltman. *Nucl. Phys.*, B44:189, 1972.